Model Predictive Control for a Heat Pump System with Thermal Storage Tanks

Economical Operation and Demand-Side Management

Weihong Tang

Master of Science Thesis

TU Delft Delft University of Technology

Delft Center for Systems and Control

Model Predictive Control for a Heat Pump System with Thermal Storage Tanks

Economical Operation and Demand-Side Management

Master of Science Thesis

For the degree of Master of Science in Systems and Control at Delft University of Technology

Weihong Tang

January 18, 2024

Faculty of Mechanical, Maritime and Materials Engineering (3mE) · Delft University of Technology

The work in this thesis was supported by Kropman B.V.. Their cooperation is hereby gratefully acknowledged.

Abstract

In light of the pressing challenges posed by global climate change and the imperative to reduce Carbon Dioxide (CO2) emissions, innovative approaches in energy management are critically important. This thesis presents an exploration of heat pumps integrated with Thermal Energy Storage (TES) systems, an area of research and application pivotal for enhancing energy efficiency and environmental sustainability. The combination of heat pumps and TES systems emerges as a key factor in reducing greenhouse gas emissions and optimizing the utilization of renewable energy. Such integration plays a crucial role in minimizing operational costs, reducing environmental negative impact, and augmenting system efficiency by enabling the storage and later use of energy from renewable sources. Moreover, this integration facilitates the effective management of demand-side energy, bolstering the capacity to incorporate fluctuating renewable generation into the energy grid. This is achieved by dynamically load shifting to balance energy supply and demand.

A central aspect of this thesis is the utilization of Model Predictive Control (MPC) for advanced energy management. The research delves into the use of MPC to optimize the operational economy of the system, aiming to maximize cost-efficiency. Additionally, an innovative MPC-based Demand-Side Management (DSM) strategy is introduced. This strategy involves two key steps: initially establishing a model to assess the system's energy flexibility, followed by harnessing this flexibility to respond to demand fluctuations. Such an approach facilitates dynamic adaptation to varying energy demands, ensuring optimal resource utilization. The predictive capability of MPC, which accounts for future disturbances including demand forecasts, electricity pricing, and weather conditions, is exploited to improve the system's responsiveness and operational efficiency.

Experimentation was conducted both in simulations and through the implementation in real systems. These practical applications demonstrated significant savings in energy costs and energy consumption, achieving economical operation. Furthermore, the execution of the proposed two-step demand-side management strategy successfully managed energy demands. This not only underscores the practical effectiveness of the proposed system but also highlights its potential in real-world scenarios.

In summary, this research underscores how the integration of heat pumps, TES systems, and advanced control strategies like MPC can significantly improve energy efficiency, reduce

operational costs, and enhance energy flexibility. It highlights the vital role of incorporating sophisticated control mechanisms into sustainable energy systems, aligning with the strategic goals of modern energy policies and advancing the field of sustainable energy management.

Table of Contents

Acknowledgements v

1 Introduction 1
- 1-1 Motivation . . . 2
- 1-2 Research Objectives . . . 3
- 1-3 Contributions . . . 4
- 1-4 Structure of This Thesis . . . 5

2 System Description and Control-Oriented Model Development 7
- 2-1 System Description . . . 7
  - 2-1-1 Heat Pump System . . . 9
  - 2-1-2 Thermal Energy Storage System . . . 10
- 2-2 Modelling Assessment Criteria . . . 12
- 2-3 Control-Oriented Models for the Heat Pump System and Thermal Storage Tanks 14
  - 2-3-1 Heat Pump . . . 14
  - 2-3-2 Heat Exchanger . . . 16
  - 2-3-3 Water Thermal Storage . . . 18
  - 2-3-4 Entire System . . . 21
- 2-4 Prediction of Hot Water Consumption . . . 29
  - 2-4-1 Data Analysis . . . 29
  - 2-4-2 Prediction Model Development . . . 31

3 MPC for Economical Operation 39
- 3-1 Original Control Strategy . . . 39
- 3-2 Objectives of the Control Strategy . . . 40
- 3-3 Model Predictive Control . . . 41
- 3-4 MPC Configuration . . . 43

3-4-1 Physical Constraints . . . 43
3-4-2 Economic MPC . . . 44
3-5 Techniques for Computational Feasibility and Efficiency of MPC . . . 45
3-5-1 Slack Factors . . . 45
3-5-2 Move Blocking Strategy . . . 47
3-6 Simulation Results . . . 48
3-6-1 MPC Computation Time . . . 48
3-6-2 Electricity Price . . . 49
3-6-3 Energy Cost Saving . . . 50
3-7 Real Implementation Results . . . 53

4 MPC-Based Demand-Side Management **57**
4-1 Introduction and Motivation . . . 57
4-2 Objectives of Demand-Side Management . . . 58
4-3 Two-Step Demand-Side Management Strategy . . . 59
4-3-1 Flexibility Assessment . . . 59
4-3-2 Flexibility Exploitation . . . 62
4-4 Simulation Results . . . 63
4-5 Real Implementation Results . . . 65

5 Conclusions **67**
5-1 Summary . . . 67
5-2 Future Work . . . 68

A Supplementary Materials **69**
A-1 Additional Experimental Results . . . 69
A-2 Control-Oriented Model Details . . . 71
A-2-1 Description and identification result of symbols . . . 71
A-2-2 Details of Model 2 . . . 74

Bibliography **75**

Glossary **79**
List of Acronyms . . . 79
List of Symbols . . . 79

Acknowledgements

I would like to express my deepest gratitude to all those who have supported and assisted me during my thesis work. First and foremost, I extend my heartfelt thanks to my supervisor, Tamas Keviczky, who is one of the finest teachers I have had the privilege to encounter. His guidance has been invaluable in my academic journey, particularly in the conduct of research. Beyond academics, his influence has profoundly shaped my attitude towards life and work. I am incredibly fortunate to have been his student; the discussions and interactions during our meetings over the past year have imparted practical experiences and perspectives that will greatly benefit me in my future endeavors, both academically and in life.

My appreciation also goes to Yun Li, my daily supervisor. Our frequent meetings have been most enriching, and as a newcomer to the path of research, I have greatly benefited from his patient instruction. Whenever I encountered confusion or difficulties, he was always there to offer timely assistance. His unwavering patience and willingness to teach me, along with his comprehensive and unreserved guidance, have been instrumental in my research journey.

Special thanks are due to Shalika Walker from Kropman B.V.. Her assistance during my time at Kropman B.V. was invaluable. She not only facilitated my interactions with various company departments but also ensured that I had timely access to the necessary learning materials and support. Her help greatly enhanced my experience and understanding. I would also like to extend my gratitude to Jos Ruijter from a.s.r., Kevin de Bont, Jan-Willem Dubbeldam, Mark Lambert, Joep van der Velden, and all the others from Kropman B.V. who have been of help. Without their support, acquiring a comprehensive understanding of heat pumps and thermal energy storage would have been challenging. I am particularly grateful for the opportunity they provided to conduct experiments on real systems, which allowed for the validation of our proposed algorithms.

Lastly, I wish to thank my family and friends for their continued support throughout this journey. Pursuing studies far from home comes with its challenges, and it is thanks to their efforts that I have been able to successfully complete my studies.

Delft, University of Technology — Weihong Tang
January 18, 2024

Chapter 1

Introduction

Climate change has become an increasingly urgent global issue, leading to significant policy responses across nations. The Dutch government and the European Union have set ambitious targets for reducing Carbon Dioxide (CO2) emissions and increasing the use of new energy sources. By 2030, the EU aims to reduce CO2 emissions by at least 55% compared to 1990 levels, while the Netherlands is targeting a 60% reduction. Moreover, there is a goal to ensure that at least 27% of energy comes from new sources by 2030, striving towards carbon neutrality and a sustainable energy supply by 2050 [23]. However, the rise in variable renewable electricity generation presents challenges in balancing supply and demand and maintaining grid stability, mainly due to the intermittent nature of renewable sources. This scenario underscores the importance of innovative solutions in storage technology and Demand-Side Management (DSM) [6], including the integration of heat pumps with Thermal Energy Storage (TES) systems and the implementation of effective DSM strategies.

The intersection of heat pumps with TES systems and DSM techniques is particularly noteworthy in the context of energy efficiency and environmental sustainability. Heat pumps are recognized for their high efficiency and significant contribution to reducing greenhouse gas emissions, which emphasizes the role of heat pumps in enhancing energy efficiency and reducing emissions in renewable energy systems [28]. Their ability to adjust heat output in line with the availability of renewable power positions them as economically viable alternatives to district heating [21]. Furthermore, the integration of thermal storage tanks with heat pumps, enhances this efficiency by storing energy captured by heat pumps or generated by solar panels for later use [3]. This integration approach is promising in enhancing overall system efficiency, reducing environmental impact, and lowering operational costs [2][13].

In addition, the further integration of heating and electricity networks through heat pumps and TES systems enhances the capacity for DSM. This enables the integration of more variable renewable generation into the energy system [34]. By shifting electrical load from on-peak to off-peak hours, and potentially to times with excess renewable electricity, these systems contribute significantly to DSM [3]. The combination of heat pumps and TES not only leads to efficiency improvements but also offers environmental and economic benefits, aligning with the strategic objectives of modern energy policies. Their role in energy markets

is becoming increasingly important, contributing to reductions in operational costs and CO2 emissions, and enhancing system agility through DSM [31].

In this context of integrating heat pumps with TES for improved energy management, Model Predictive Control (MPC) is recognized as a powerful and effective tool. Its application in heat pump systems significantly optimizes performance by minimizing power consumption while maintaining heating capacity [38][40]. Compared to traditional control methods, MPC is particularly adept at exploiting energy storage and predicting future disturbances, which includes demand forecasts [6], electricity prices (also referred to as Economic Model Predictive Control) [24], and weather conditions [29]. By efficiently handling system constraints, MPC ensures that operations remain within safe and efficient boundaries [24]. Additionally, control actions optimized based on a prediction horizon significantly enhance DSM capabilities [6], aligning with the strategic objectives of reducing emissions and improving overall energy efficiency in the face of evolving energy demands.

1-1 Motivation

This research is driven by several key motivations that address both current challenges and future opportunities in the field of energy management and sustainability. The following points outline the primary factors that have inspired and directed our study, highlighting the growing importance of heat pumps, the challenges of renewable energy integration, the potential of integrating heat pumps with storage systems and smart grids, and the advancement of system energy flexibility through DSM.

- **The growing importance of heat pumps:**

  Heat pumps are increasingly recognized as a crucial low CO2 emission technology, especially pertinent in the current era of developing standards for low and zero-carbon housing [16]. Their market potential is particularly notable in the European Union, which promotes their widespread adoption to improve energy efficiency and utilize renewable energy sources. The EU directive on renewables includes heat pumps among the technologies enabling the exploitation of renewable sources [32]. This growing significance is further evidenced by the record sales of heat pumps in Europe, reaching 3 million units in 2022, which indicates a 38% growth and contributes to a total of 20 million units in operation [12]. In the Netherlands, the government aims to install one million heat pumps by 2030 as part of its sustainable building environment program.

- **Challenges in renewable energy integration:**

  With increasing dependence on renewable energy sources, introducing flexibility into the power system is crucial for ensuring stability [16]. The widespread introduction of fluctuating Renewable Energy Sources (RES) has made balancing power demand and supply increasingly challenging, raising the likelihood of frequency deviations. To mitigate these deviations, there is a growing need for control energy. However, the traditional approach of depending on generators for this control energy poses economic and environmental challenges, emphasizing the need for more sustainable and cost-effective solutions [30].

- **Potential of heat pump integration with storage systems and smart grids:**

  Addressing the challenges presented by renewable energy integration calls for innovative solutions, among which the combination of heat pumps with thermal energy storage systems and smart grids stands prominent [3]. This integration provides a comprehensive approach to energy management. Thermal energy storage systems serve as a crucial buffer, allowing for thermal load shifting. This capability is not only essential for stabilizing the grid in the face of increasing usage of renewable energy but also offers an efficient way to store energy, aligning with fluctuating demand or electricity prices [17]. Thus, this integration represents a forward-thinking strategy to enhance energy efficiency and grid reliability.

- **Advancing system energy flexibility through DSM:**

  Further enhancing the energy flexibility of systems, especially in light of the challenges posed by renewable energy integration, can be effectively achieved through DSM [20]. DSM refers to the methods and strategies used to manage consumer demand (from demand-side) for energy. By adjusting or shifting energy use patterns, DSM plays a pivotal role in aligning energy demand with supply in a more dynamic and responsive manner. One critical aspect of DSM, particularly relevant in the context of heat pump operation, is addressing the issue of electricity demand peaking. Heat pumps, while efficient, can cause significant peaks in electricity demand, particularly in utility buildings where there are limits on the peak electricity that can be drawn from the grid. These peaks can strain the energy infrastructure and lead to inefficiencies. By enabling buildings to respond to real-time requirements of the electricity grid, such as through the use of real-time pricing or direct control mechanisms, DSM can significantly contribute to mitigating these demand peaks, leading to a more balanced and efficient energy system [7]. This approach not only complements the integration of heat pumps and smart grid technologies but also represents a key step towards a more adaptable and sustainable energy infrastructure.

1-2 Research Objectives

Building upon the foundational insights from our previous literature review [36], this thesis focuses on applying advanced control algorithms, specifically MPC, to a real-world heat pump system with thermal storage tanks. The primary goals are to achieve economical operation and effective demand-side management. The research is structured around the following objectives:

- **System Modeling Performance:**

  To critically evaluate the developed control-oriented models for heat pumps and thermal energy storage systems, assessing their accuracy and reliability in reflecting real-world dynamics and efficiencies. The goal is to ensure that these models accurately represent the operational characteristics of a heat pump system with water thermal storage tanks in the real world.

- **Design of a Prediction Model for Water Consumption:**

To develop an advanced predictive model for water consumption, aiming for high precision in forecasting. This model is intended to optimize the heat pump system's operational efficiency by enabling proactive and optimized control decisions based on anticipated future water consumption.

- **Optimizing MPC for Economical Operation:**

  To refine the MPC strategy for cost-effective energy management in our heat pump system with water thermal storage tanks. This involves tailoring the MPC to adapt to variable energy supply and demand conditions, focusing specifically on achieving economical operation.

- **Demand-Side Management Design:**

  To develop innovative DSM strategies with an emphasis on system flexibility. This involves determining the maximum duration for which the system can be shut down and leveraging this period to enhance system flexibility, such as meeting the grid's load shifting requirements.

- **Simulation and Real-World Implementation:**

  To test and evaluate our methodology in both simulated and real-world environments. This includes assessing the effectiveness of MPC in terms of energy savings, cost reduction, and enhancing energy flexibility. The objective also involves observing the practical challenges and overall performance of the system in actual operational.

1-3 Contributions

This thesis work makes several significant contributions to the field of heat pump systems with thermal energy storage, as detailed below:

- **Development of a Control-Oriented Model:**

  A comprehensive control-oriented model has been developed to effectively represent the dynamics of real heat pump systems with thermal storage tanks. This model is meticulously crafted to strike a balance between computational complexity and accuracy, ensuring that it not only reflects real-world system dynamics accurately but also remains computationally feasible for practical applications. Such a balance is crucial for its robustness, making the model an ideal foundation for further research and application in the field.

- **Design and Implementation of MPC:**

  A key contribution of this thesis is the design of a tailored MPC strategy for system control, followed by its implementation. This strategy represents a significant advancement over traditional rule-based control methods, optimizing energy usage and reducing costs while showing marked improvements in efficiency and adaptability in response to electricity market fluctuations.

- **Assessment and Exploitation of the Energy Potential through DSM:**

  The thesis introduces a two-step demand-side management framework, consisting of flexibility assessment and exploitation, and proposes a solution method based on MPC. This approach thoroughly investigates the energy flexibility of heat pump systems, implementing advanced demand response strategies and underscoring the system's adaptability in managing energy demand. This contributes significantly to DSM, enhancing sustainable and efficient energy use.

- **Tailored Control Approach for Heat Pump On/Off Control:**

  A key contribution is the development of an advanced control method specifically tailored for the on/off control of heat pumps. This approach, while based on basic control principles, demonstrates a high degree of adaptability and potential for wider application, indicating its practical relevance and scalability for diverse heat pump systems.

- **Validation through Real-World Implementation:**

  The developed algorithms and strategies have been tested and validated within a real-world system environment. This real-world application not only demonstrates the effectiveness of our proposed solutions but also highlights their viability for widespread industrial adoption.

The contributions of this thesis not only advance the understanding and capabilities of heat pump systems with thermal energy storage but also pave the way for innovative, energy-efficient, and cost-effective solutions in sustainable energy management.

1-4 Structure of This Thesis

The thesis is structured as follows:

- Chapter 2 provides an in-depth examination of the system under study, focusing on its key components such as the heat pump, the heat exchanger, and water thermal storage tanks. It details the development of a control-oriented model for each component and the integration of these models into a comprehensive system model. The chapter also discusses the model identification process and presents the demand prediction model used in our research.

- Chapter 3 introduces the original control methods and outlines the objectives for designing new control strategies, with a focus on achieving economical operation. It delves into MPC, detailing the specific MPC configuration employed in our research. Additionally, the chapter discusses techniques to enhance the computational feasibility and efficiency of MPC. It concludes with the presentation of simulations and tests conducted on the real system to validate the proposed control strategies.

- Chapter 4 addresses the rationale for implementing DSM, specifically through the design of MPC-based strategies. It introduces the concepts of flexibility assessment and flexibility exploitation. The chapter explores methods for implementing these concepts

and integrating them with MPC for effective DSM. Concluding the chapter are simulations and real-system tests that demonstrate the practical application and effectiveness of these strategies.

- Chapter 5 provides a comprehensive summary of the thesis. It reflects on the findings and offers suggestions for future work and potential areas of exploration building on this thesis research.

Chapter 2

System Description and Control-Oriented Model Development

This chapter provides a detailed description of the physical system considered for control in this thesis, as well as the control-oriented modeling of its components. Section 2-1 presents an overview of the system, including brief descriptions of the two key subsystems that constitute it. Section 2-2 delves into model assessment, discussing the error metrics employed to evaluate model performance. Subsequent modeling of the essential parts is thoroughly described in Section 2-3. Here, the individual subsystem models are developed and later integrated into a comprehensive model of the entire system. This section also covers model identification and validation to ensure the models' accuracy and reliability. Finally, Section 2-4 introduces the demand prediction model utilized in this study. This predictive model is integral to forecasting and managing the system's performance.

2-1 System Description

This thesis explores the air-to-water Carbon Dioxide (CO2) heat pump system, an innovative technology implemented by Kropman B.V. at the ASR headquarters in Utrecht. The actual heat pump system with thermal energy storage is illustrated in Figure 2-1. This advanced system plays a crucial role in providing domestic hot water for various office applications, including kitchens and gym shower facilities. Its significance is highlighted by its efficient, sustainable approach to hot water supply, particularly notable for its load-shifting capabilities, an essential feature in today's energy landscape. The principal scheme of the system, demonstrating its comprehensive layout and functionality including key components such as a heat pump, a heat exchanger, and thermal storage tanks, is depicted in Figure 2-2. All relevant sensor information can be monitored remotely, as shown in Figure 2-3.

The system consists of two primary subsystems: the heat pump system and the thermal energy storage system. The heat pump system includes a heat pump, a heat exchanger, and the water circuit connecting them. This subsystem is primarily responsible for heat

(a) CO2 air-to-water heat pump **(b)** Two 500L water tank

Figure 2-1: The heat pump system with thermal energy storage

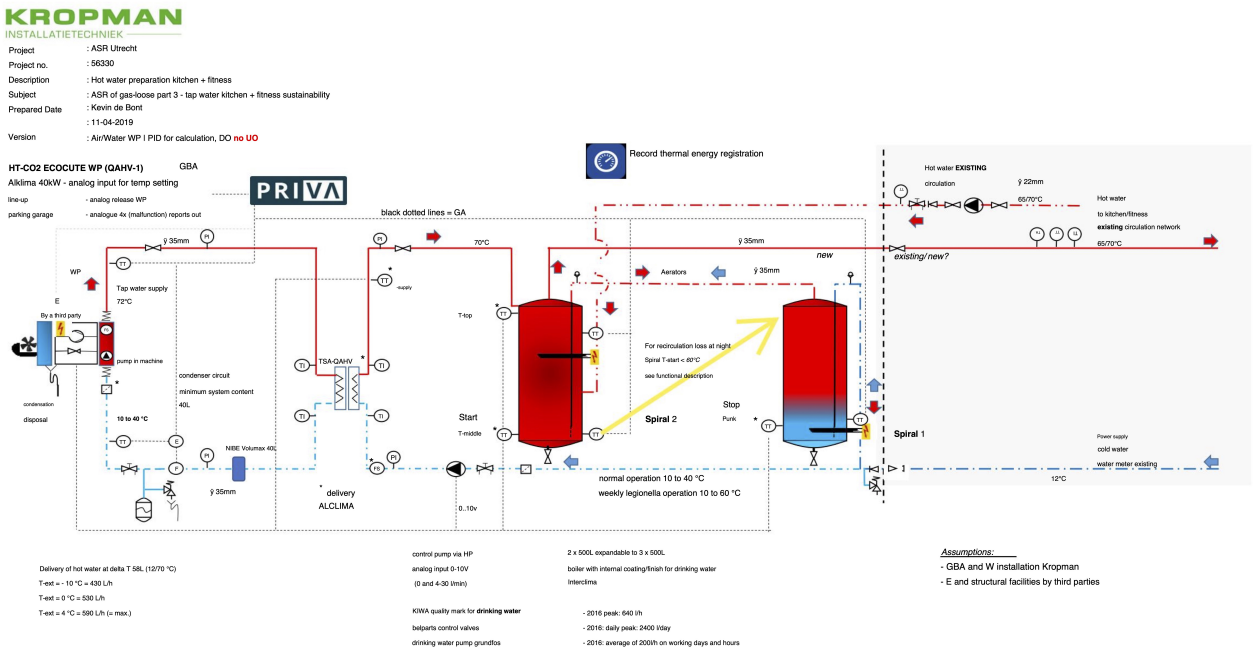

Figure 2-2: Principle scheme of the system

extraction and temperature regulation. The thermal energy storage system, comprising two thermal storage water tanks and their associated supply and makeup water pipelines, plays a vital role in ensuring a steady supply of hot water, adapting to fluctuating water demands. A detailed schematic representation of the entire system, highlighting the interconnectivity and functions of these subsystems, is presented in Figure 2-4. Red pipes transport heated water, blue pipes carry water awaiting heating, and the green pipe serves the demand side, respectively. The specific components and their attributes are described in Table 2-1.

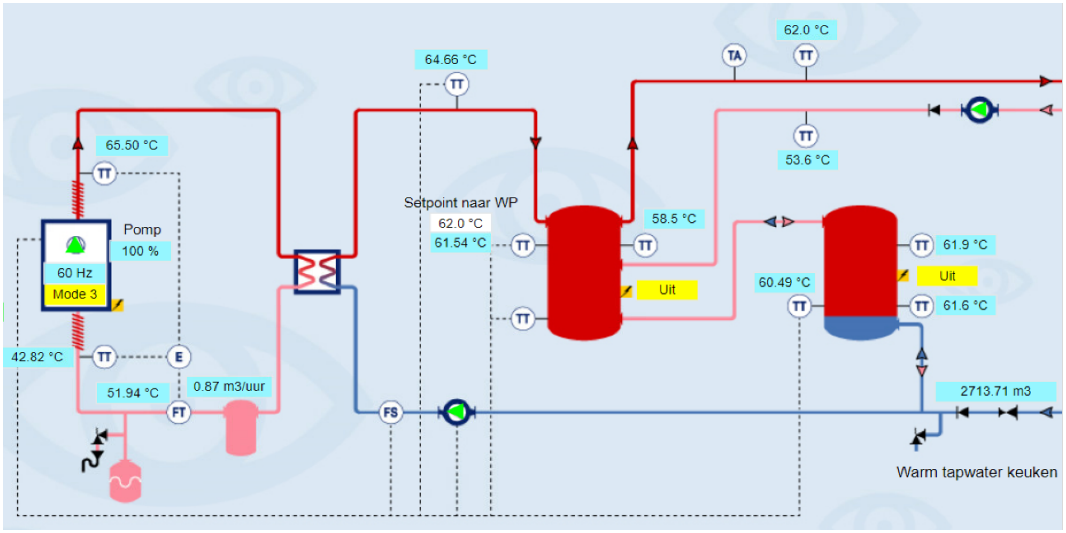

Figure 2-3: Screenshot of remote monitoring

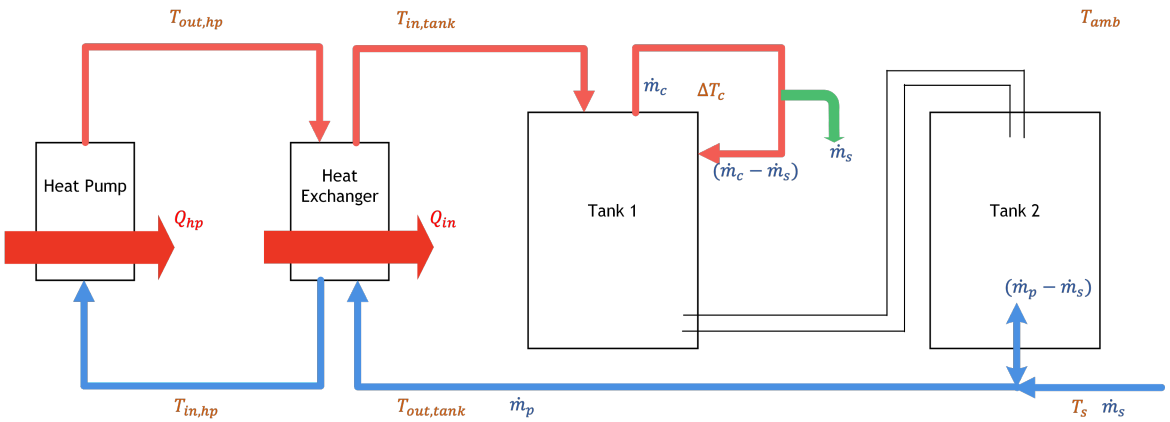

Figure 2-4: Diagram of energy flow for the entire system

2-1-1 Heat Pump System

Figure 2-5 outlines the operational scheme of the heat pump system, a crucial component of the air-to-water CO2 heat pump system. This type of system, air-to-water, implies that air acts as the heat source, transferring heat to water. In this setup, CO2 is utilized as the refrigerant fluid. At its heart, the heat pump operates by extracting heat from the ambient air and then elevating the temperature of the CO2 refrigerant. The captured heat is efficiently transferred to water, a process fundamental to the system's ability to supply hot water efficiently [8].

Considering the operational complexity and the necessity for safety, the control of the heat pump is limited to a straightforward yet effective on-off mechanism. This rule-based control design is critical for ensuring both operational efficiency and safety. Specifically, the system activates the heat pump when the upper water temperature in the first tank exceeds a predetermined threshold and deactivates it once the bottom water temperature in the second tank

Symbol	Description
Q_{hp}	Input heat of the heat pump
Q_{in}	Heat transferred from the heat pump to the storage system through the heat exchanger
$\dot{m}_p$	Flow rate in the main circulation pipe
$\dot{m}_s$	Flow rate in the supplement pipe
$\dot{m}_c$	Flow rate in the demand circulation pipe
T_s	Temperature of the water in supply pipe
$T_{in,tank}$	Temperature of the inlet water of the water tank
$T_{out,tank}$	Temperature of the outlet water of the water tank
$T_{in,hp}$	Temperature of the inlet water of the heat pump
$T_{out,hp}$	Temperature of the outlet water of the heat pump
ΔT_c	Temperature difference in the demand pipe
T_{amb}	Ambient air temperature

Table 2-1: Symbol description

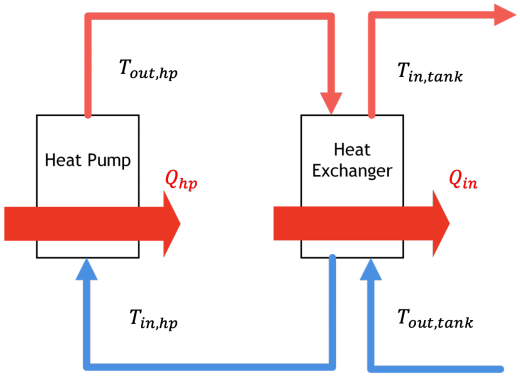

Figure 2-5: Heat pump system

falls to a set lower limit. This focused approach to on-off control is key to the emphasis of the thesis on the control aspect of the heat pump, thus obviating the need for an in-depth analysis of internal components such as compressors and condensers.

Additionally, Figure 2-6 displays the scheme of the heat exchanger. According to the manufacturer's documentation of the heat pump system, effective heat exchange is achieved under optimal conditions with a 5°C temperature difference ΔT_{he} between the heat pump's outlet water temperature ($T_{out,hp}$) and the water tank's inlet temperature ($T_{in,tank}$).

2-1-2 Thermal Energy Storage System

The thermal energy storage system is pivotal in the operation of the air-to-water CO2 heat pump system. Its fundamental role is to store heated water, ensuring a consistent supply of hot water, even during periods of heightened demand. This subsystem, comprised of two 500L water tanks referred to as Tank 1 and Tank 2, is illustrated in Figure 2-7. A key feature of this configuration is the connection between the bottom of Tank 1 and the top of Tank 2,

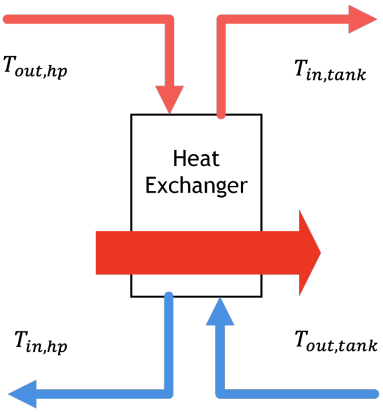

Figure 2-6: Heat exchanger

facilitating efficient water transfer and storage.

Within this subsystem, water replenishment operates on a one-to-one basis. This approach ensures that the quantity of water consumed is precisely replenished, meaning the flow rate at the replenishment end matches the flow rate of water exiting the demand side. As water demand varies, the flow rate dynamically adjusts to maintain this balance, ensuring that the flow rate is not constant. This dynamic adjustment is critical in responding to fluctuating demands while maintaining system efficiency. Moreover, both water tanks are consistently kept at full capacity. During the replenishment process, water from Tank 2 flows into Tank 1, thereby guaranteeing an uninterrupted supply of hot water.

This meticulous strategy for maintaining a continuous and balanced water supply is crucial for the efficient and effective operation of the subsystem. It highlights the importance of well-conceived control strategies in optimizing the performance of such integrated systems. The design of the two-tank system, with its specific capacity and interconnection, plays a significant role in achieving the desired thermal energy storage capacity and responsiveness to varying water demands.

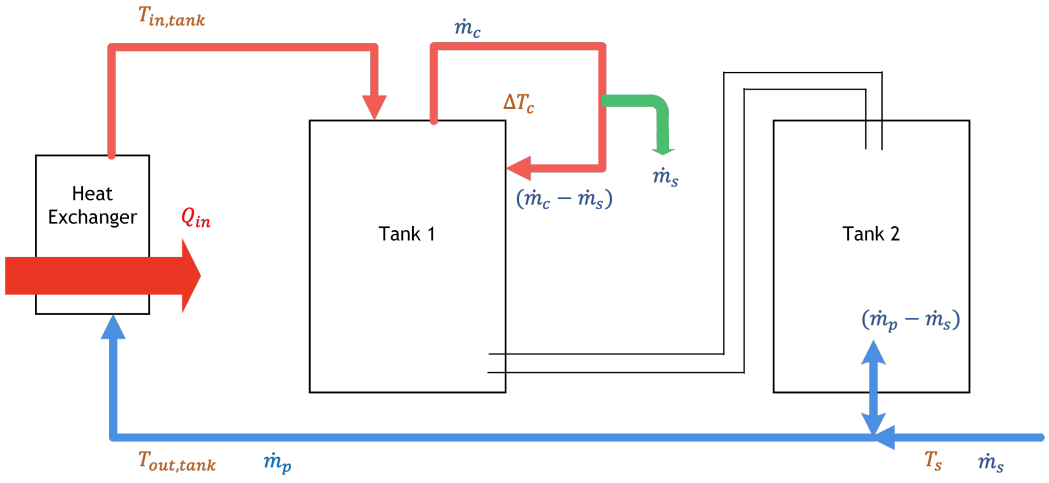

Figure 2-7: Thermal energy storage system

2-2 Modelling Assessment Criteria

Before delving into the specifics of our models, it is essential to introduce the metrics used for model evaluation. These metrics are crucial as they provide objective criteria to assess the accuracy and effectiveness of our models.

- **Root Mean Square Error (RMSE):**

  Root Mean Square Error (RMSE) is a widely used measure of the differences between values predicted by a model and the values observed [25]. It is defined as:

$$\text{RMSE}(\boldsymbol{y}, \hat{\boldsymbol{y}}) = \sqrt{\frac{|\boldsymbol{y} - \hat{\boldsymbol{y}}|_2^2}{N}} \tag{2-1}$$

  Here, y represents the observed values, $\hat{y}$ are the predicted values, and N is the number of observations. RMSE is particularly helpful as it gives a clear indication of the magnitude of prediction errors. The primary advantage of RMSE is its interpretability in the same units as the predicted variable. However, it can be overly sensitive to outliers, making it less reliable when outliers are a significant factor.

- **Mean Absolute Percentage Error (MAPE):**

  Mean Absolute Percentage Error (MAPE) is another critical metric for model assessment. It is the average of the absolute percentage errors [10] and is given by:

$$\text{MAPE}(\boldsymbol{y}, \hat{\boldsymbol{y}}) = \frac{100\%}{N} \sum_{i=1}^{N} \left| \frac{y_i - \hat{y_i}}{y_i} \right| \tag{2-2}$$

  MAPE provides a clear percentage-based measure of error, making it intuitively easy to understand and interpret. However, it can be misleading if there are zero or near-zero actual values in the data, as the percentage error becomes undefined or disproportionately high.

- **Variance Accounted For (VAF):**

  Variance Accounted For (VAF) is another common metric for model performance evaluation. It quantifies the proportion of variance in the observed data that is explained by the model [37]. The VAF is calculated as follows:

$$\text{VAF}(\boldsymbol{y}, \hat{\boldsymbol{y}}) = \left(1 - \frac{var(\boldsymbol{y} - \hat{\boldsymbol{y}})}{var(\boldsymbol{y})}\right) \cdot 100\% \tag{2-3}$$

  Here, *var* means the variance function. The VAF is expressed as a percentage, where higher values indicate a better model fit to the data. This metric is intuitive and easy to interpret, providing a clear, percentage-based indication of the model's explanatory power. It also offers a normalized measure of model accuracy, facilitating comparisons across different models or datasets.

In Table 2-2, we present a comprehensive comparison of the three error metrics used in our model assessment: RMSE, MAPE, and VAF. Each metric is evaluated based on its advantages and disadvantages. RMSE is recognized for providing a clear magnitude of prediction errors and is interpretable in the same units as the predicted variable. However, its sensitivity to outliers may affect its reliability. MAPE is advantageous for its intuitive, percentage-based error measure, which is easy to comprehend and interpret. Nonetheless, it may be misleading in datasets where actual values are zero or near-zero. VAF offers a normalized measure of model accuracy and is useful for comparing across different models or datasets, though it may not fully represent the model's predictive accuracy in certain scenarios. Table 2-2 assists in understanding the applicability and limitations of each metric within the context of our model assessment.

Metric	**Advantages**	**Disadvantages**
RMSE	Provides a clear magnitude of prediction errors and interpretable in the same units as the predicted variable.	Overly sensitive to outliers, which can affect its reliability.
MAPE	Offers an intuitive percentage-based error measure, easy to understand and interpret.	Misleading if actual values are zero or near-zero; percentage error becomes undefined or disproportionately high.
VAF	Offers a normalized measure of model accuracy, easy to interpret, and useful for comparing across models.	May not fully represent the model's predictive accuracy if the observed data has a low variance.

Table 2-2: Comparison of error metrics: RMSE, MAPE, and VAF

It is important to note that in our process of system identification and validation for the entire system, we have chosen RMSE and MAPE as our primary metrics for model assessment. This selection is influenced by the specific limitations associated with our data access. Our data, including crucial parameters like water consumption, was available only at hourly intervals. This granularity of data presents a significant limitation, as it does not allow for the capture of minute-level variations in water usage within each hour. Consequently, this restriction leads to an inability to effectively capture short-term temperature variations. This limitation particularly impacts VAF, as VAF relies on capturing and explaining the variance within the data. Given our data's limited resolution, the VAF metric would not be able to effectively represent the short-term fluctuations and thus would not provide a fully accurate measure of the model's performance. Therefore, given these data constraints, RMSE and MAPE are deemed more appropriate for our model assessment. These metrics are less sensitive to the lack of finer temporal resolution in the data and offer a more reliable measure of our model's accuracy and effectiveness, considering the available data's nature and scope.

2-3 Control-Oriented Models for the Heat Pump System and Thermal Storage Tanks

2-3-1 Heat Pump

In our study of the heat pump system, we focus on a control strategy limited to on-off operation. This decision is driven by the nature of the heat pump as an actuator within the entire system. To model the heat pump's behavior, we employ the Coefficient of Performance (COP) equation. The COP offers a simplified yet meaningful measure of efficiency, making it particularly useful in scenarios where detailed component information is either not crucial or is lacking. This modeling approach strikes a balance between computational simplicity and accuracy, which is essential for our study. It allows us to represent the system's output heat energy relative to its input electrical energy, aligning with a black-box modeling philosophy. In this context, the operation of the heat pump can be described by the following equation:

$$Q_{hp} = P_{hp} \times COP \tag{2-4}$$

Here, P_{hp} represents the heat pump's power, while COP stands for the coefficient of performance. This formula is instrumental in integrating the on-off control mechanism into our control framework, enhancing both efficiency and predictability.

Coefficient of Performance (COP)

The COP is a crucial measure of a heat pump's efficiency, representing the ratio of useful heat transfer to work input [39]. It provides an efficient way to estimate the performance of the heat pump without the need for extensive and complex computations, thereby ensuring a practical approach in our study. The COP equation is formulated as:

$$COP = \frac{Q_{hp}}{P_{hp}} \tag{2-5}$$

where Q_{hp} denotes the heat produced by the heat pump and P_{hp} is the energy input. The COP is crucial for determining the efficiency of the heat pump, where a higher COP indicates a more efficient system. Accurate modeling of the COP is essential for predicting the performance of the heat pump. Various methodologies exist for modeling the COP, taking into account multiple factors that affect heat pump operation.

For air-source heat pumps, the COP is often modeled as a function of ambient temperature [6]. Our heat pump model, which falls under the air-source category, is based on the research in [15]. Following the research, we have chosen to use the heat pump's inlet water temperature $T_{in,hp}$ and the ambient temperature T_{amb} as the primary variables in our COP equation. We have developed two models to encapsulate the heat pump's performance:

$$COP1 = a_1 + a_2 \cdot T_{in,hp} + a_3 \cdot T_{in,hp}^2 + a_4 \cdot T_{amb} + a_5 \cdot T_{in,hp} \cdot T_{amb} \tag{2-6}$$

$$COP2 = a_1 + a_2 \cdot T_{in,hp} + a_3 \cdot T_{amb} + a_4 \cdot T_{in,hp} \cdot T_{amb} \tag{2-7}$$

The first model incorporates both linear and quadratic terms, including the interaction effect between inlet water and ambient temperatures. Although more complex, this model allows for a detailed representation of various operational scenarios. The second model, simpler in its formulation by omitting the quadratic term, still accounts for the interaction between these two temperature variables. Both models are in line with our methodological approach of starting with simpler models and progressively incorporating more complexity as needed.

Regression Analysis

Figure 2-8 and Figure 2-9 present the manufacturers' data sheets available for our analysis. Figure 2-8 illustrates the variation in COP values at different inlet water temperatures, with outlet water temperatures ranging from 80 to 90 °C. Each point on the graph represents a distinct data point, with the lines depicting the general trend. The data points are color-coded, with blue points representing an ambient temperature of 18.5 °C, and red points indicating an ambient temperature of 12.5 °C. Similarly, Figure 2-9 displays data for scenarios with outlet water temperatures between 70 and 80 °C, using the same color scheme to differentiate ambient temperatures. This extensive dataset was crucial for our regression analysis, where we applied polynomial curve fitting to determine the best fit for our data.

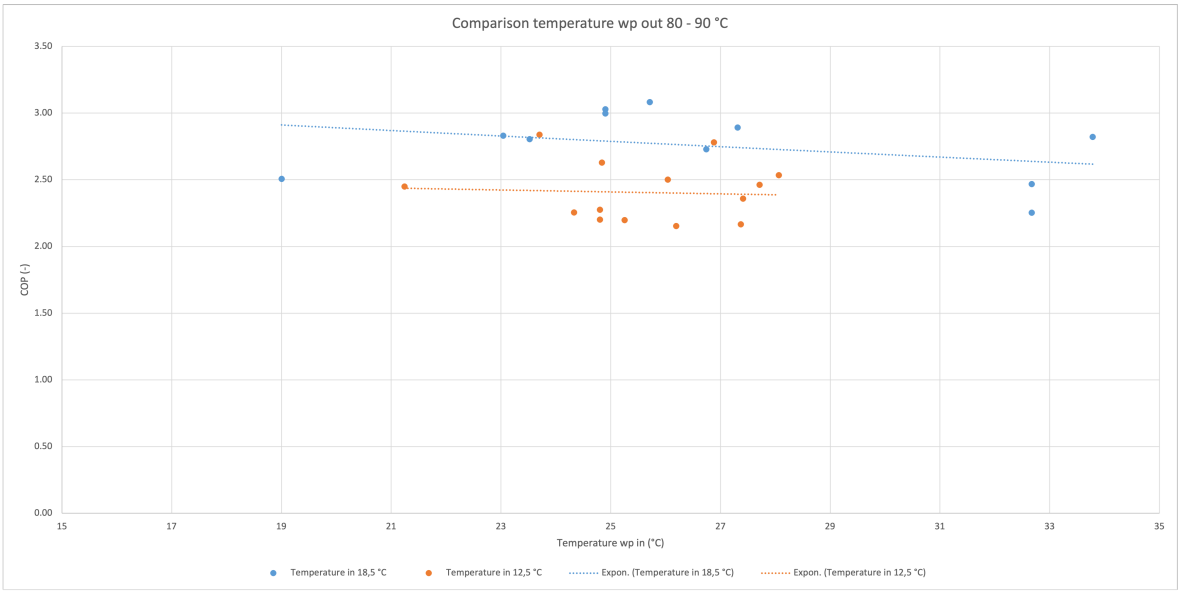

Figure 2-8: COP with different ambient temperatures (outlet water temperatures ranging from 80 to 90 °C)

The outcomes of this regression analysis are shown in Figure 2-10 and Figure 2-11, which depict the regression results for our $COP1$ and $COP2$ models, respectively. As evident from these figures, both models demonstrate low RMSEs, below 10% MAPEs and over 80% VAFs, indicating they capture a significant portion of the total data variation and provide reliable predictions with minimal errors.

The derived equations for these models are:

$$COP1 = 3.2914 - 0.0403 \cdot T_{in,hp} - 0.0000 \cdot T_{in,hp}^2 + 0.0232 \cdot T_{amb} + 0.0002 \cdot T_{in,hp} \cdot T_{amb} \quad (2\text{-}8)$$

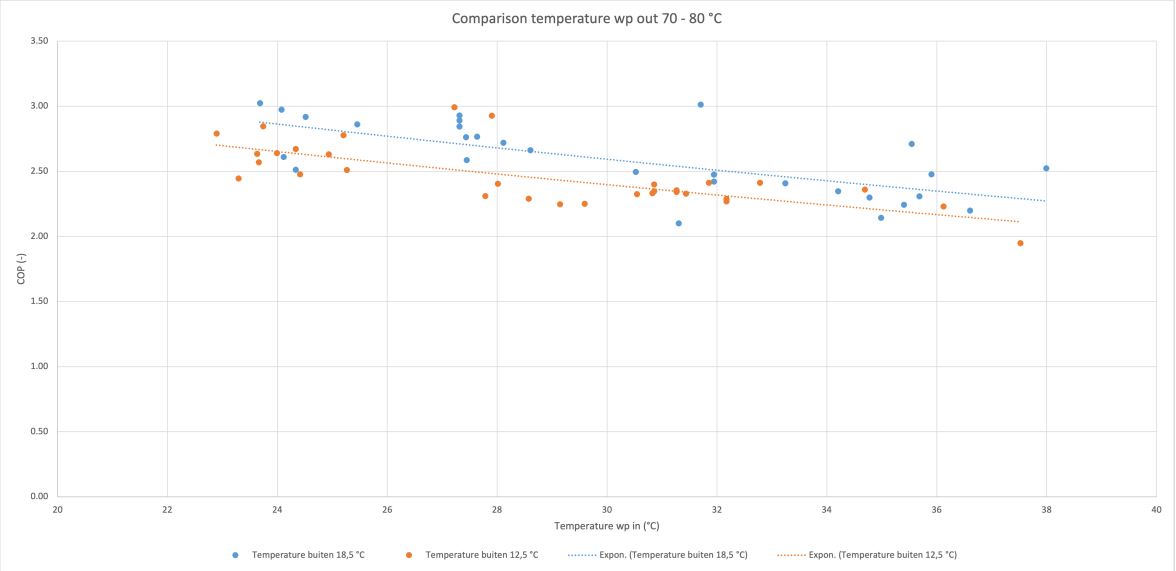

Figure 2-9: COP with different ambient temperatures (outlet water temperatures ranging from 70 to 80 °C)

$$COP2 = 3.3297 - 0.0423 \cdot T_{in,hp} + 0.0219 \cdot T_{amb} + 0.0003 \cdot T_{in,hp} \cdot T_{amb} \tag{2-9}$$

A notable observation from our analysis is the minimal impact of the quadratic term for $T_{in,hp}$ in the $COP1$ equation. The coefficient following the decimal point consists of four zeros, indicating this term may not be critically influential for the model's performance. This suggests the feasibility of a satisfactory COP equation using only first-degree terms, a notion supported by the fitting results of $COP2$.

2-3-2 Heat Exchanger

As previously mentioned in Section 2-1-1, under ideal conditions, heat exchange in the system is expected to occur with a 5°C temperature difference ΔT_{he} between the outlet water temperature of the heat pump section $T_{out,hp}$ and the inlet water temperature of the water tank $T_{in,tank}$. Our aim was to determine the actual temperature difference during the operation of the heat pump we studied. To achieve this, we focused on a specific day, May 8, 2023, for our analysis. Figure 2-12 showcases our findings, where the operational state of the heat pump is represented by the orange line. We observed that the temperature difference, illustrated by the blue line, predominantly fluctuated around 2.5°C during stable operation, as highlighted by the green line.

The larger temperature difference observed at the start phase can be attributed to the pre-existing temperature difference before the heat pump's activation. Once the heat pump begins its operation, the temperature difference stabilizes at approximately 2.5°C. The discrepancy observed during the end phase is likely due to a delay in the flow meter's response, suggesting that the heat pump might have ceased functioning by that time.

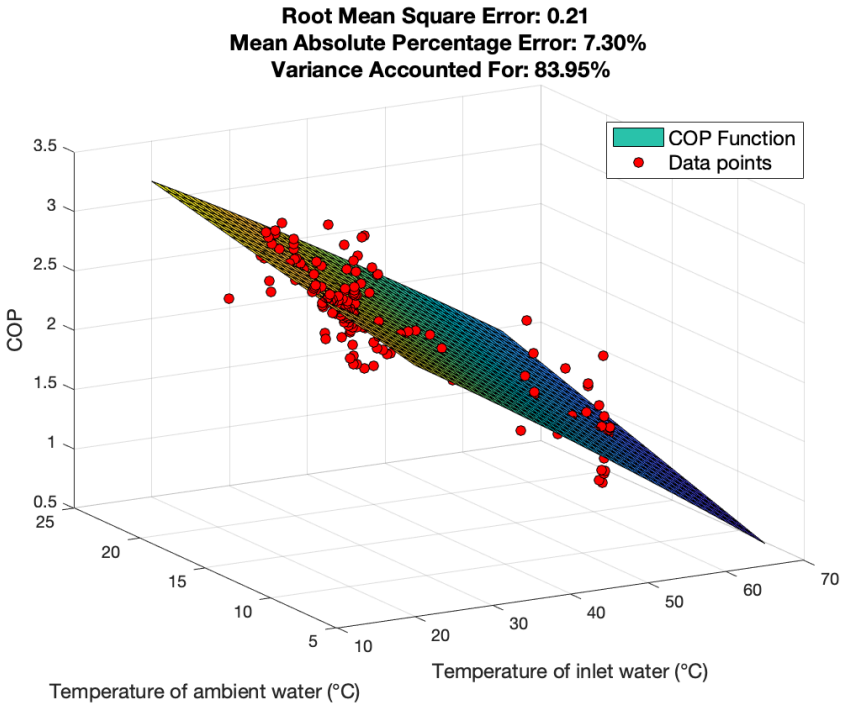

Figure 2-10: Plot of the $COP1$ function with the original data points

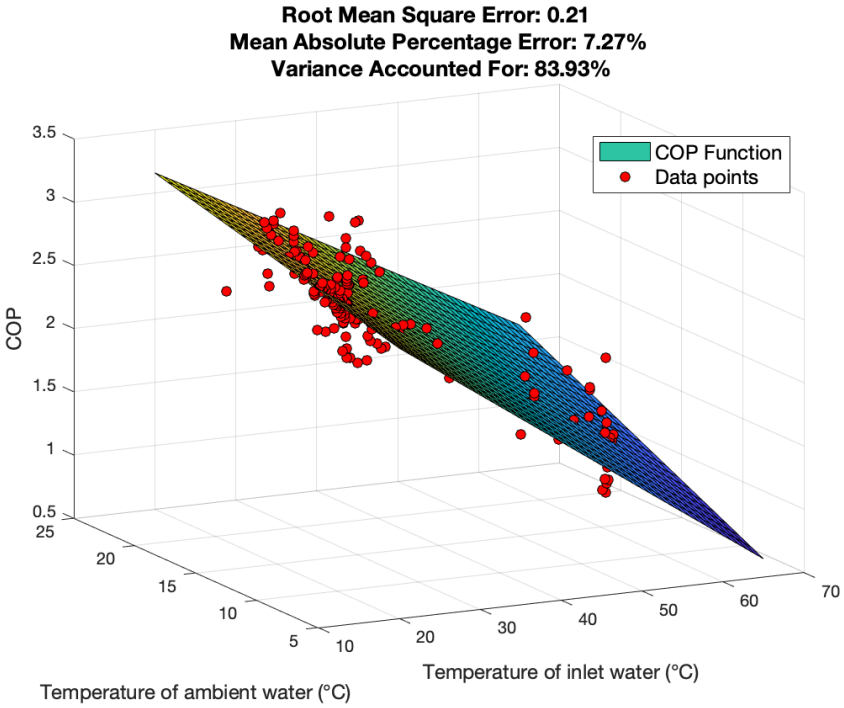

Figure 2-11: Plot of the $COP2$ function with the original data points

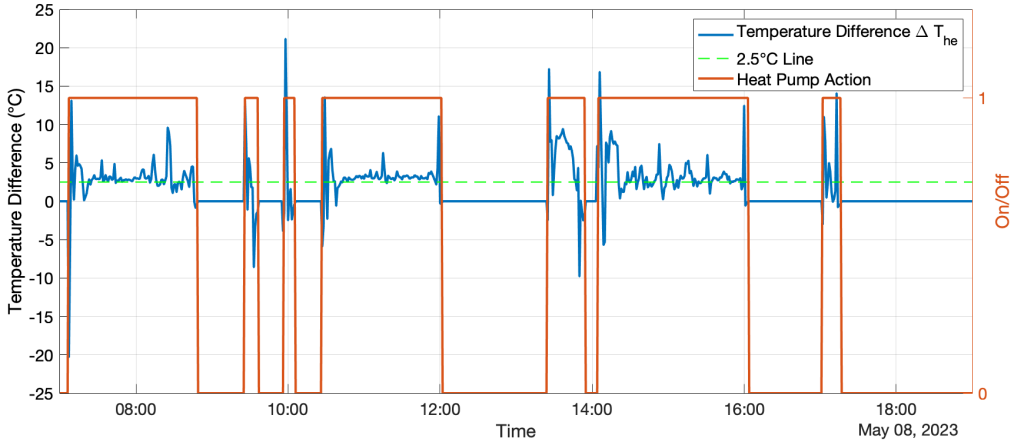

Figure 2-12: Temperature difference between outlet water of the heat pump and outlet water of the heat exchanger

2-3-3 Water Thermal Storage

Stratified Tank Model

In our research, the Stratified Tank Model, a prominent method in thermal energy storage, was utilized to model our hot water storage tank. This approach conceptualizes the tank as being divided into N distinct, equivalent segments or layers. Each segment functions as an individual node, maintaining a uniform temperature [4]. The stratification methodology is particularly advantageous for accurately representing the thermal dynamics within the tank, striking a balance between the model's complexity and its precision.

The heat dynamics within each segment of the tank are illustrated in Figure 2-13. In this depiction, each node or layer undergoes various thermal interactions:

- Heat Pump Transfer $\dot{Q}_{hp,j}$: The heat input from the heat pump to layer j.
- Wall Heat Loss $\dot{Q}_{wall,j}$: The heat lost from the layer j to the tank wall.
- Layer Heat Transfer $\dot{Q}_{j+1}$ and $\dot{Q}_{j-1}$: The spontaneous heat transfer between layer j and its adjacent layers $j+1$ and $j-1$, respectively.

The energy balance equation, which is central to this model, is outlined as follows:

$$\begin{aligned} m_j c_p \frac{dT}{dt} &= -\dot{Q}_{\text{wall},j} + \dot{Q}_{j-1} - \dot{Q}_{j+1} + \dot{Q}_{\text{conv}} \\ \dot{Q}_{\text{conv}} &= \dot{m}_t c_p \left(T_{j-1} - T_j\right) \\ \dot{Q}_{j+1} &= R_j \left(T_j - T_{j+1}\right), \quad \dot{Q}_{j-1} = R_j \left(T_{j-1} - T_j\right), \\ \dot{Q}_{\text{wall},j} &= R_w \left(T_j - T_0\right) \end{aligned} \tag{2-10}$$

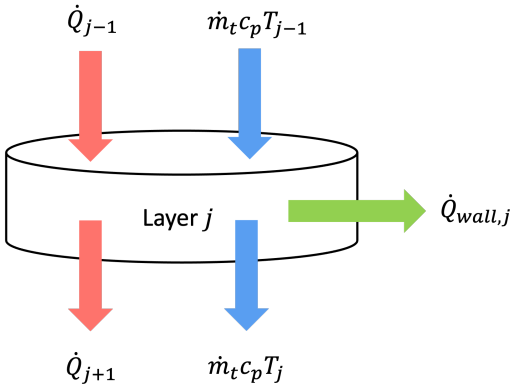

Figure 2-13: Heat flow diagram of a single layer of TES

In this equation, m_j represents the mass of layer j, T_j is the corresponding temperature, c_p and $\dot{m}_t$ denote the specific heat capacity of the water and the water mass flow rate within the tank layers, respectively, and $\dot{Q}_{conv}$ represents the heat conversion by water flow.

This energy balance equation is crucial for modeling the dynamics of each layer. It captures the essential thermal behavior and interactions with adjacent layers, providing a relatively simple yet accurate representation of the thermal dynamics of tanks. This simplicity is key for easy integration of the model into broader system-level simulations, maintaining reasonable accuracy in portraying the thermal behavior of the tanks.

The Number of Tank Layers

In the development of our stratified thermal storage model, a critical aspect was determining the optimal number of layers to accurately represent the system's dynamics. While intuitively, a greater number of layers might seem to offer a more detailed system depiction, this increase in granularity also leads to heightened model complexity and prolonged simulation times. Additionally, it cannot necessarily guarantee enhanced accuracy.

To ascertain the ideal stratification, we conducted experimental tests using two water tanks. The model's effectiveness was evaluated based on the RMSE criterion. The relationship between the number of layers in the thermal storage tanks and the resulting modeling errors was visually represented in Figure 2-14 and Figure 2-15, using temperature data from May 1, 2023. Figure 2-14 illustrates the error at each temperature measurement point (upper layer of tank 1 and both upper and bottom layers of tank 2) for different numbers of layers. Figure 2-15 aggregates these errors across all measurement points, showing the total error for each layer configuration in both tanks. The minimum error point, marked in red, indicates the combination of 2 layers in Tank 1 and 4 layers in Tank 2.

Our analysis revealed that a model with 2 layers in Tank 1 and 4 layers in Tank 2 yielded the most accurate results. This finding challenged the conventional belief that more layers would inherently enhance model precision. One potential explanation for this outcome could be the discrepancy between the actual and modeled sensor positions. We initially assumed sensor placement at the top layer of the first tank and at both the top and bottom layers of the second tank. However, an excessive number of layers might lead to a significant deviation

of the modeled sensor positions from their actual locations. Additionally, the intrinsic heat transfer dynamics within the tanks could contribute to this finding. An increase in the number of layers might elongate the heat flow pathway, resulting in more diffusion and mixing within the tank, which could inadvertently influence the accuracy of our modeling. Moreover, a more segmented model might amplify minor inaccuracies in the model's assumptions or parameter estimations, increasing the overall error.

Therefore, based on our experimental results and analysis, we have adopted a model with 2 layers for Tank 1 and 4 layers for Tank 2. This configuration offers an effective balance between modeling accuracy and computational efficiency, making it the most suitable choice for our system. Our system with the stratified tank model is presented as shown in Figure 2-16. The corresponding tank symbol descriptions for these components are detailed in Table 2-3.

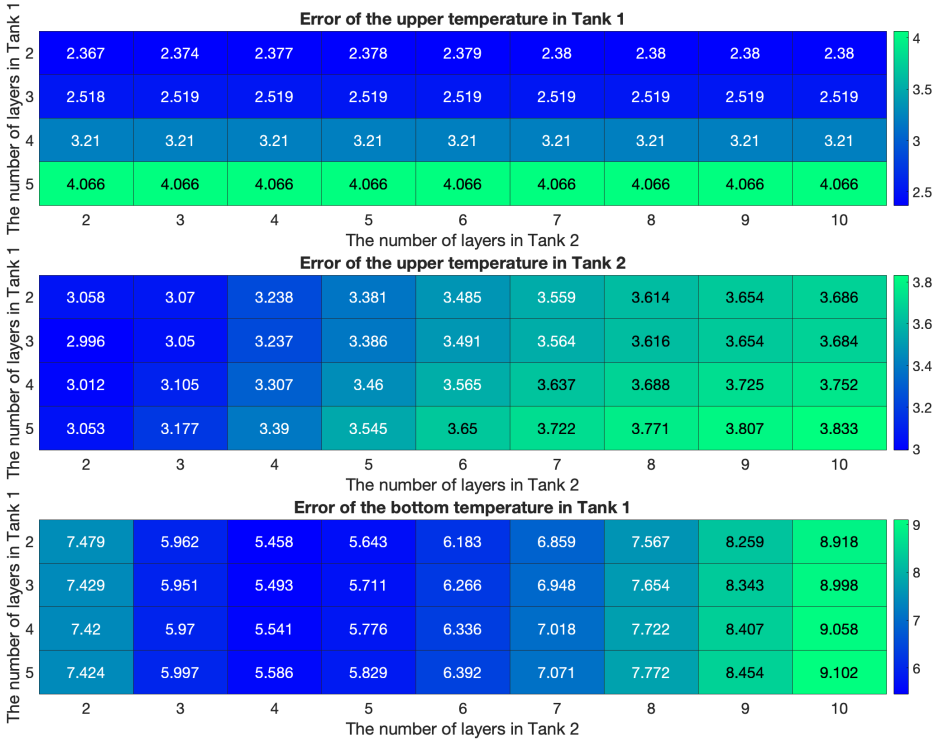

Figure 2-14: RMSE of temperatures with the different numbers of layers

Symbol	Description
T_1	The temperature of the 1st layer of the water tanks
T_2	The temperature of the 2nd layer of the water tanks
T_3	The temperature of the 3rd layer of the water tanks
T_4	The temperature of the 4th layer of the water tanks
T_5	The temperature of the 5th layer of the water tanks
T_6	The temperature of the 6th layer of the water tanks

Table 2-3: Tank symbol description

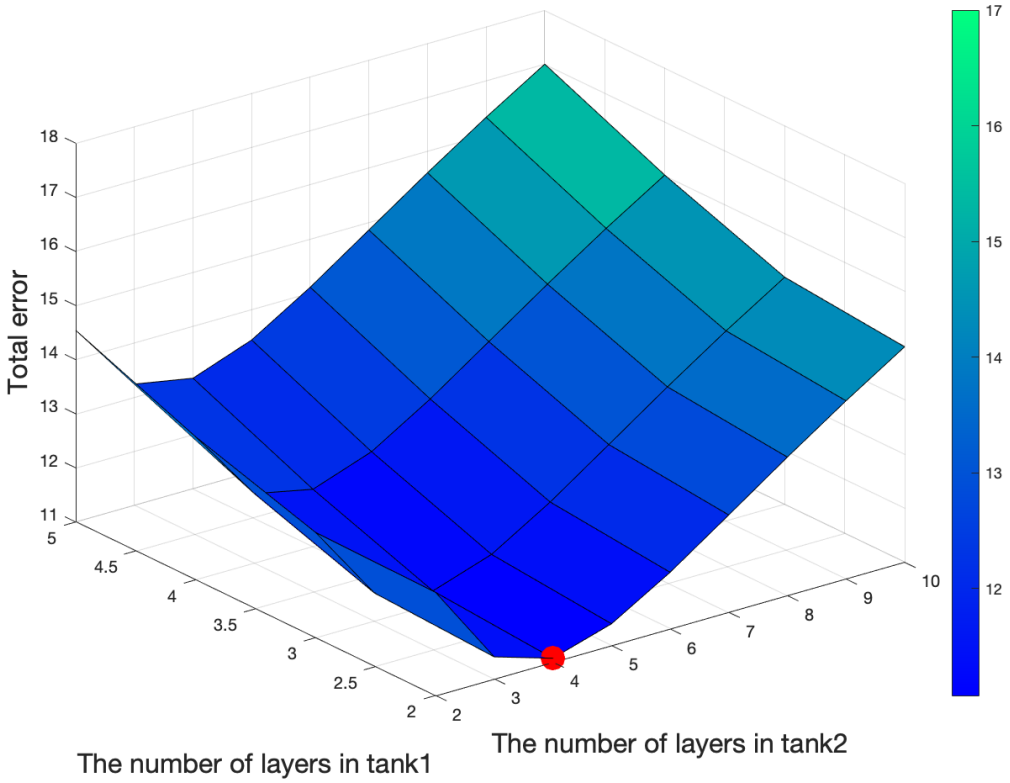

Figure 2-15: Total RMSE of temperatures with the different numbers of layers

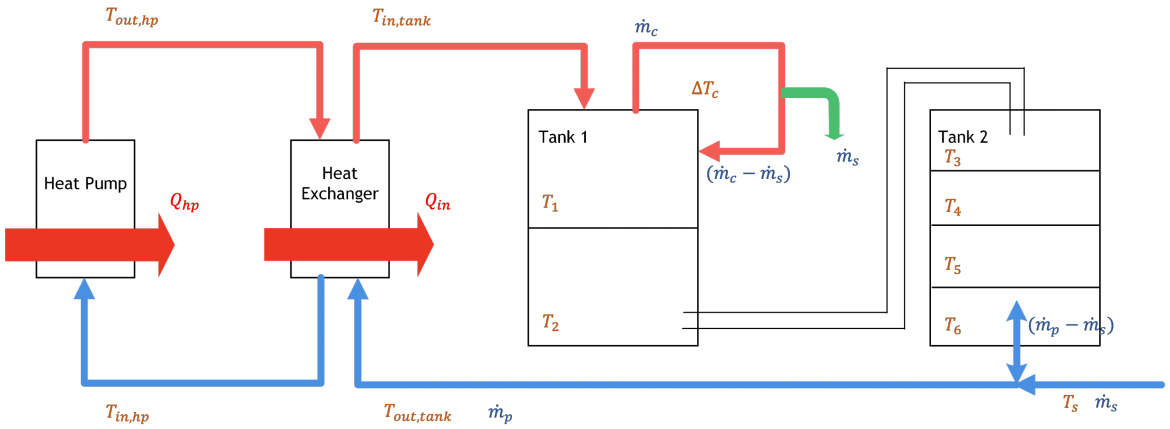

Figure 2-16: Diagram of the entire system with the stratified tank model

2-3-4 Entire System

Integrated System Modeling

Building upon the foundational elements established in Subsections 2-3-1 (Heat Pump), 2-3-2 (Heat Exchanger), and 2-3-3 (Thermal Energy Storage), we have synthesized these compo-

nents to develop a comprehensive model of our system. In this integrated model, various temperature variables are designated as state variables, forming the basis of our system dynamics. The structure of our state vectors is defined in Table 2-4.

State	Description	Units
x^1	The outlet water temperature of the heat pump $T_{out,hp}$	°C
x^2	The inlet water temperature of the heat pump $T_{in,hp}$	°C
x^3	The inlet water temperature of the tank $T_{in,tank}$	°C
x^4	The outlet water temperature of the tank $T_{out,tank}$	°C
x^5	The temperature of the 1st layer of the water tanks T_1	°C
x^6	The temperature of the 2nd layer of the water tanks T_2	°C
x^7	The temperature of the 3rd layer of the water tanks T_3	°C
x^8	The temperature of the 4th layer of the water tanks T_4	°C
x^9	The temperature of the 5th layer of the water tanks T_5	°C
x^{10}	The temperature of the 6th layer of the water tanks T_6	°C

Table 2-4: State description

For the integrated system, we have Eq. (2-11). Eq. (2-11a), Eq. (2-11b), Eq. (2-11c) and Eq. (2-11d) are the equations of the heat pump system segment. It is notable that x_1, x_2, x_3 exhibit dual-model behavior based on the control variable u, which corresponds to the operational status of the heat pump (either active or inactive). When the heat pump is operational, the pipeline dynamics are primarily influenced by its output. In contrast, during the dormant phase of the heat pump, passive heat dissipation is the dominant factor. The variable x_4 represents the outlet water temperature of the tank. Given the lack of a corresponding temperature sensor, direct temperature data cannot be used for identifying thermal dynamic parameters related to x_4. Therefore, we use the bottom layer temperature of the second tank x_{10} and the supply water temperature T_s to estimate the outlet water temperature of the tank x_4.

Eq. (2-11e), Eq. (2-11f), Eq. (2-11g), Eq. (2-11h), Eq. (2-11i) and Eq. (2-11j) are adopted for the thermal energy storage system part. These equations are derived from a stratified tank model, in which the first and second tanks are divided into two and four layers, respectively. Each layer functions as an individual node with its specific temperature state. For future references within this thesis, this integrated model Eq. (2-11) is formally designated as **Model 1**. The detailed symbol description is shown in Table A-1.

$$x_{k+1}^1 = \left(x_k^2 + \frac{Q_{hp}}{m_{\dot{p}} c_p}\right) u_k + \left(x_k^1 - \frac{\left(R_{\text{pipe1}}(x_k^1 - T_k^{\text{amb}}) + R_{\text{pipes}}(x_k^1 - x_k^2)\right) \cdot dk}{m_{\text{pipe1}} c_p}\right)(1 - u_k) \tag{2-11a}$$

$$x_{k+1}^2 = \left(x_{k+1}^4 + \Delta T_{he}\right) u_k + \left(x_k^2 - \frac{\left(R_{\text{pipe2}}(x_k^2 - T_k^{\text{amb}}) + R_{\text{pipes}}(x_k^2 - x_k^1)\right) \cdot dk}{m_{\text{pipe2}} c_p}\right)(1 - u_k) \tag{2-11b}$$

$$\begin{aligned} x_{k+1}^3 = &\left(x_{k+1}^1 - \Delta T_{he}\right) u_k + \left(x_k^3 - \frac{\left(R_{\text{pipe3}}(x_k^3 - T_k^{\text{amb}})\right) \cdot dk}{m_{\text{pipe3}} c_p}\right)(1 - u_k) \\ &- \left(\frac{\left(R_{\text{pipe,upper}}(x_k^3 - x_k^5) + R_{\text{pipe,bottom}}(x_k^3 - x_k^{10})\right) \cdot dk}{m_{\text{pipe3}} c_p}\right)(1 - u_k) \end{aligned} \tag{2-11c}$$

$$x_{k+1}^4 = T_{\text{s}} \frac{\dot{m}_s}{\dot{m}_p} + x_k^{10}\left(1 - \frac{\dot{m}_s}{\dot{m}_p}\right) \tag{2-11d}$$

$$x_{k+1}^5 = x_k^5 + \frac{\dot{m}_p c_p \left(x_k^3 - x_k^5\right) u_k - (\dot{m}_c - \dot{m}_s) c_p \triangle T_c - R_{12}(x_k^5 - x_k^6) + \dot{m}_s c_p (x_k^6 - x_k^5)(1 - u_k)}{m_1 c_p} dk \tag{2-11e}$$

$$x_{k+1}^6 = x_k^6 + \frac{(\dot{m}_p - \dot{m}_s) c_p \left(x_k^5 - x_k^6\right) u_k + R_{12}(x_k^5 - x_k^6) - R_{23}(x_k^6 - x_k^7) + \dot{m}_s c_p (x_k^7 - x_k^6)(1 - u_k)}{m_2 c_p} dk \tag{2-11f}$$

$$x_{k+1}^7 = x_k^7 + \frac{(\dot{m}_p - \dot{m}_s) c_p \left(x_k^6 - x_k^7\right) u_k + R_{23}(x_k^6 - x_k^7) - R_{34}(x_k^7 - x_k^8) + \dot{m}_s c_p (x_k^8 - x_k^7)(1 - u_k)}{m_3 c_p} dk \tag{2-11g}$$

$$x_{k+1}^8 = x_k^8 + \frac{(\dot{m}_p - \dot{m}_s) c_p \left(x_k^7 - x_k^8\right) u_k + R_{34}(x_k^7 - x_k^8) - R_{45}(x_k^8 - x_k^9) + \dot{m}_s c_p (x_k^9 - x_k^8)(1 - u_k)}{m_4 c_p} dk \tag{2-11h}$$

$$x_{k+1}^9 = x_k^9 + \frac{(\dot{m}_p - \dot{m}_s) c_p \left(x_k^8 - x_k^9\right) u_k + R_{45}(x_k^8 - x_k^9) - R_{56}(x_k^9 - x_k^{10}) + \dot{m}_s c_p (x_k^{10} - x_k^9)(1 - u_k)}{m_5 c_p} dk \tag{2-11i}$$

$$x_{k+1}^{10} = x_k^{10} + \frac{(\dot{m}_p - \dot{m}_s) c_p \left(x_k^9 - x_k^{10}\right) u_k + R_{56}(x_k^9 - x_k^{10}) + \dot{m}_s c_p (T_s - x_k^{10})(1 - u_k)}{m_6 c_p} dk \tag{2-11j}$$

Model Adjustment for Improved Prediction Performance

In addition to our initial model, **Model 1**, we have proposed further optimizations based on data analysis.

- Addressing Temperature Drop in the Upper Layer of the Tank

  An analysis of historical data revealed a notable temperature drop in the upper layer of the tank following the heat pump's deactivation. This phenomenon occurs because, after shutdown, the water pump in the pipeline circuit remains active for about 5 minutes, leading to increased heat loss. Figure 2-17 depicts this behavior, with the blue line indicating the heat pump's on/off status and the black line representing the Figure 2-17 temperature of Tank 1 .

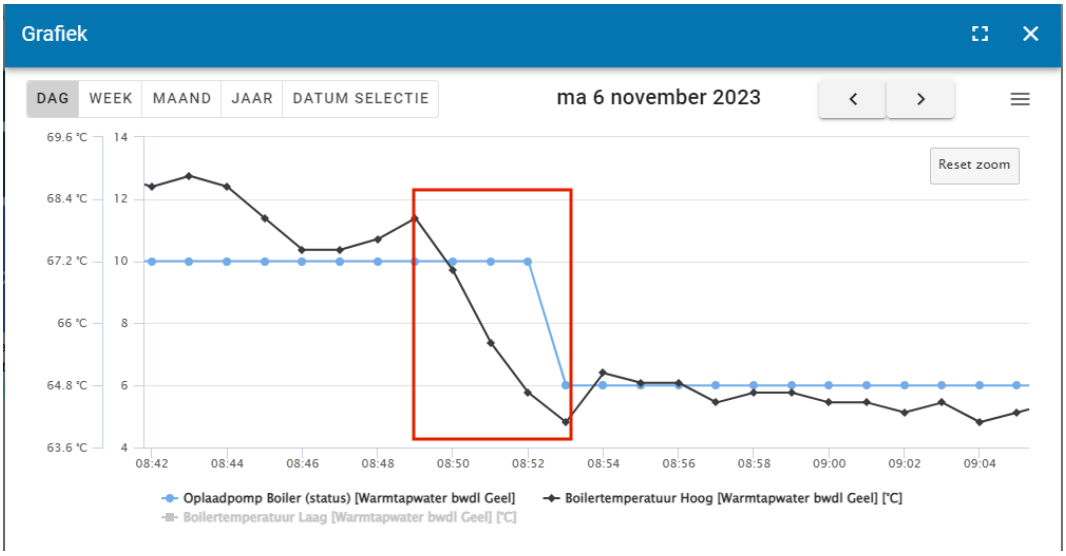

Figure 2-17: Temperature drop after the shutdown of the heat pump

To better represent this observed behavior, we propose adding a compensatory term to the existing equation for the upper layer temperature of the tank. The compensatory term is as follows.

$$\Delta T_{off} \cdot (u_k - u_{k-1}) \cdot u_{k-1} \tag{2-12}$$

Here, ΔT_{off} represents the observed temperature drop, which we set as 2.5°C in our model. This refinement aims to improve the model's accuracy in reflecting the temperature dynamics of the tank's upper layer.

- Refining the Heat Pump System Model

  When examining the temperature data of the pipes in the heat pump system, we noticed that the temperature tends to fluctuate rapidly and significantly, as shown in Figure 2-18. It would pose challenges in accurately tracking the temperature state variables. With a sampling time of 5 minutes, these swift changes are difficult to capture. To overcome this, we considered simplifying the model by reducing the number of state

variables related to the temperatures of the heat pump pipes. Figure 2-19 shows the revised schematic of the heat pump system.

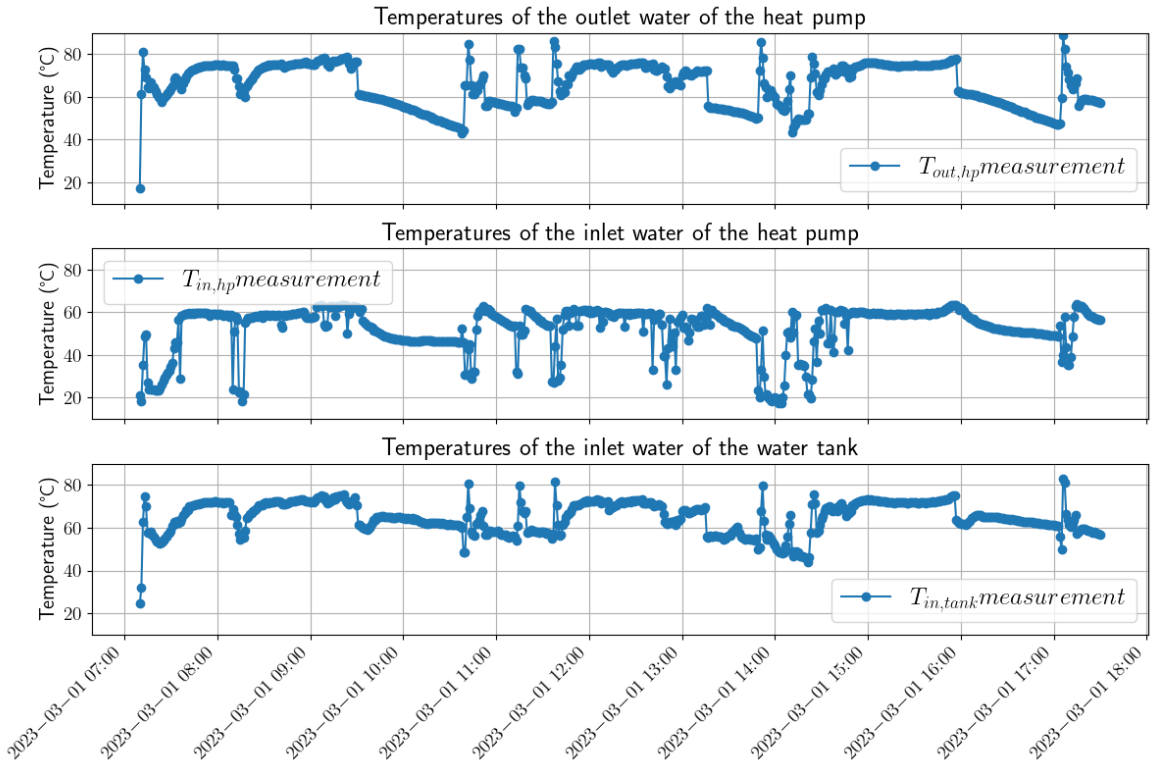

Figure 2-18: Temperatures of pipes on March 1, 2023

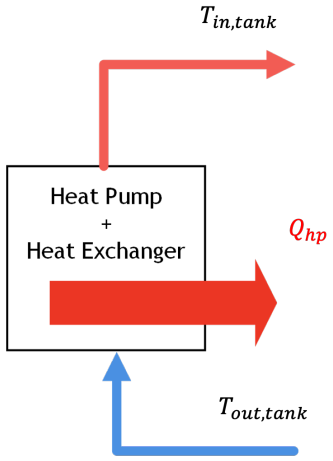

Figure 2-19: New heat pump schematic diagram

The original COP equation, which was dependent on the inlet water temperature of the heat pump $T_{in,hp}$ and ambient air temperature T_{amb}, is shown in Eq. (2-7). Based on our earlier findings regarding the heat exchanger, we noted a temperature difference ΔT_{he} between the inlet water temperature of the heat pump $T_{in,hp}$ and the outlet water

temperature of the tank $T_{out,tank}$. Consequently, the revised COP equation is as follows:

$$COP = a_1 + a_2 \cdot (T_{out,tank} - \Delta T_{he}) + a_3 \cdot T_{amb} + a_4 \cdot (T_{out,tank} - \Delta T_{he}) \cdot T_{amb} \quad (2\text{-}13)$$

The enhancements incorporated in this model lead us to formally designate it as **Model 2**. The equations and symbol description are shown in Eq. (A-1) and Table A-2 respectively. Similar to **Model 1**, **Model 2** will be referred to consistently throughout the thesis for ease of reference and coherence in discussion.

Interpolation Estimation for Water Consumption

To facilitate a comprehensive understanding of water consumption patterns, our model is configured to sample data every 5 minutes. This granularity is crucial for identifying short-term fluctuations in water usage, which are not captured by hourly data. To bridge this gap, we perform an interpolation estimation, as exemplified by the data from March 1, 2023, depicted in Figure 2-20.

This figure illustrates the results of our spline interpolation method applied to hourly average data. We considered a data offset, shifting the hourly values to the midpoint of each hour. This adjustment is based on the rationale that the recorded hourly averages are more likely to occur around the middle rather than the endpoints. As such, the original hourly data, shown by the solid blue line, is adjusted to align with these midpoints. The dotted orange line then represents the interpolated data, providing a visual estimate of the water consumption trends at 5-minute intervals throughout the day.

By adjusting the original data points to the hourly midpoints before interpolation, we enhance the model's ability to reflect the true water consumption within each hour. While this method could improve the accuracy of our 5-minute interval estimates, it is important to note that it still does not capture the exact peak moments of water consumption within each hour. This limitation is a significant factor that can influence the model's accuracy and effectiveness in real-time applications.

Identification and Validation

The process of model identification involved the selection of data spanning ten days (five days each in March and October 2023). This step was crucial for initial model tuning. Subsequently, we embarked on a comprehensive validation phase, utilizing data from the entire months of March and August 2023. The data for this phase was sampled at intervals of 5 minutes.

Figure 2-21 illustrates the simulation results for a specific day from the training dataset, providing a visual representation of the performance of the model during the identification stage. Table 2-5 presents detailed outcomes of this process, quantifying the accuracy and efficiency of the model.

In a similar vein, for the identification of the enhanced **Model 2**, we selected data from the same periods in March and October 2023. This selection was instrumental in refining and

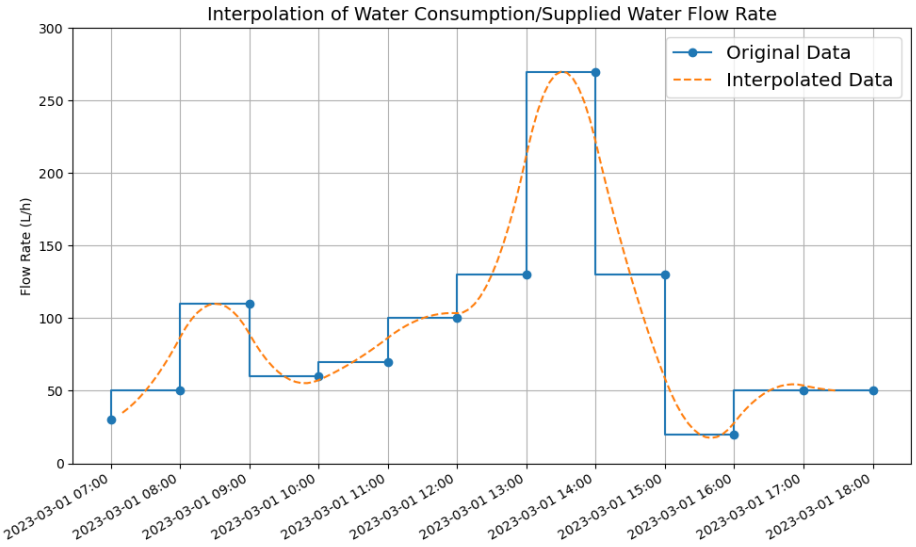

Figure 2-20: Interpolation result of the flow rate of supplied water on March 1, 2023

validating the improvements implemented in the model. To assert the robustness of these enhancements, a thorough validation was conducted using extensive datasets from the whole months of March and August 2023.

Figure 2-22 displays the simulation results for a day within the training dataset, showcasing the refined model's performance post-improvement. Furthermore, Table 2-6 outlines the results from the model identification process, offering quantitative evidence of the improvements' impact on the model's precision.

Temperature of upper layer of tank 1 T_1	Training Set (10 days)	Testing Set 1 (March: 23 days)	Testing Set 2 (August: 23 days)
Root Mean Square Error (RMSE)	4.22°C	4.10°C	5.84°C
Mean Absolute Percentage Error (MAPE)	5.06%	4.94%	5.84%

Table 2-5: Model Validation with Model 1

Temperature of upper layer of tank 1 T_1	Training Set (10 days)	Testing Set 1 (March: 23 days)	Testing Set 2 (August: 23 days)
Root Mean Square Error (RMSE)	3.98°C	3.48°C	4.58°C
Mean Absolute Percentage Error (MAPE)	4.82%	4.31%	5.90%

Table 2-6: Model Validation with Model 2

Table 2-7 offers a clear comparison between the two models across various datasets. We use the RMSE of the temperature variable T_1 as a benchmark for this comparison. As shown

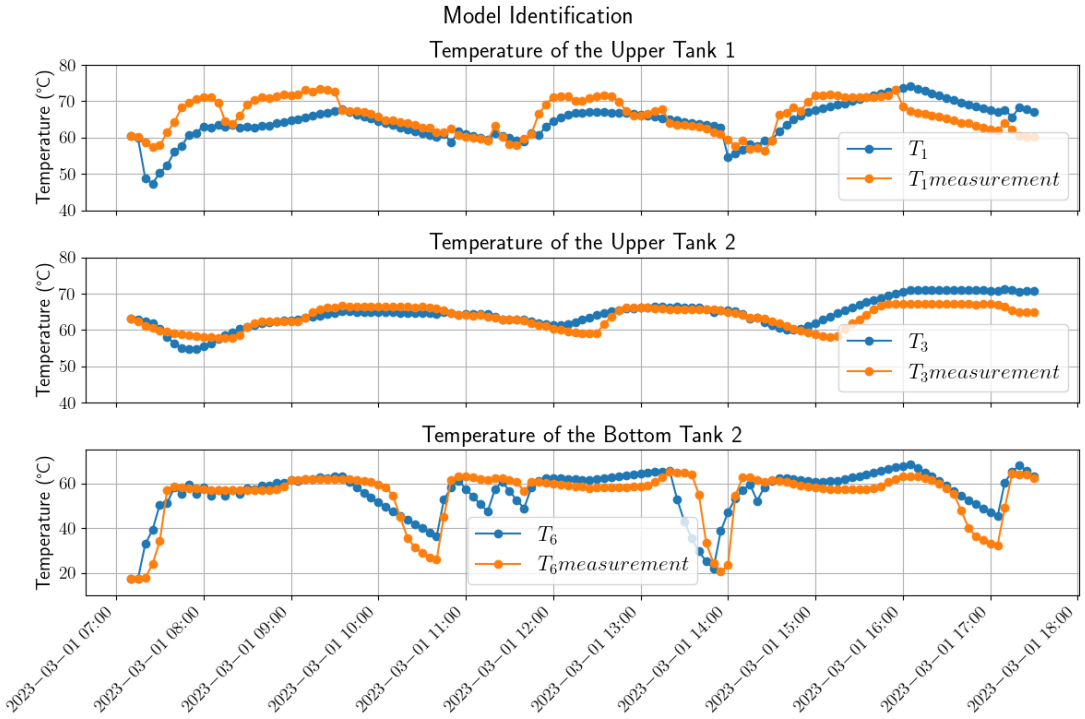

Figure 2-21: Identification result of Model 1 on March 1, 2023

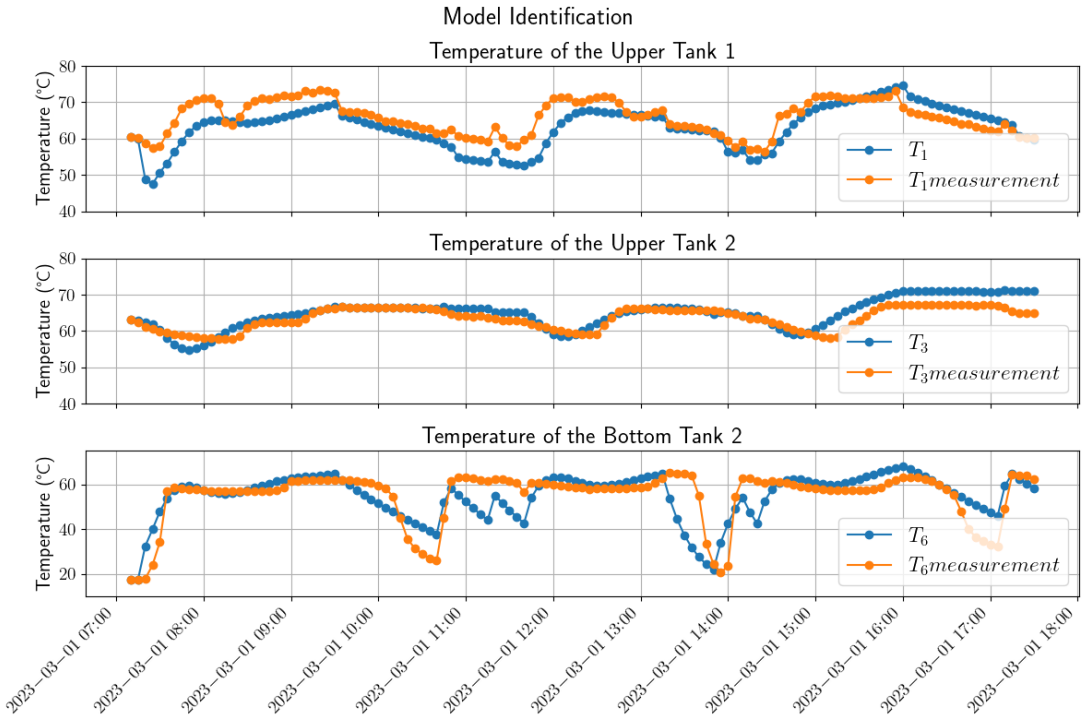

Figure 2-22: Identification result of Model 2 on March 1, 2023

in Table 2-7, **Model 2** consistently demonstrates lower RMSE values compared to **Model 1** across all test sets. This decrease in RMSE with **Model 2** signifies not just enhanced model precision, but it also opens doors for more effective applications in environments where accurate temperature control and prediction are crucial.

Furthermore, a notable advantage of **Model 2** lies in its reduced complexity, thanks to fewer variables. This simplification is expected to lead to considerable benefits in computation time, particularly during the Model Predictive Control (MPC) design phase. The diminished computational demands of **Model 2** are anticipated to not only streamline processes but also significantly boost overall efficiency, which is paramount in practical applications.

In Section 3-6-1, we will delve deeper into the implications of these improvements on MPC design. This exploration will cover aspects of computation efficiency and practical usability, offering a comprehensive understanding of how the advancements in **Model 2** can be effectively translated into real-world scenarios.

RMSE of T_1	Training Set (12 days)	Testing Set 1 (March: 23 days)	Testing Set 2 (August: 23 days)
Model 1	4.22°C (100%)	4.35°C (100%)	6.76°C (100%)
Model 2	3.98°C (94.31%)	3.48°C (80.00%)	4.58°C (67.75%)

Table 2-7: Comparison between Model 1 and Model 2

2-4 Prediction of Hot Water Consumption

2-4-1 Data Analysis

Before designing water consumption prediction models, it is imperative to gain a deep understanding of our dataset. The inherent patterns within the data can greatly influence the model's performance. A fundamental goal of this data analysis is to uncover latent patterns or trends in water consumption data, which are essential for informed decision-making. Recognizing these patterns not only informs our choice of modeling approach but also highlights potential challenges, especially in the context of the data limitations previously discussed.

Our analysis utilizes data from week 50 of 2022 (Dec 12-18, 2022), offering a detailed view of consumption patterns. As illustrated in Figure 2-23, comparing water consumption with heat demand Q_{dem} reveals parallel patterns, underscoring the relevance of heat consumption as a pivotal metric in our model.

In an effort to uncover deeper insights and identify recurring consumption patterns, we examined heatmaps for water two specific weeks: week 50 of 2022 (Dec 12-18, 2022) and week 12 of 2023 (Mar 20-26, 2023), as depicted in Figure 2-24 and Figure 2-25. The data reveals a distinct periodicity in water consumption, with notable consumption peaks around 15:00.

Identifying these clear patterns in water and heat consumption is instrumental in laying the groundwork for implementing forecasting models. In our subsequent analyses, we opt

for the Seasonal Autoregressive Integrated Moving Average (SARIMA) model, owing to its effectiveness in capturing the seasonal variations in data patterns. The choice of SARIMA over more complex deep learning approaches is driven by the nature of our available data. We primarily rely on historical water consumption data, which is a single-dimensional dataset, without access to potentially influential variables such as the number of individuals arriving at the office building on a particular day. These variables can be potent determinants of water consumption, yet their absence makes deep learning models, which excel in multi-dimensional and complex data scenarios, less suitable for our context. Hence, SARIMA, with its capability to model univariate time series data with seasonal components, emerges as the more appropriate choice for our analysis.

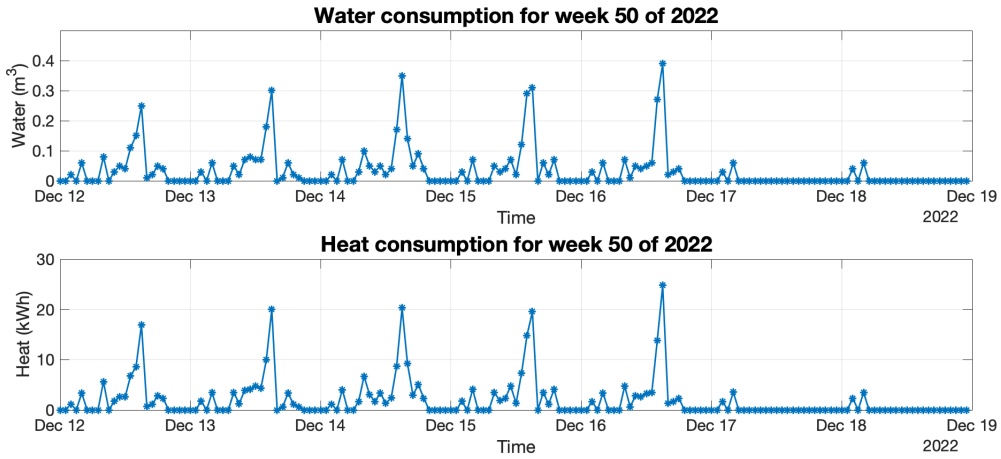

Figure 2-23: Water consumption and heat consumption in week 50 of 2022

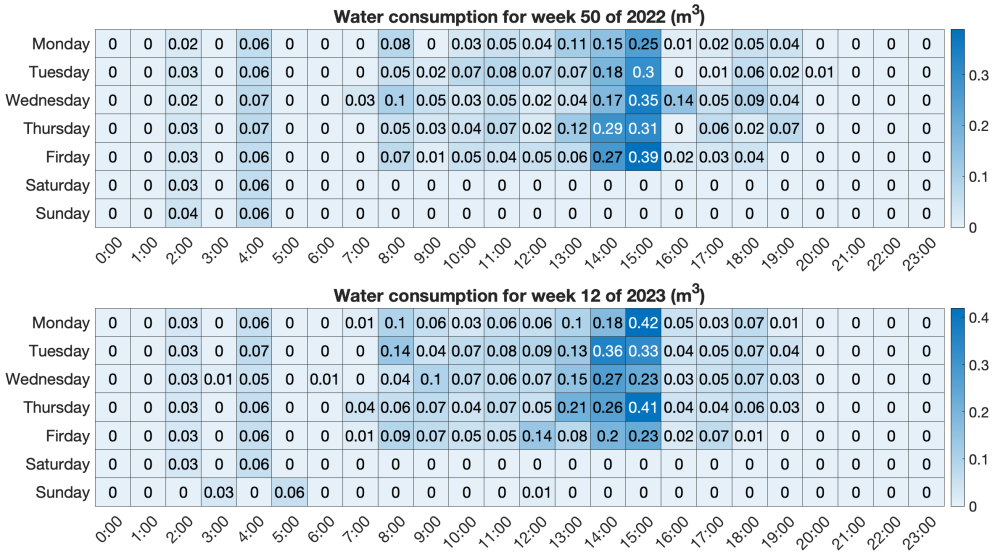

Figure 2-24: Heat map for water consumption in week 50 of 2022 and week 12 of 2023

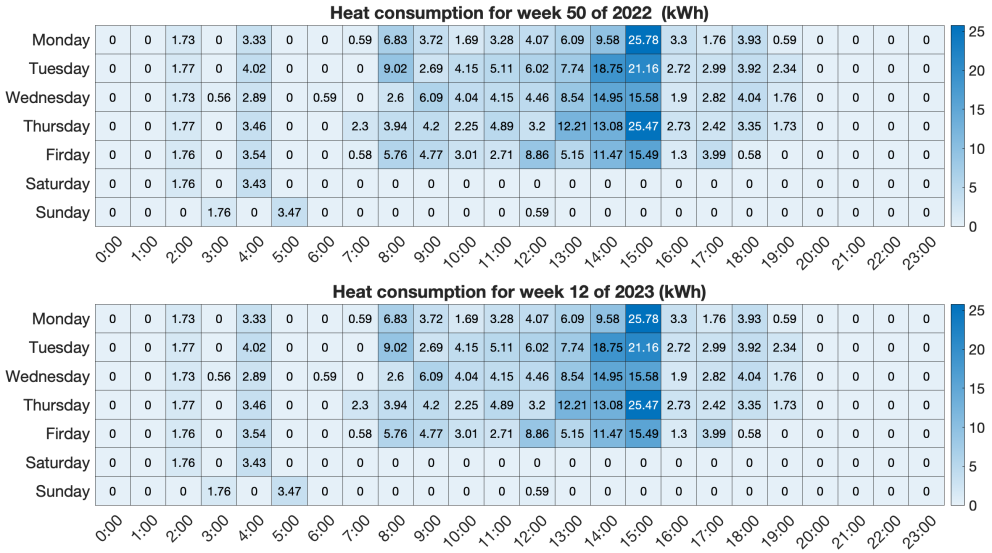

Figure 2-25: Heat map for heat consumption in week 50 of 2022 and week 12 of 2023

2-4-2 Prediction Model Development

Seasonal Autoregressive Integrated Moving Average (SARIMA)

SARIMA model represents an advancement in forecasting methodology, extending the Autoregressive Integrated Moving Average (ARIMA) framework to adeptly handle seasonality in time series data. SARIMA is particularly effective for datasets exhibiting seasonal patterns, as it intricately blends components of seasonality, trend, and noise [9].

Typically, SARIMA models are typically denoted as SARIMA(p, d, q)(P, D, Q)s, where:

- p and P represent the order of the non-seasonal and seasonal Autoregressive (AR) terms, respectively.
- d and D denote the order of non-seasonal and seasonal differencing.
- q and Q indicate the order of the non-seasonal and seasonal Moving Average (MA) terms.
- s is the seasonality period of the time series

The mathematical representation of a SARIMA model is:

$$\begin{aligned} Y_t =& c + \phi_1 Y_{t-1} + \cdots + \phi_p Y_{t-p} + \Phi_1 Y_{t-P} + \cdots + \Phi_P Y_{t-PS} \\ & - \theta_1 \varepsilon_{t-1} - \cdots - \theta_q \varepsilon_{t-q} - \Theta_1 \varepsilon_{t-Q} - \cdots - \Theta_Q \varepsilon_{t-QS} + \varepsilon_t \end{aligned} \tag{2-14}$$

where:

- Y_t is the time series.

- c is a constant.
- ϕ and Φ_p are the coefficients for the non-seasonal and seasonal AR terms, respectively.
- θ and Θ are the coefficients for the non-seasonal and seasonal MA terms, respectively.
- ε_t is the error term at time t.

To elucidate the concept of seasonality within SARIMA models, we consider our hourly water consumption data. Figure 2-26 illustrates an example of how seasonality is captured in SARIMA. In the context of daily seasonality, where $s = 24$, each segment corresponds to an hour of the day, and the model uses data from the same hour in previous days (e.g., Y_{t-24},$Y_{t-24\times2}$,...) to predict the current or upcoming hour (Y_t). This daily cycle assumes that patterns repeat every 24 hours, a common scenario in water consumption behaviors. Additionally, the model can capture weekly seasonality by setting $s = 24 \times 7$, which extends the pattern recognition over a seven-day cycle. In this case, the model uses data from the same hour on the corresponding day of previous weeks (e.g., $Y_{t-24\times7}$,$Y_{t-24\times7\times2}$,...) to forecast the water consumption for that hour on the current or upcoming week. This approach is particularly useful for capturing behaviors that repeat on a weekly basis, such as increased water usage on certain days of the week.

The SARIMA model's ability to incorporate both non-seasonal and seasonal elements makes it a robust tool for forecasting in contexts where these patterns are prominent. Its flexibility in handling different orders of autoregressive and moving average components allows for fine-tuned modeling of complex time series data.

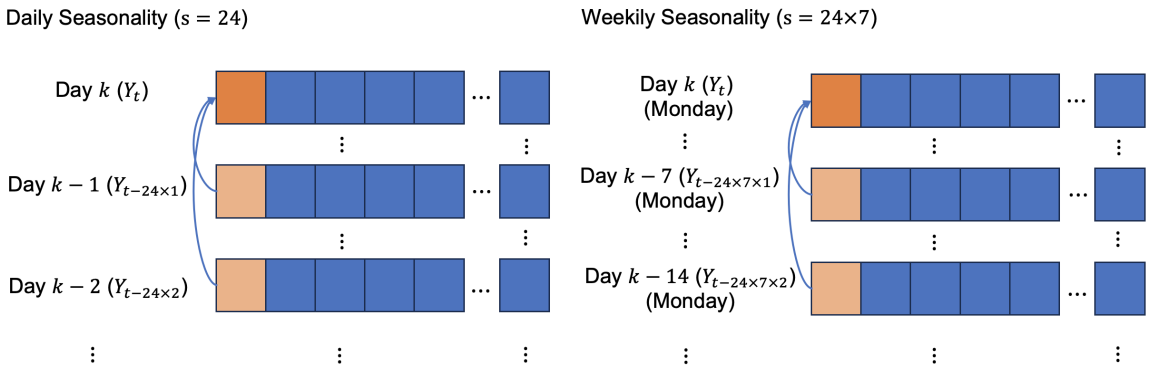

Figure 2-26: SARIMA with diffierent seasonality

Prediction Results

For model training, our dataset comprised water consumption data from January 9, 2023, to March 5, 2023, a period spanning 56 days. Figure 2-27 depicts the water usage during this period. Utilizing this training set, our objective was to predict the subsequent week's water consumption (March 6 to March 10, 2023). To reduce noise and improve the model's predictive accuracy, we limited our focus to data from working hours between 7 am and 6 pm on weekdays.

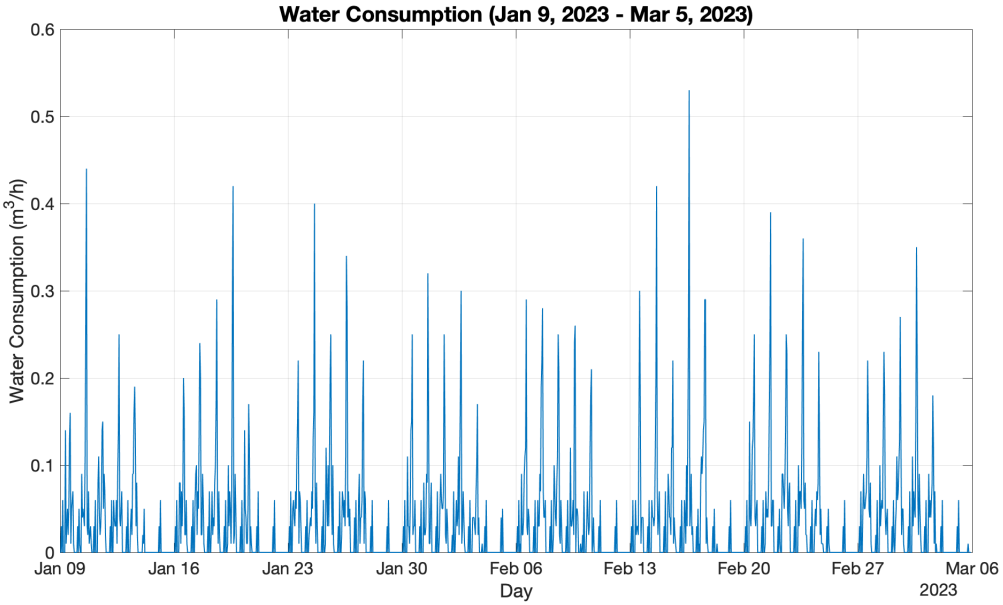

Figure 2-27: Water consumption from Jan 9, 2023 to Mar 5, 2023

The training of the models utilized MATLAB's ARIMA function from the Econometrics Toolbox. We crafted two distinct models to capture the inherent seasonality within our data: one with daily seasonality (Seasonality = 12 hours, due to focusing on half-day intervals) and another with weekly seasonality (Seasonality = 12×5 hours, accounting for the weekday working hours only). Additionally, we explored a combined SARIMA model $Y_{combine}$ that considers both daily SARIMA model Y_{daily} and weekly SARIMA model Y_{weekly}. The combined model was constructed using the following formulation:

$$Y_{combine} = \alpha Y_{weekly} + (1 - \alpha) Y_{daily} \tag{2-15}$$

Here, we have selected an α value of 0.8, giving more weight to the weekly component based on preliminary analyses suggesting a stronger weekly pattern.

The water consumption of the predictions using the weekly, daily, and combined SARIMA models are displayed in Figure 2-28, Figure 2-29, and Figure 2-30, respectively. The effectiveness of the SARIMA models in predicting water consumption is quantitatively summarized in Table 2-8. This table compares the performance of the weekly, daily, and combined SARIMA models over the prediction period from March 6 to March 10, 2023. From the RMSE values, we observe that the weekly and combined SARIMA models have an equal performance, with a lower error rate than the daily model. This suggests that the weekly model and the combined model are more precise in capturing the actual consumption patterns for this specific period. Furthermore, the VAF values corroborate this finding, with the combined SARIMA model marginally outperforming the weekly model, indicating that it can account for a slightly higher proportion of the variance in the observed data.

This analysis suggests that while daily seasonality is present, the weekly and combined models, which incorporate a broader temporal context, provide a more accurate and comprehensive

understanding of water consumption patterns. Additionally, combined models have slightly better performance than weekly models.

Mar 6-10, 2023	Weekly SARIMA	Daily SARIMA	Combined SARIMA
Root Mean Square Error (RMSE)	0.04 m^3/h	0.05 m^3/h	0.04 m^3/h
Variance Accounted For (VAF)	82.01%	72.99%	82.33%

Table 2-8: Water consumption SARIMA model performances

Similarly, the predictive efficacy of the SARIMA models regarding heat consumption is visually represented by the results displayed in Figure 2-31 for the weekly model, Figure 2-32 for the daily model, and Figure 2-33 for the combined model. These figures highlight the heat consumption forecasts across the specified period, allowing for a direct comparison of how each model variant aligns with the actual consumption trends. The summarized results of these predictions are concisely presented in Table 2-9.

Mar 6-10, 2023	Weekly SARIMA	Daily SARIMA	Combined SARIMA
Root Mean Square Error (RMSE)	2.34 kWh	2.97 kWh	2.33 kWh
Variance Accounted For (VAF)	84.09%	75.34%	84.37%

Table 2-9: Heat consumption SARIMA model performances

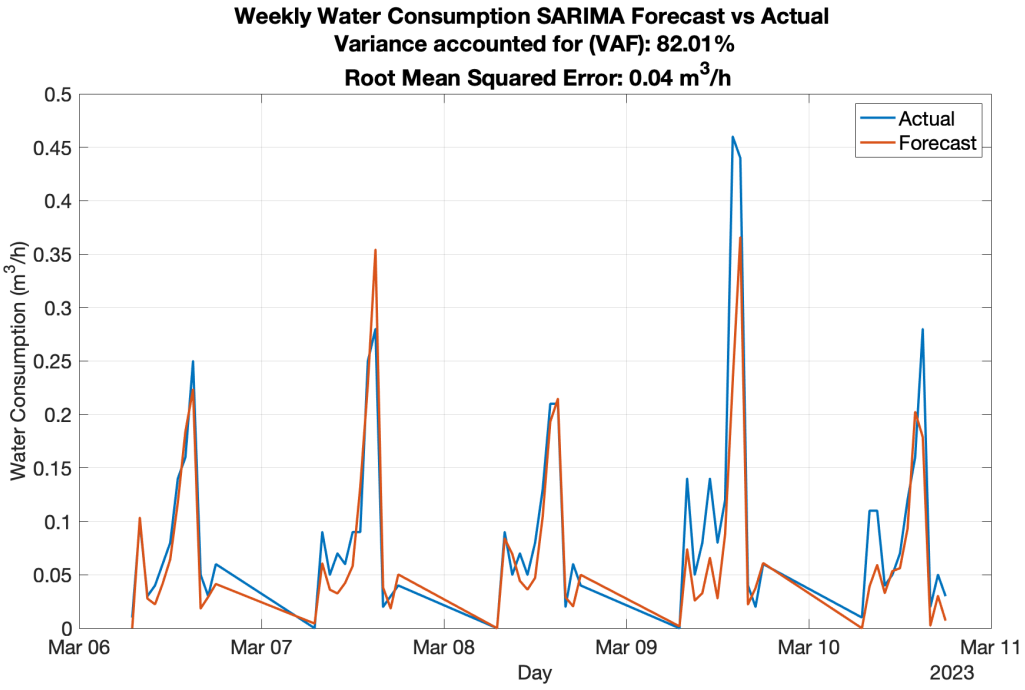

Figure 2-28: Water consumption weekly SARIMA forecast

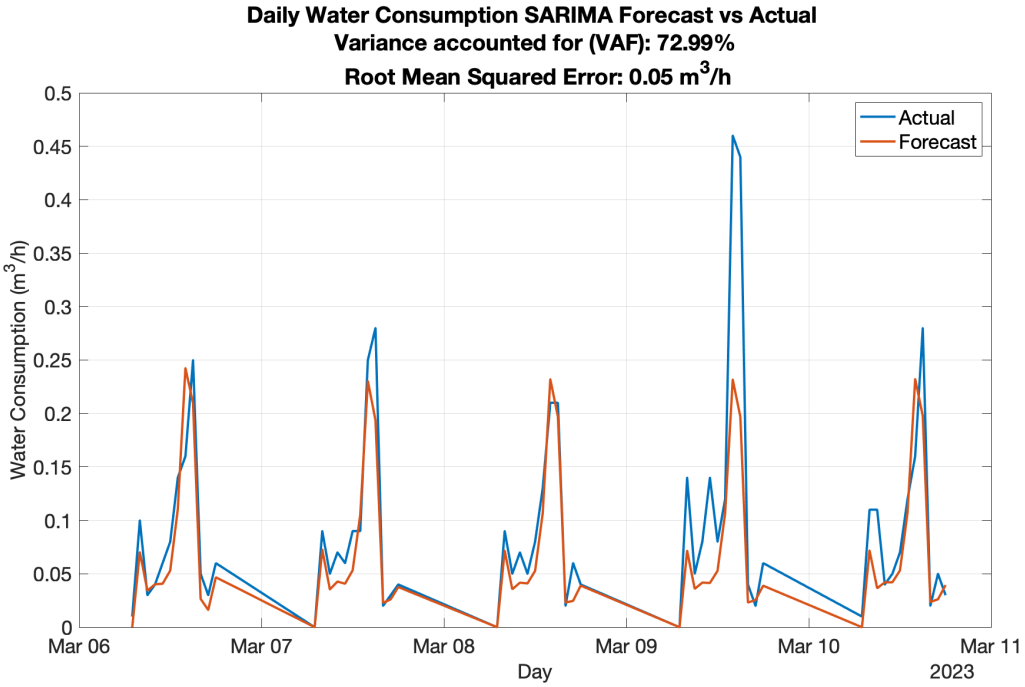

Figure 2-29: Water consumption daily SARIMA forecast

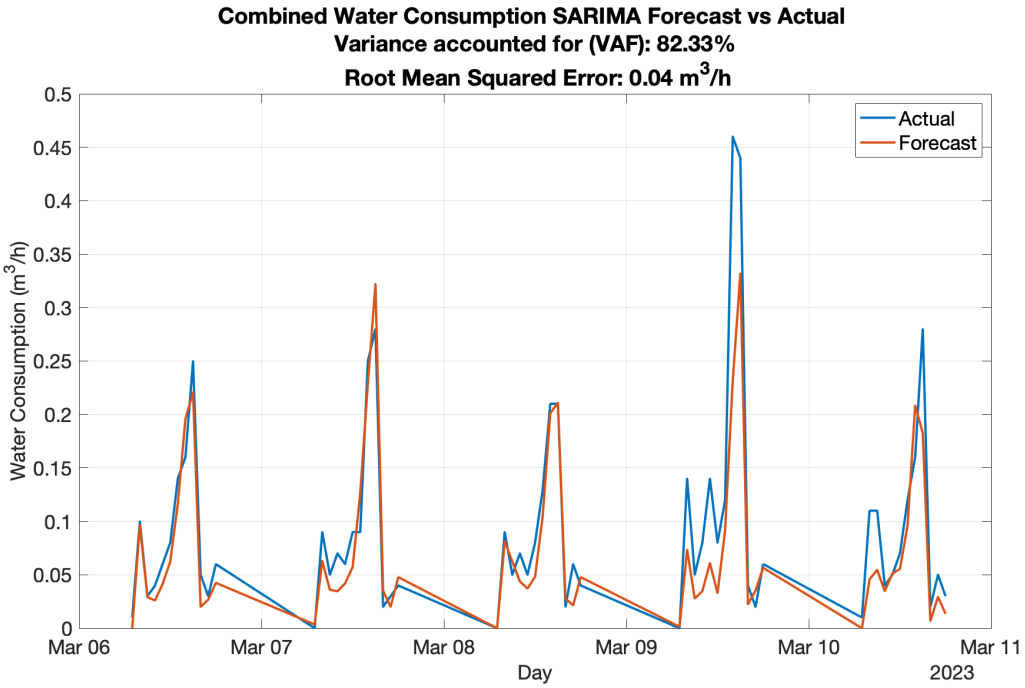

Figure 2-30: Water consumption combined SARIMA forecast

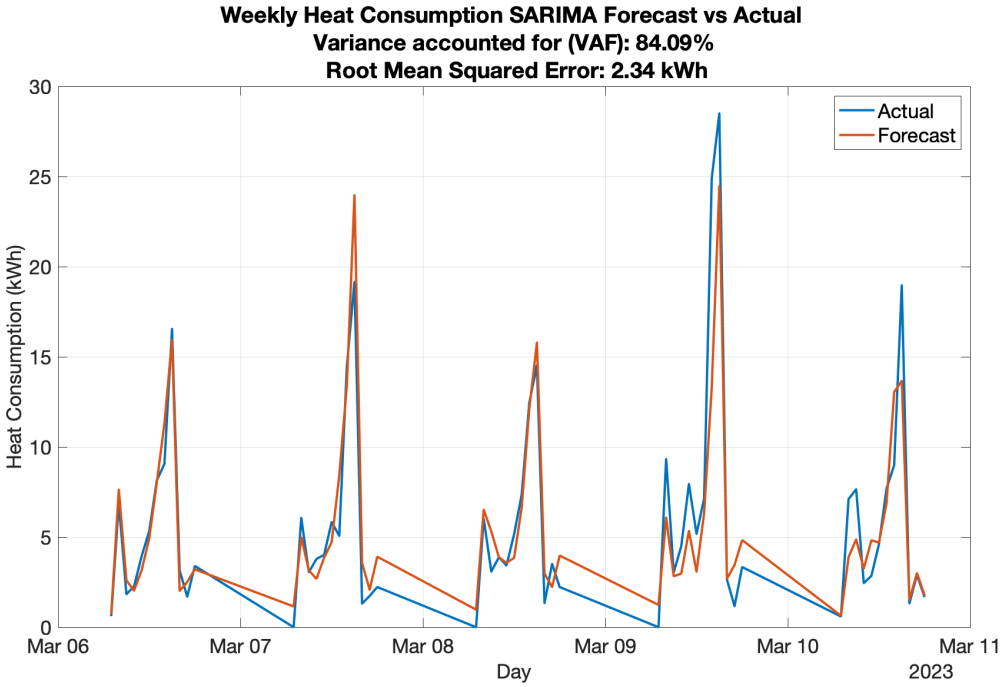

Figure 2-31: Heat consumption weekly SARIMA forecast

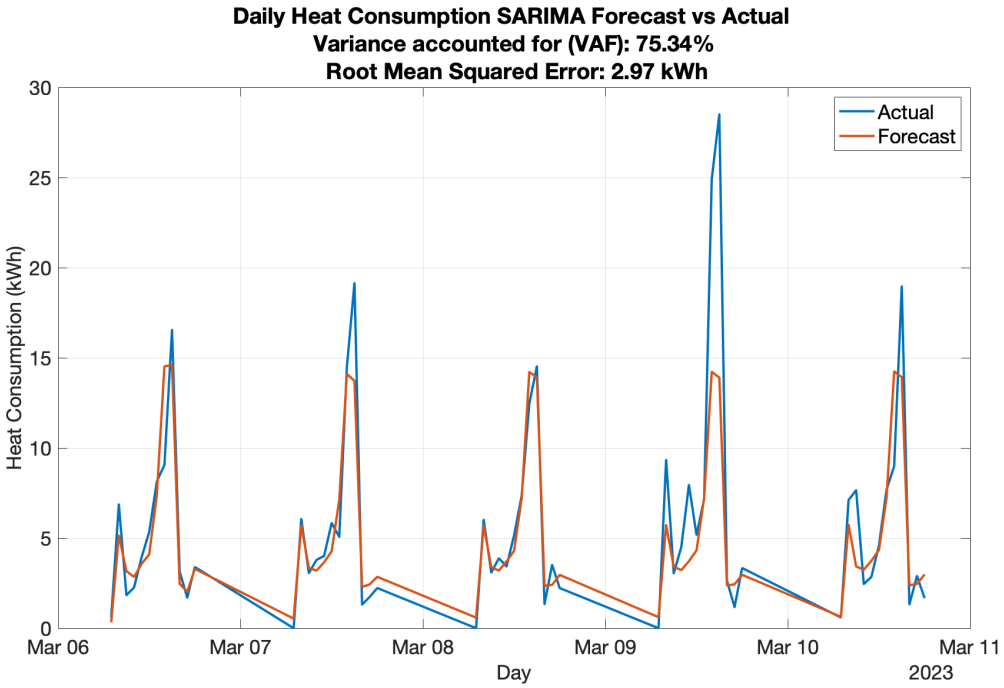

Figure 2-32: Heat consumption daily SARIMA forecast

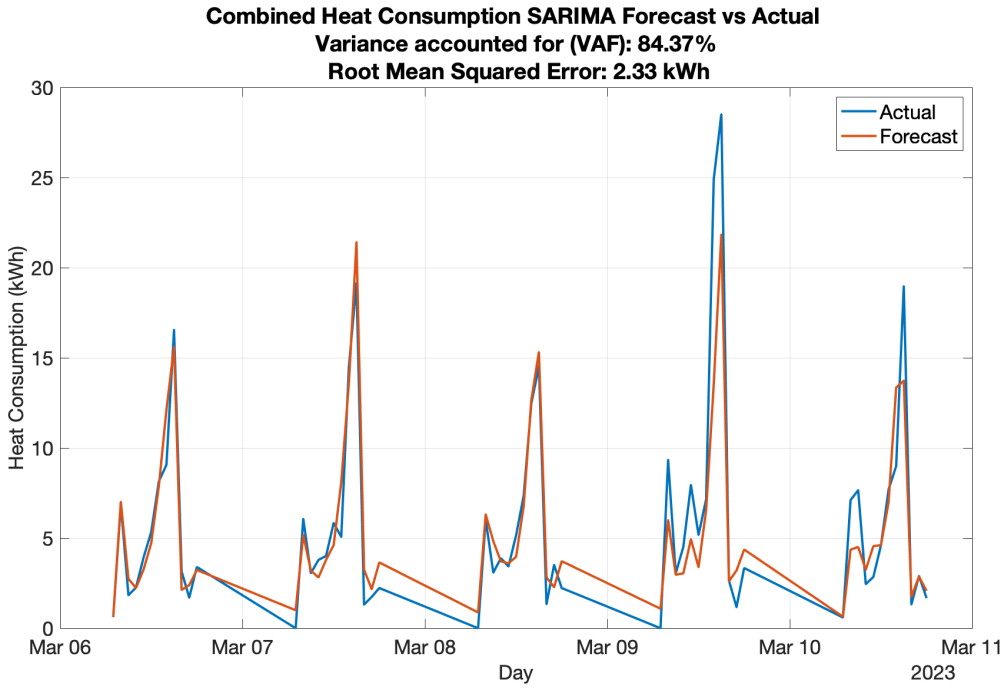

Figure 2-33: Heat consumption combined SARIMA forecast

Chapter 3

MPC for Economical Operation

This chapter focuses on the design and evaluation of control strategies specifically for a heat pump system with thermal storage tanks, employing Model Predictive Control (MPC) to achieve economical operation. It begins in Section 3-1 with a review of the original control strategy and its application in the operational heat pump system. Section 3-2 outlines the specific objectives aimed at enhancing the system's energy efficiency and responsiveness. Following this, the chapter introduces the MPC in Section 3-3, detailing its theoretical foundation and ability to predict future system behavior. Sections 3-4 and 3-5 delve into the configuration design and the techniques for computational feasibility and efficiency of the MPC, respectively. Finally, Sections 3-6 and 3-7 focus on demonstrating the results and analysis of simulations and real implementation tests. These tests not only validate the efficacy of the MPC strategy in reducing energy costs but also illustrate its feasibility in real-world operational environments. The findings of these analyses underscore the chapter's comprehensive study of control strategies, providing robust support and evidence for achieving an economically efficient control of heat pump systems.

3-1 Original Control Strategy

As is common with many existing heat pump systems, the control strategy currently employed in the HP system of the Kropman B.V. test buildings is rule-based control. The core of the strategy is based on temperature regulation within the water tanks, which directly influences the activation and deactivation of the heat pump. Specifically, the system activates the heat pump when the upper temperature in the first water tank exceeds a set point of 62°C. This set point is chosen to maintain the water tank's upper temperature mostly above 60°C, providing a 2°C temperature buffer. Conversely, the heat pump is deactivated when the lower temperature of the second water tank reaches the same set temperature of 62°C. However, while this buffer ensures a certain level of thermal stability, it can lead to thermal energy wastage and reduced efficiency, as the system often operates at a higher temperature than necessary.

This rule-based approach, while ensuring a basic level of thermal efficiency and stability, has limitations due to its simplicity. It does not account for dynamic hot water consumption and time-varying electricity prices, which are essential for optimizing the system's operation in terms of energy and cost efficiency. Additionally, the current strategy does not utilize demand forecasting and dynamic system predictions, which would allow the system to proactively respond to changes in demand and system conditions. These predictive elements, coupled with considerations of electricity pricing, could significantly improve the system's performance, making it more energy-efficient and cost-effective under varying conditions.

The limitations of this rule-based approach highlight the need for a more advanced control strategy, setting the stage for the exploration of MPC in the subsequent sections of this chapter.

3-2 Objectives of the Control Strategy

In this section, we outline the primary objectives that guide the development and implementation of our control strategy for the heat pump system with thermal energy tanks. These objectives are crucial in defining the direction of our research and the design of the control system. They include:

- **Reduction of Energy Usage:**

  The original control strategy of our system, which is rule-based, operates the heat pump solely based on the temperature readings of the water tanks. While straightforward, this approach lacks flexibility and can lead to unnecessary energy consumption. It operates in a rather reactive manner, initiating the heat pump's action based on the current state without considering future states and demands.

  Our aim is to transcend this limitation by adopting a more proactive control strategy. By anticipating future states and demands, we can achieve a more nuanced and flexible operation of the heat pump. This foresight allows us to optimize the system's energy use, reducing wastage and improving overall efficiency. The goal is to ensure that the heat pump is operational only when necessary, reducing its runtime during periods of low demand or when the storage has sufficient energy, thereby significantly cutting down on overall energy consumption.

- **Minimizing Energy Costs through Electricity Price Integration:**

  The previous control strategy of our heat pump system did not take into account the fluctuating costs of electricity, leading to potential inefficiencies in energy cost management. Without considering electricity pricing, the system could inadvertently operate more intensively during peak pricing periods, inadvertently increasing operational costs.

  To address this, we have revised our control strategy to incorporate electricity pricing, thereby aligning the operation of the heat pump with the dynamic electricity market. This integration allows the system to be more active during off-peak hours with lower electricity prices and conserve energy during peak hours when prices are high. This economically advanced approach optimizes operational costs without compromising efficiency or performance, making our system adaptively responsive to energy market fluctuations.

By focusing on these goals, we aim to develop a control strategy that is both responsive to immediate operational needs and adaptable to fluctuations in the energy price market.

3-3 Model Predictive Control

MPC represents an advanced control strategy that leverages a model of the system to predict future states and make informed control decisions [33]. This approach is highly effective for complex systems where future states are uncertain and require optimization over time [18]. MPC distinguishes itself by continuously solving an optimization problem at each control step, aiming to minimize a cost function over a set future prediction horizon while conforming to the constraints of the system [1]. The outcome of this optimization dictates the subsequent control actions.

In the context of our heat pump system, which operates on binary control actions denoted as $u_k \in \{0, 1\}$ to represent the on/off state, as detailed in Section 2-1-1, we apply a specialized variant of MPC known as Mixed-Integer Model Predictive Control (MI-MPC). This adaptation is necessary due to the binary nature of our control signals, on/off signals [26].

Figure 3-1 illustrates the MPC framework tailored for our system. At the core of the MPC is the Dynamic System Model, which receives inputs from two critical components: the States X_k of the system and the Predictive Demand $\hat{d}_k$. The States represent the real-time measurements of temperatures at various points in the system, such as tanks and pipes. The Predictive Demand is generated by the Demand Forecast module, which anticipates future water usage patterns. These inputs are fed into the Dynamic System Model to project the system's future states, denoted as Predictive States $\hat{X}_k$. The Optimizer then uses these projections to solve an optimization problem at each control step, determining the optimal Control Input u_k, which dictates the heat pump's on/off status. This input aims to minimize the cost function while ensuring that the operational constraints are satisfied. The Plant represents the physical real system, with the States X_k being influenced by both the Control Input u_k and the external Demand d_k. By continuously updating the system model with real-time data, the MPC framework can proactively adjust to changing conditions, ensuring efficient and stable operation of our system.

Problem Formulation

Following this schematic representation, the MI-MPC framework for our system treats the control inputs as mixed-integer variables within the optimization process. This necessitates tailored adjustments in both the objective function and the constraints to effectively incorporate these discrete control variables. The formulation of the MI-MPC problem for our system is as follows:

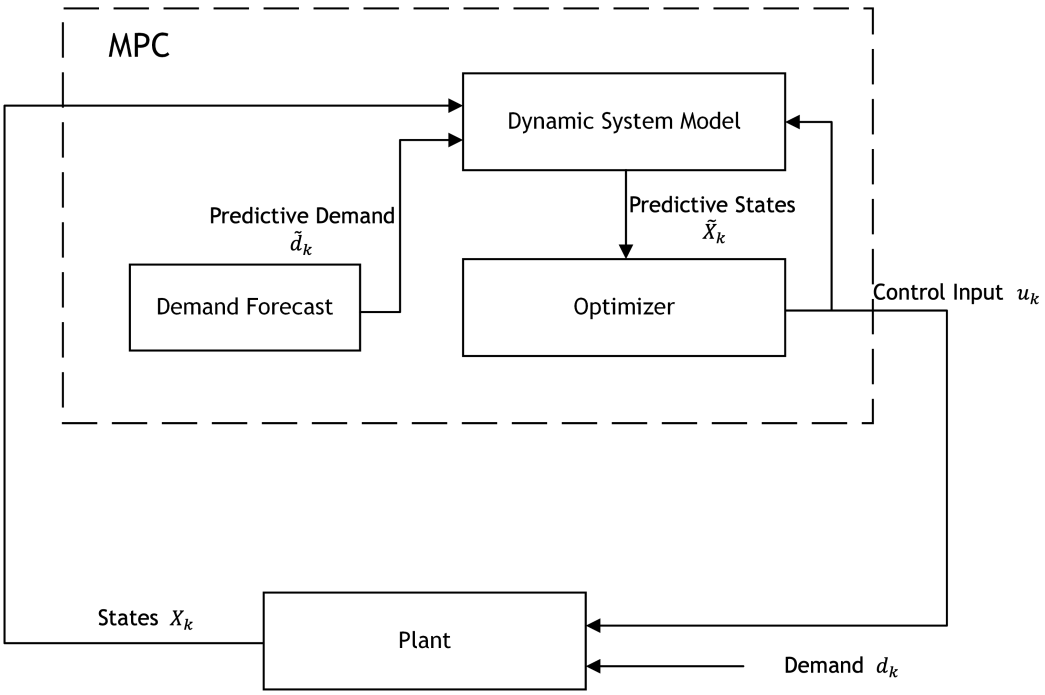

Figure 3-1: MPC framework

$$\min_{u_0,\ldots,u_{N-1}} J_{mpc} = \sum_{k=0}^{N-1} J(x_{k+1}, u_k, d_k) \tag{3-1}$$

$$\text{s.t.} \quad x_{k+1} = f(x_k, u_k, d_k), \forall k = 0, 1, \ldots, N-1 \tag{3-2}$$

$$X_N \in \mathcal{X} \tag{3-3}$$

$$U_N \in \mathcal{U} \tag{3-4}$$

$$u_k \in \{0, 1\}, \forall k = 0, 1, \ldots, N-1 \tag{3-5}$$

$$x_0 = x_{initial} \tag{3-6}$$

Where:

- x_k represents states of the system, the temperatures at pipes and tanks of the system, which are updated using temperature sensors. $x_{initial}$ is the initial condition.
- u_k is the binary control signal corresponding to the heat pump's on/off status.
- d_k denotes water consumption, acting as a disturbance in our model. A water consumption predictive model will be developed as part of this research.
- $U_N = \begin{bmatrix} u_0 & u_1 & \cdots & u_{N-1} \end{bmatrix}^T$ and $X_N = \begin{bmatrix} x_0 & x_1 & \cdots & x_{N-1} \end{bmatrix}^T$ are the vectors of binary control signal and states of the system.
- $\mathcal{X}$ and $\mathcal{U}$ are the additional constraint sets for the states and control inputs, respectively, such as safety or operational limits.

- $J_{mpc} = \sum_{k=0}^{N-1} J(x_{k+1}, u_k, d_k)$ is the objective function of the optimization problem. It is formulated to minimize some aspect of the system's behavior, such as energy usage, or operational costs.
- $f(x_k, u_k, d_k)$ represents the system dynamics, which is a crucial part of the control-oriented model developed in Section 2-3-4. This model, either **Model 1** or **Model 2** as mentioned earlier, encompasses a comprehensive representation of the heat pump system. It includes a Coefficient of Performance (COP) model for the heat pump and a stratified tank model for thermal storage tanks. These components are combined to simulate the dynamics of the system accurately.

The implementation of MPC, particularly in its mixed-integer form, offers several advantages over the basic rule-based control strategy initially discussed. It allows for proactive adjustments in control actions by anticipating future system states, thereby enhancing efficiency and performance. This predictive ability is especially beneficial in managing the dynamic and sometimes unpredictable nature of the heat pump system, aligning with our goals for economical operation.

3-4 MPC Configuration

3-4-1 Physical Constraints

In configuring the MPC for our heat pump system, it is essential to incorporate specific physical constraints. These constraints are not only imperative for ensuring the system's safe and efficient operation but also play a crucial role in meeting demand requirements and maintaining health standards.

- Upper Temperature of Tank 1:

  The upper layer of Tank 1 is directly connected to the hot water supply pipeline, often considered as the Hot Tap Water Temperature. It is critical that the upper temperature of Tank 1 T_1 does not consistently fall below 60°C. This is primarily to meet two key requirements: customer expectations for hot water supply and control measures against legionella bacteria. The desirable temperature range for hot tap water is approximately 55-75°C. While slight deviations from this range can be tolerated under specific conditions like peak demand periods or temporary operational issues with the heat pump, these are exceptions rather than the norm. Based on the state description in Table 2-4, T_1 is the state x^5 in our system model. $T_{1,k}$ and x_k^5 are T_1 and x^5 at timestamp k, respectively. Then, we have the following constraints:

$$\begin{aligned} 55 \leq & T_{1,k} \leq 75 \\ 55 \leq & x_k^5 \leq 75 \end{aligned} \tag{3-7}$$

  Moreover, it is preferred to maintain the temperature most of the time above 60°C. This practice is crucial for controlling the growth of legionella bacteria, which thrive between 20°C and 50°C. By keeping the temperature above this threshold, the proliferation of

these bacteria is inhibited, ensuring the sanitary safety of the hot water supply. Then, we have the following constraints:

$$\begin{aligned} T_{1,k} &\geq 60 \\ x_k^5 &\geq 60 \end{aligned} \tag{3-8}$$

- Heat Pump Switching Frequency:

  Another vital constraint involves the frequency with which the heat pump is turned on and off. Excessive switching can accelerate wear and tear, potentially leading to damage to the heat pump. To mitigate this, a constraint has been established to regulate the switching frequency, carefully balancing operational efficiency with the longevity of the equipment. The constraint is formalized as follows:

$$\sum_{j=-\mathrm{n_{last}}}^{-1} (u_{j+1} - u_j)^2 \leq \mathrm{N_{control}} \tag{3-9}$$

  Here, $\mathrm{n_{last}}$ represents the number of past control steps considered in addition to the current control step. $\mathrm{N_{control}}$ denotes the maximum number of switch operations allowed within these past steps and the current step. Specifically, we set $\mathrm{n_{last}}$ to 7 and $\mathrm{N_{control}}$ to 1. This means that, including the current time step, we have a total of 8 steps within a 40-minute window (as each step is 5 minutes apart, hence $5 \times 8 = 40$). During this 40-minute period, only one switch operation is permitted. In other words, the heat pump must maintain its state, either on or off, for a minimum duration of 40 minutes.

These physical constraints are integrated into the MPC problem formulation. Then, in Eq. (3-3) and Eq. (3-4), the additional constraint sets become as follows.

$$\mathcal{X} := \left\{ X_N \;\middle|\; \begin{matrix} 55 \leq x_k^5 \leq 75 \\ x_k^5 \geq 60 \end{matrix} , \forall k = 0, 1, \ldots, N-1 \right\} \tag{3-10}$$

$$\mathcal{U} := \left\{ U_N \;\middle|\; \textstyle\sum_{j=-\mathrm{n_{last}}}^{-1} (u_{j+1} - u_j)^2 \leq \mathrm{N_{control}} \right\} \tag{3-11}$$

This integration helps in guiding the selection of optimal control actions. In the objective function of the MPC, appropriate weights are assigned to these constraints to balance the trade-offs among energy efficiency, cost, and user comfort. This ensures that the system operates not only within safe and efficient parameters but also in a manner that aligns with user expectations and health regulations.

3-4-2 Economic MPC

Economic Model Predictive Control (EMPC) is a control strategy that is fundamentally focused on cost optimization. Generally, EMPC can encompass a wide range of cost considerations depending on the specific application and operational objectives. It is designed to factor in various economic parameters to guide the decision-making process within the system.

In the specific context of our research on the heat pump system, the EMPC is tailored to incorporate real-time electricity pricing. This adaptation allows us to directly address the costs associated with the energy consumption of the heat pump, particularly considering the fluctuations in electricity pricing over time.

Then, our objective function J_{mpc} shown in Eq. (3-1) can be represented as follows.

$$J_{eco} = \sum_{k=0}^{N-1} w_1 C_k P_k^{hp} u_k \tag{3-12}$$

Where:

- w_1 is the weighting factor, representing the relative importance of the cost in the objective function.
- C_k represents the cost of electricity at each time step.
- P_k^{hp} is the power consumption of the heat pump.
- u_k indicates the operational state of the heat pump, whether it is on (1) or off (0).

By integrating electricity pricing into the objective function of the MPC, our system is adept at adjusting the operation of the heat pump in response to varying electricity prices. This not only promotes economic efficiency but also emphasizes the importance of minimizing energy consumption. Thus, our EMPC strategy ensures that the heat pump system operates in a manner that is both cost-effective and energy-efficient, aligning with our overarching goals of sustainability and economic practicality.

3-5 Techniques for Computational Feasibility and Efficiency of MPC

3-5-1 Slack Factors

In the realm of MPC, ensuring the feasibility of the control strategy is of paramount importance. Infeasibility in MPC, meaning the inability to find a solution that satisfies all the constraints, can lead to several adverse outcomes. These may include the failure of the system to respond adequately to system demands, potential operational instability, or even system shutdowns in extreme cases. Such scenarios are particularly undesirable in our heat pump system with thermal storage tanks, where maintaining continuous operation is crucial.

To address this challenge, one effective method is the transformation of hard constraints into soft constraints using slack variables. Hard constraints are strict requirements that the control strategy must satisfy, but their rigidity can sometimes make finding a feasible solution difficult, especially in complex or unpredictable operational environments. By introducing slack variables, we can convert these hard constraints into soft constraints, allowing for a certain degree of flexibility. For example, in [41], a penalty term is added to the slack variables, to ensure that state constraints like wheel slip do not lead to infeasibility in the design of the nonlinear MPC controller.

To implement this, specific constraints of our system, as initially represented in Eq. (3-7), Eq. (3-8), and Eq. (3-9), are modified to include slack variables. The revised formulations are as follows:

$$55 - \delta_k^1 \leq x_k^5 \leq 75 + \delta_k^1, \forall k = 0, 1 \ldots, N-1 \tag{3-13}$$

$$x_k^5 \geq 60 - \delta_k^2, \forall k = 0, 1 \ldots, N-1 \tag{3-14}$$

$$\sum_{j=-\mathrm{n_{last}}}^{-1} (u_{j+1} - u_j)^2 \leq \mathrm{N_{control}} + \delta^{num} \tag{3-15}$$

In these equations, $\delta^1 \in \mathbb{R}^N$, $\delta^2 \in \mathbb{R}^N$ and $\delta^{num} \in \mathbb{R}$ represent the slack factors introduced, where N denotes the length of the prediction horizon. These slack factors, δ_1 and δ_2, associated with temperature, are designed to have a flexibility range up to 10 degrees, and δ_N for the switching frequency is limited to a maximum of 5 switches, ensuring that they enhance the system's adaptability while maintaining operational integrity. The constraints corresponding to these slack factors are defined as:

$$\begin{aligned} 0 \leq & \delta_k^1 \leq 10, \forall k = 0, 1 \ldots, N-1 \\ 0 \leq & \delta_k^2 \leq 10, \forall k = 0, 1 \ldots, N-1 \\ 0 \leq & \delta^{num} \leq 5 \end{aligned} \tag{3-16}$$

Furthermore, to ensure that these slack variables are effectively managed within the MPC framework, corresponding terms are added to the objective function. This addition allows the system to weigh the trade-offs between adhering to the original constraints and allowing for slight deviations where necessary. The objective term related to slack variables is represented by the equation:

$$J_{slack} = \sum_{k=0}^{N-1} \left(w_2 \delta_k^1 + w_3 \delta_k^2 \right) + w_4 \delta^{num} \tag{3-17}$$

Here, w_2, w_3, and w_4 are the weighting factors associated with the slack variables. In the context of our heat pump system, these weighting factors are set to be large numbers. The rationale for using large weights is to ensure that the deviation from the original constraints is minimized and only allowed when absolutely necessary. By assigning high values to these weights, the MPC is encouraged to prioritize adherence to the original constraints as much as possible, resorting to slack only in scenarios where it is essential to maintain the feasibility of the solution. This approach ensures that the system operates closely to the desired performance parameters, while still maintaining the flexibility provided by the slack variables.

Then, our objective function J_{mpc} as in Eq. (3-1) becomes:

$$\begin{aligned} J_{mpc} &= J_{eco} + J_{slack} \\ &= \sum_{k=0}^{N-1} \left(w_1 C_k P_k^{\mathrm{hp}} u_k + w_2 \delta_k^1 + w_3 \delta_k^2 \right) + w_4 \delta^{num} \end{aligned} \tag{3-18}$$

Integrating slack factors into the MPC enhances the flexibility and robustness of the control strategy, making it more adaptable to real-world conditions. Particularly in scenarios where strict adherence to hard constraints might be challenging or impractical, slack variables allow the control strategy to remain operational by slightly adjusting constraints when necessary. This adjustment not only prevents infeasibility but also ensures that the system continues to operate efficiently, despite minor deviations from the ideal constraint parameters.

3-5-2 Move Blocking Strategy

As we try to refine the control over our heat pump system within the MPC framework, we recognize the value of extending the prediction horizon to better anticipate future demands and temperature states. Nonetheless, a longer prediction horizon poses computational challenges, notably increasing the computation time pf MPC, which could lead to performance inefficiencies. Given our system operates with a sample time of 5 minutes, we must constrain the maximum computation time for MPC updates to under one minute to avoid introducing errors and to maintain system responsiveness.

To address this, we employ a Move Blocking Strategy in our MPC design. This technique involves segmenting the prediction horizon into variable-sized blocks [35]. The initial segment of the horizon is divided into smaller time blocks, which allows for more accurate and responsive control actions that can address immediate system states and short-term demand forecasts. As the prediction extends further into the future, the size of the time blocks increases. This is based on the premise that the necessity for precision in control actions decreases as the time horizon extends, due to the diminishing influence of such actions over an extended forecast period.

Figure 3-2 provides a visual representation of the Move Blocking Strategy in action, comparing a standard MPC signal with one utilizing move blocking over a 20-step prediction horizon. In this illustration, the prediction horizon is divided into blocks of varying sizes to demonstrate the efficiency of this strategy. Specifically, the horizon consists of three distinct block types. One-step region, highlighted in red, consists of five blocks where each block represents a single step. This allows for precise control adjustments responding to immediate system requirements. Two-step region, colored in green, comprises three blocks, with each block encompassing two steps. This section reflects a mid-term forecast, where control precision is balanced with computational efficiency. Three-step region, shaded in blue, also includes three blocks, but each block spans three steps. The three-step region is where control actions have a less effect, and a coarse adjustment is sufficient.

The adoption of this move blocking strategy enables us to maintain a longer prediction horizon without incurring prohibitive computation times. It strikes a critical balance, allowing the MPC to function effectively in real-time, aligning the timeliness of control actions with the computational constraints.

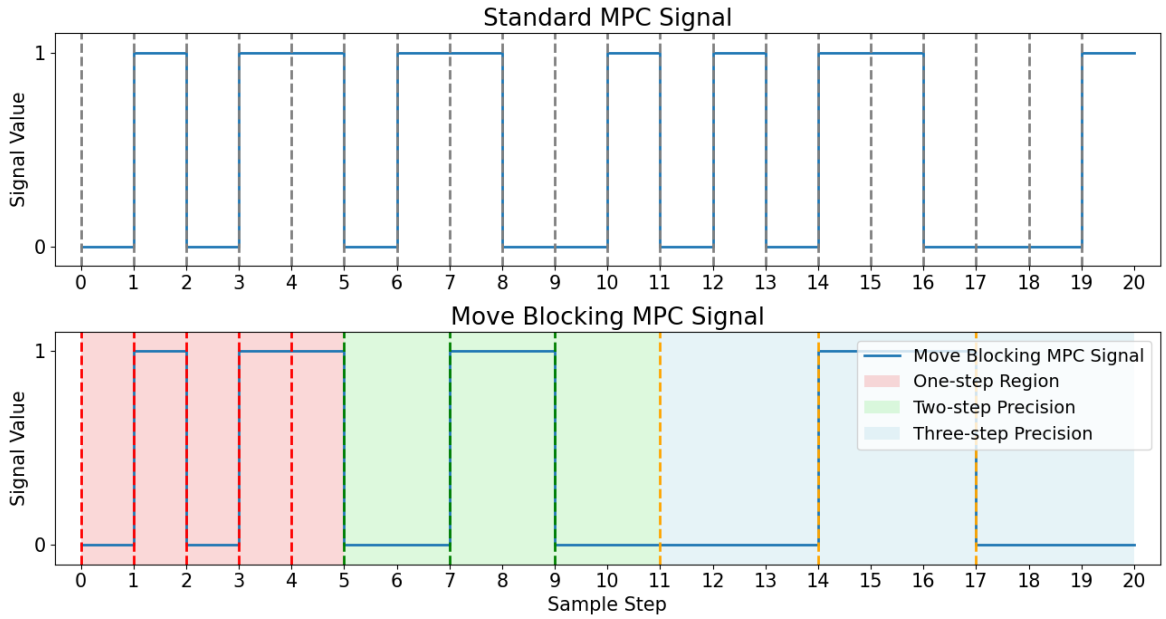

Figure 3-2: Example of a Move Blocking Strategy

3-6 Simulation Results

3-6-1 MPC Computation Time

In this subsection, we present the results of our simulations comparing MPC computation times. These simulations are crucial for evaluating the efficiency of our control strategies under different modeling and configuration scenarios.

Comparison Between Model 1 and Model 2

The MPC computation times for **Model 1** and **Model 2** are delineated in Section 2-3-4. Utilizing a standard control strategy, the control horizon consisted of 20-minute steps (four sample steps per control step).

Table 3-1 shows the results. With an identical prediction horizon length, **Model 2** showcases a marked enhancement in MPC computation time over **Model 1**. This improvement, coupled with better model identification precision, as presented in Table 2-5 and Table 2-6 from Section 2-3-4, clearly suggests that **Model 2** is the preferable choice for our system. Hence, we will proceed with **Model 2** for all further simulations and practical implementations.

Comparison Between Standard Strategy and Move Blocking Strategy

Subsequently, we evaluated the standard strategy against the move blocking strategy with respect to MPC update time. The move blocking strategy employs a differentiated step duration within the control horizon to attain a complete 6-hour prediction horizon.

Mar 6, 2023 (6-hour Standard Control Horizon)	Model 1	Model 2
Minimum Update Time	11.74 s	3.22 s
Maximum Update Time	301.19 s	82.18 s
Average Update Time	72.96 s	21.62 s

Table 3-1: MPC update time of Model 1 and Model2

Table 3-2 presents these findings. Under the standard strategy, the maximum update time exceeded one minute, which is too long for our system, as it is designed to update the control signal every five minutes. On the contrary, the move blocking strategy proficiently retained the maximum update time under one minute. This underscores its effectiveness in reducing computation overhead while preserving predictive accuracy, thereby meeting the stringent real-time operational demands of our system.

Mar 6, 2023	Standard Control Horizon (6 Hours)	Move Blocking Control Horizon (6 Hours)
Minimum Update Time	3.22 s	0.51 s
Maximum Update Time	82.18 s	15.68 s
Average Update Time	21.62 s	9.16 s

Table 3-2: MPC update time of Model 2 with 6-hour standard control horizon and move blocking control horizon

3-6-2 Electricity Price

The cost of electricity plays a crucial role in the EMPC of our heat pump system. To integrate this factor, we sourced day-ahead electricity price data from the European Network of Transmission System Operators for Electricity (ENTSO-E) [14], which provides a forecast of electricity prices.

As depicted in Figure 3-3, an examination of the electricity price trends over the first ten days of March 2023 was conducted, with a particular focus on the operational hours of our heat pump system (07:10 to 17:30). There is a discernible pattern where electricity prices typically peak during early morning hours (07:00 to 11:00) and late afternoon (16:00 to 18:00). Conversely, the midday hours (11:00 to 16:00) often see a dip in prices.

Given the regularity observed in these pricing patterns, we have chosen the data from March 1, 2023, as a benchmark for our simulation studies. The price profile for this day, as represented in Figure 3-4, will act as a typical day for our analysis. This approach allows for a standardized assessment in our simulation scenarios, providing a consistent basis to evaluate the impact of electricity prices on the EMPC decision-making process.

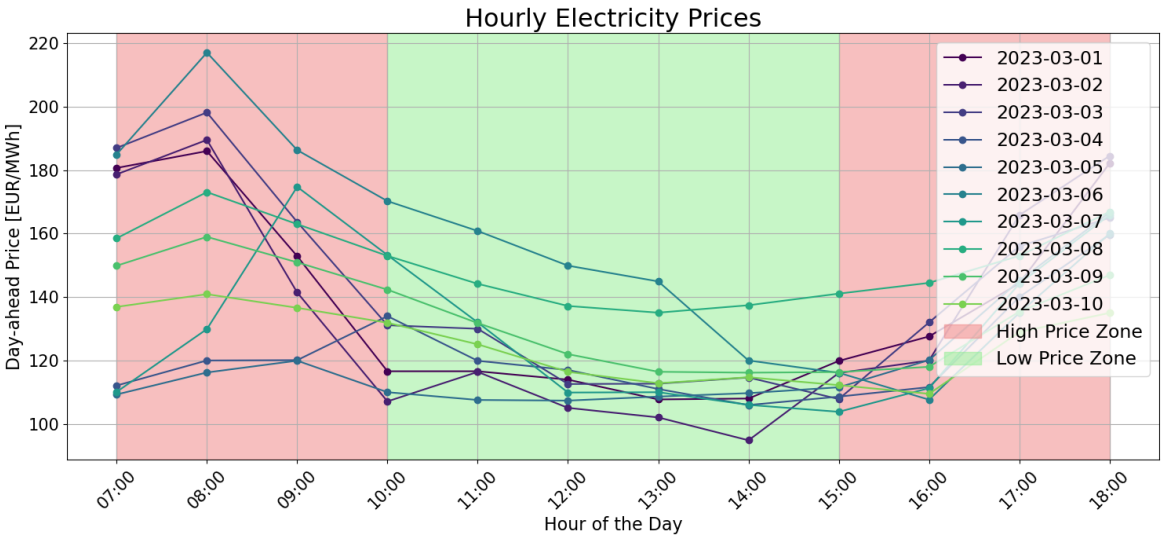

Figure 3-3: Hourly electricity prices for each day in the first 10 days of March 2023

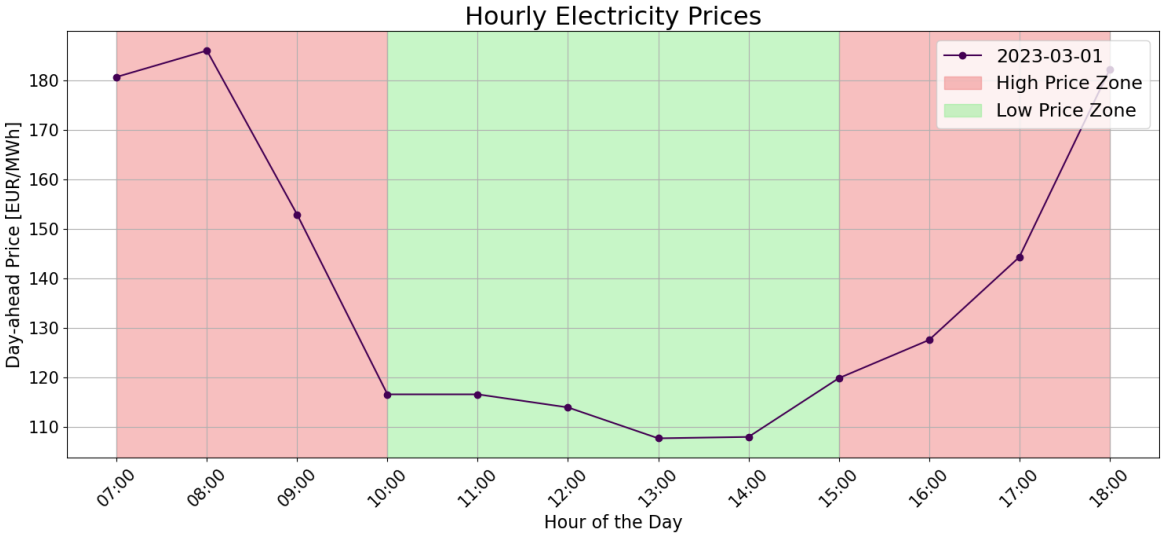

Figure 3-4: Hourly electricity prices for Mar 1, 2023

3-6-3 Energy Cost Saving

In this subsection, the energy cost savings facilitated by the EMPC strategy are brought into focus through a series of simulations. The analysis of these simulations is crucial, as it illustrates the tangible benefits of employing our EMPC strategy, particularly in the context of reducing operational expenses.

Simulation Results for a Specific Day

The simulation conducted on March 6, 2023 served as a foundational analysis, providing valuable insights into the daily operation of the system and the potential cost savings achievable

through our strategies.

Figure 3-5 illustrates the results of this simulation, highlighting the day-to-day performance of the EMPC strategy. The figure notably features low electricity price periods marked in green and the operation percentages of the heat pump during the different electricity price periods of the day. Specifically, during the first low electricity price period, the operation percentage under the MPC strategy was 61.76%, slightly lower than the original strategy's 64.71%. This modest reduction is due to the MPC strategy's efficient initial heating requirements as work hours commence. During the high electricity price period, the MPC strategy significantly reduces the heat pump's operation to 56.67%, compared to the original strategy's 61.67%. This considerable reduction is a reflection of the MPC's sensitivity to electricity pricing, effectively minimizing operational costs without compromising the system's thermal requirements. In the second low electricity price period, following the peak water usage hours (between 13:00 and 15:00), the MPC strategy further decreases the heat pump's operation to 38.71%, compared to the original strategy's 58.06%. This substantial decrease demonstrates the MPC's adaptability to both electricity pricing and the reduced heating demand after peak hours.

Table 3-3 summarizes the performance comparison between the original and MPC strategies on March 6, 2023. The MPC strategy showed a reduction in electricity costs from 8.69 Euro to 7.45 Euro (85.73% of the original strategy) and a decrease in energy consumption from 64.17 kWh to 55.83 kWh (87.00% of the original strategy). Moreover, throughout the simulation, the temperature T_1 was successfully maintained within the expected range of 55°C to 75°C, demonstrating the strategy's ability to manage system operations within predefined temperature constraints. Specifically, the MPC strategy outperformed the original in maintaining the upper water tank temperature above 60°C. The MPC strategy showed a lower number of violation steps below 60°C compared to the original strategy, with 8 violation steps for MPC against 20 for the original. This metric indicates how often the temperature in the water tank fell below the desired threshold of 60°C. The average temperature deviation below 60°C was also smaller under the MPC strategy, with differences of 0.05°C and 0.24°C for MPC and original strategies, respectively, and maximum deviations of 1.94°C for MPC versus 4.43°C for the original strategy.

These results collectively demonstrate the multifaceted effectiveness of the MPC strategy. By operating the heat pump less frequently, especially during periods of high electricity prices, the MPC strategy not only conserves energy but also adeptly adapts to varying demand patterns throughout the day. This adaptability leads to significant cost savings and improved energy efficiency. At the same time, the MPC strategy effectively maintains water temperature within the desired range. It performs better than the original strategy in both cost efficiency and temperature control.

Simulation Results for a Week

To broaden our understanding of the EMPC's capabilities, we conducted a week-long simulation from March 6 to March 10, 2023. Table 3-4 presents a detailed comparison of the week-long performance between the original control strategy and the Economic MPC strategy.

Throughout the week, as reflected in Table 3-4, the EMPC strategy consistently achieved lower energy consumption and operational costs than the original strategy. Energy consumption decreased progressively with longer control horizons, with the Move Blocking Control

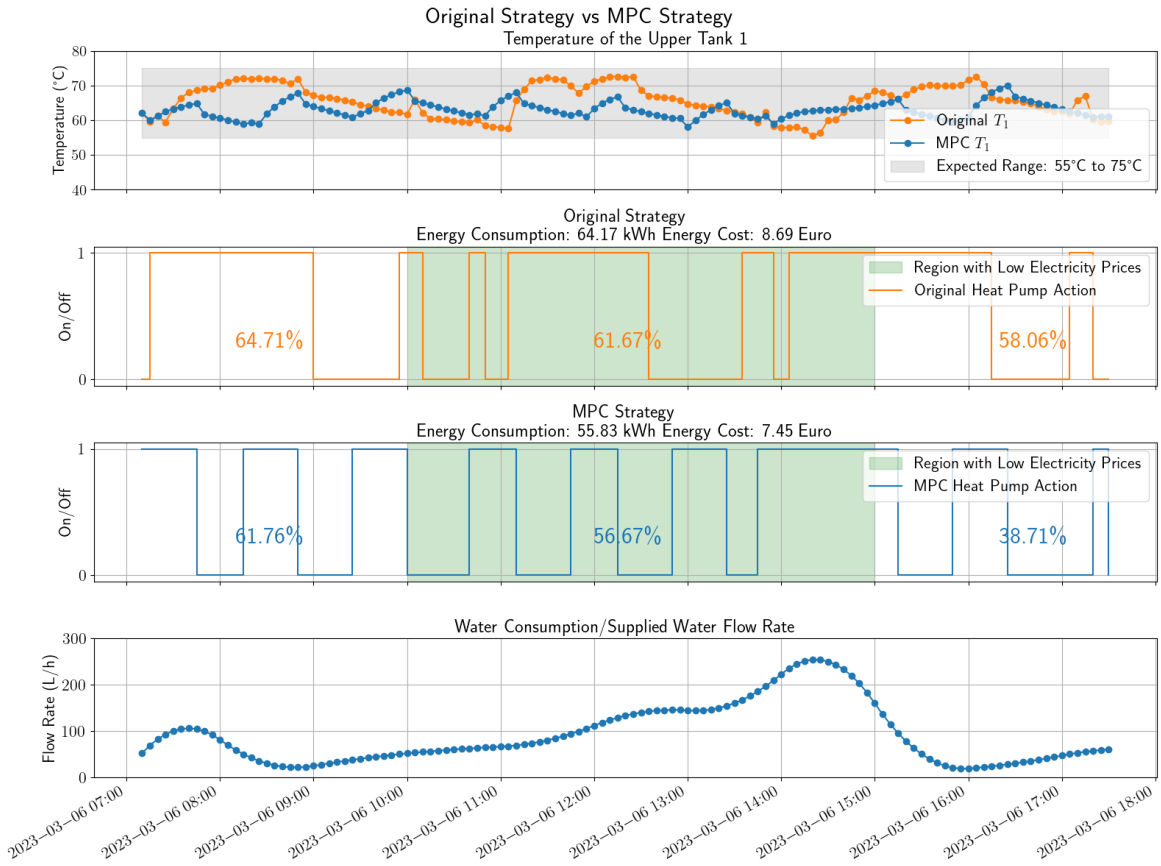

Figure 3-5: Simulation result for energy cost saving on Mar 6, 2023

Mar 6, 2023	Original Strategy	MPC Strategy
Energy consumption (kWh)	64.17 (100%)	55.83 (87.00%)
Energy cost (Euro)	8.69 (100%)	7.45 (85.73%)
The number of violation steps below 60°C (5-min sample time)	20	8
Average violation temperature difference below 60°C (°C)	0.24	0.05
Maximum violation temperature (°C)	4.43	1.94

Table 3-3: Performance of the original and MPC strategies on Mar 6, 2023

Horizon of 6 hours reaching the lowest consumption at 308.33 kWh, which is 91.36% of the consumption under the original strategy. Similarly, energy costs were reduced to 87.38% of the original strategy's costs when employing the Move Blocking Strategy. Despite the MPC strategy's increased number of violation steps, the overall temperature control remained within acceptable limits. The average violation temperature difference below 60°C remained below

0.62°C, and the peak temperature violation was contained at 5.39°C, underscoring the strategy's effectiveness in temperature regulation despite a more aggressive energy cost-saving approach.

Figure 3-6 offers a weekly overview of the temperature profiles under both the original and EMPC strategies. The EMPC strategy demonstrates a commendable ability to maintain temperature stability, with the average temperature consistently above the critical 60°C threshold. Notably, the MPC strategy managed to keep the upper tank temperature within a tighter range compared to the original strategy, as evidenced by the red shaded area in the figure. This indicates a more controlled and efficient heating process, avoiding the extremes that can lead to energy wastage.

The week-long simulation results substantiate the EMPC strategy's capability in curtailing energy costs, confirming the observations made from the single-day analysis. The more detailed and extended assessment provides a nuanced understanding of the strategy's performance, illustrating its significant potential for cost savings in a real-world operational setting.

Mar 6 – 10, 2023	Original Strategy	MPC (Standard control horizon, 2 hour)	MPC (Standard control horizon, 4 hour)	MPC (Standard control horizon, 5 hour)	MPC (Moving block control horizon, 6 hour)
Energy consumption (kWh)	337.50 (100%)	311.67 (92.35%)	315.00 (93.33%)	310.83 (92.10%)	308.33 (91.36%)
Energy cost (Euro)	45.57 (100%)	40.42 (88.70%)	40.74 (89.40%)	40.16 (88.13%)	39.82 (87.38%)
The number of violation steps below 60°C (5-min sample time)	97	147	152	168	209
Average violation temperature difference below 60 °C (°C)	0.27	0.43	0.44	0.47	0.62
Maximum violation temperature (°C)	6.26	6.39	5.33	5.22	5.39

Table 3-4: Performance of the original strategy and MPC strategies from Mar 6 to Mar 10, 2023

3-7 Real Implementation Results

On November 16, 2023, we conducted a test with the primary goal of reducing energy costs while maintaining system efficiency. The results are illustrated in Figure 3-7. Subsequently, we compared water consumption on the test day with historical data to establish the consistency and reliability of the system under different conditions.

The historical data from October 4, 2023 is illustrated in Figure 3-8. Figure 3-9 compares the water consumption patterns between our test date, November 16, 2023, and a previous date, October 4, 2023, revealing a close alignment in usage patterns between the two dates. The similarity in water usage on these two distinct dates validates our selection of October 4 as a suitable baseline for comparison.

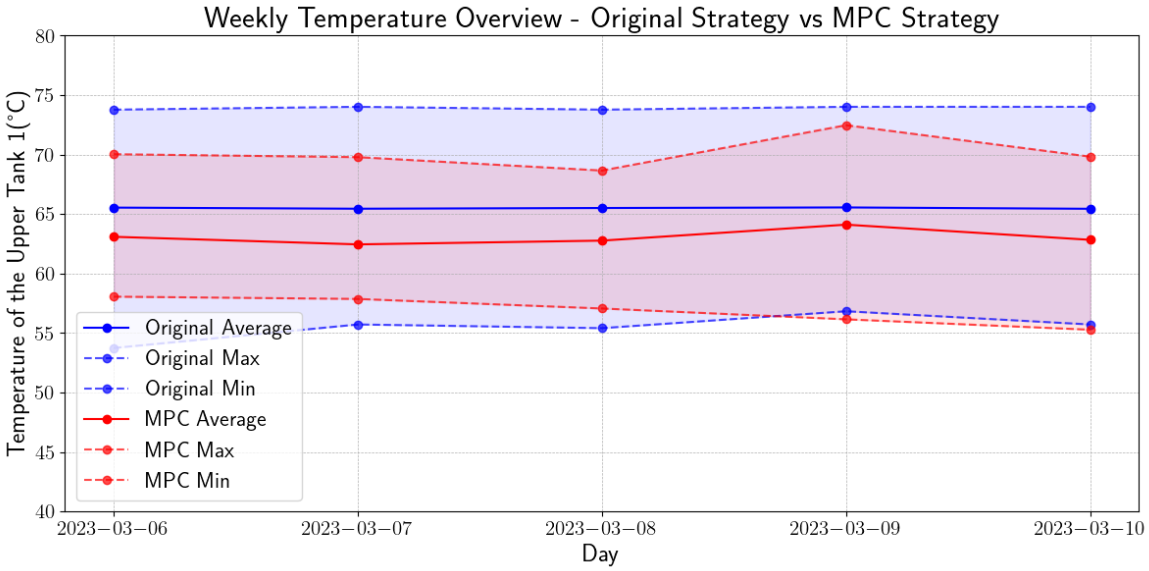

Figure 3-6: Weekly temperature overview of the original strategy and MPC strategies from Mar 6 to Mar 10, 2023

Table 3-5 summarizes the performance of strategies. The MPC strategy implemented on November 16, 2023, yielded significant improvements over the original strategy from October 4, 2023. Energy consumption decreased to 65.83 kWh, reaching 94.04% of the energy used by the original strategy. Moreover, the energy cost was reduced from 9.63 Euro to 8.64 Euro, amounting to 89.72% of the cost incurred under the original strategy. These reductions in energy and cost illustrate the tangible benefits of the MPC approach.

However, the number of temperature violation steps below 60°C increased from 23 to 35 when transitioning from the original to the MPC strategy. Despite this increase, the average temperature difference for violations below 60°C was lower at 0.43°C, compared to 0.58°C in the original strategy. Furthermore, the maximum temperature violation was significantly mitigated, from 7.16°C down to 4.43°C, under the MPC strategy. This underscores the enhanced precision of the MPC in maintaining temperature within expected range, even while optimizing for cost and energy savings.

The successful real-world application of the MPC strategy on November 16, 2023 validates its effectiveness and showcases its scalability. Although there was a minor increase in the number of small temperature deviations, the overall control of temperature was more efficient, leading to considerable energy savings. These outcomes reinforce the EMPC strategy as a practical and enhanced alternative to the original strategy, with significant implications for real-world energy systems management.

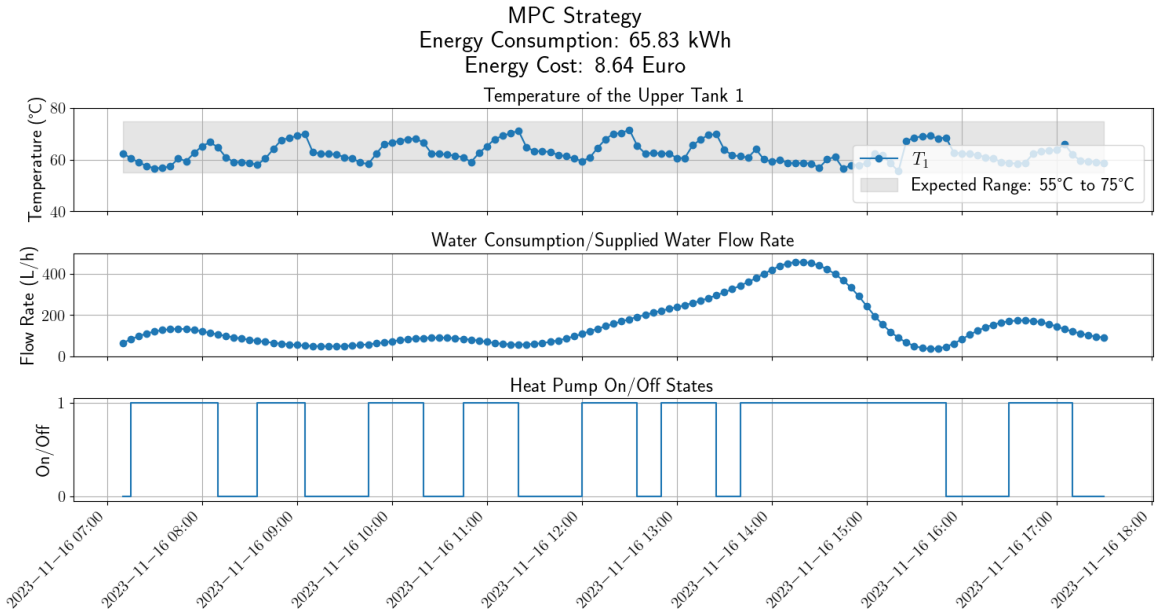

Figure 3-7: Result of the implementation for economical operation on Nov 16, 2023

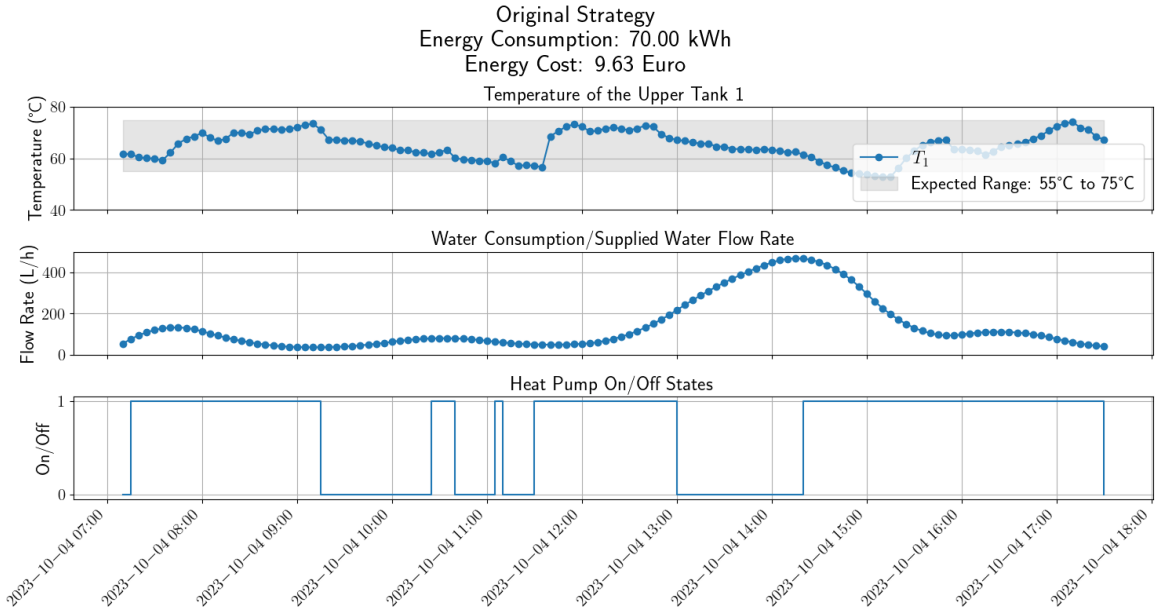

Figure 3-8: Historical data from Oct 4, 2023

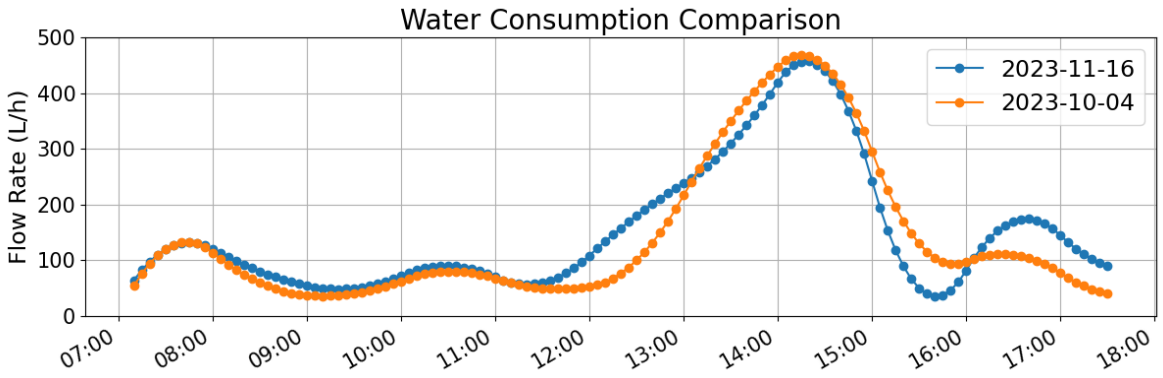

Figure 3-9: Water consumption comparison between Nov 16, 2023 and Oct 4, 2023

	Original Strategy (Oct 4, 2023)	MPC Strategy (Nov 16, 2023)
Energy consumption (kWh)	70 (100%)	65.83 (94.04%)
Energy cost (Euro)	9.63 (100%)	8.64 (89.72%)
The number of violation steps below 60°C (5-min sample time)	23	35
Average violation temperature difference below 60°C (°C)	0.58	0.43
Maximum violation temperature (°C)	7.16	4.43

Table 3-5: Performance of the original strategy on Oct 4, 2023 and the MPC strategy on Nov 16, 2023

Chapter 4

MPC-Based Demand-Side Management

This chapter further explores control strategies with an emphasis on demand-side management within the context of Model Predictive Control (MPC). Section 4-1 provides an introduction to Demand-Side Management (DSM) and the motivation for its implementation. Section 4-2 outlines the objectives of demand-side management. Section 4-3 focuses a proposed strategy, a two-step demand-side management strategy, which elaborates on the processes of Flexibility Assessment and Exploitation. The chapter concludes with Sections 4-4 and 4-5, which present the results and analysis of simulations and real implementation tests, respectively.

4-1 Introduction and Motivation

As the integration of Renewable Energy Sources (RES) continues to escalate, addressing their inherent characteristics, such as volatility, intermittency, uncertainty, and limited controllability, becomes increasingly imperative. In response to these characteristics, the role of DSM has emerged as a pivotal counterpart to traditional supply-side efforts that focus on the production and distribution of energy.

DSM encompasses a broad range of strategies aimed at influencing consumer energy consumption to better align with energy availability and system needs. Unlike supply-side management, DSM directly involves end-users, empowering them to play a significant role in the energy landscape through energy consumption patterns.

There are generally two types of DSM programs:

- Price-based programs [21] [22], which prompt the system to adjust its energy consumption in response to economic signals like electricity prices. This approach encourages users to modify their energy usage based on the fluctuating costs of electricity, often in anticipation of day-ahead electricity price forecasts. The Economic Model Predictive

Control (EMPC) strategy, which aligns with this type of program, was discussed in detail in Chapter 3.

- Incentive-based programs [5] [11], where systems reduce their energy consumption according to specific Demand Response (DR) requests. These requests outline an energy consumption profile for a certain time period, with corresponding incentives to motivate adherence.

Given the groundwork of the EMPC strategy laid in Chapter 3, this chapter will consider the incentive-based DSM programs, proposing a two-step demand-side management strategy.

DR, a fundamental element of DSM, is a scheme intended to motivate end-users to alter their electricity usage patterns in line with fluctuations in electricity availability or price [19]. DR requests typically aim to maintain total energy consumption within set bounds [5], balancing the supply and demand of grid.

The challenge with DR lies in striking the right balance: overly ambitious DR requests could compromise system performance, while overly conservative ones might not exploit the system's full flexibility potential. This balance is predicated on an accurate assessment of the system's flexibility capabilities. Our proposed DSM strategy begins with a thorough evaluation of system flexibility, followed by the strategic deployment of this flexibility through targeted DR measures. This two-step approach seeks to optimize the system's flexibility utilization, ensuring a harmonious balance between energy savings and the maintenance of operational integrity.

4-2 Objectives of Demand-Side Management

The objectives of demand-side management within our control strategy are twofold: first, to evaluate and optimize the energy flexibility of our heat pump system, and second, to harness thermal energy storage as a tool for exploitation of energy flexibility potential through implementing effective DR.

The first focus is on evaluating the energy flexibility of the heat pump system. This involves analyzing how effectively the system can adapt its energy usage patterns in response to external conditions such as changes in grid demands. The assessment of energy flexibility is crucial for understanding the system's capacity to store and shift energy usage, which is instrumental in optimizing operational efficiency and reducing costs.

The second objective revolves around the strategic use of thermal energy storage to fulfill DR request. Thermal storage acts as a buffer, allowing the system to storage energy during times of excess supply or low costs and release it during peak demand. This functionality not only improves the operational efficiency of the heat pump system but also plays a significant role in supporting grid balance and enhancing overall energy sustainability.

All in all, these objectives guide our DSM strategy towards enhancing the responsiveness of the system to energy demand fluctuations and market dynamics. This integrated approach ensures that our heat pump system operates not just with immediate efficiency but also aligns with broader objectives of energy sustainability and grid reliability.

4-3 Two-Step Demand-Side Management Strategy

Drawing inspiration from the pioneering work of Yun Li [27], we propose a two-step demand-side management strategy that focuses on assessing and exploiting the energy flexibility of our system. The schematic of this strategy is depicted in Figure 4-1.

Our DSM strategy unfolds in two key steps:

1. **Flexibility Assessment**. It involves developing a robust formula to quantitatively assess the system's flexibility potential, factoring in uncertain external conditions such as water consumption. Information regarding the flexibility capacity is systematically communicated to the grid operators.
2. **Flexibility Exploitation**. It revolves around the exploitation of this assessed flexibility through DR requests. These requests are defined for specific periods, dictating the energy consumption profile that the system should follow. By aligning the system's operation with these requests, we effectively utilize the system's inherent flexibility to meet grid demands and contribute to overall energy optimization.

By implementing these two steps, our DSM strategy aims to maximize the system's responsiveness to energy demand and market conditions, ultimately contributing to a more resilient and sustainable energy grid.

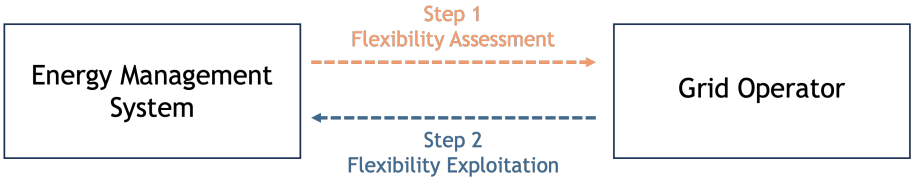

Figure 4-1: Diagram of the proposed DSM strategy

4-3-1 Flexibility Assessment

Assessment of HVAC Device Flexibility

The assessment of flexibility aims to quantify the adaptable capacity of the Heating, Ventilating and Air-Conditioning (HVAC) system—*specifically, the maximum duration the device can remain off without affecting the desired conditions.* This capability is crucial for optimizing energy usage during varying demand and supply conditions, especially when integrating renewable energy sources with their unpredictable nature.

Our approach to assessing flexibility involves the use of binary decision variables that accommodate the on/off control nature of our HVAC system. Through this method, we can delineate the periods during which the system can afford to be non-operational, thereby offering potential for energy savings and operational optimization.

In our formulation, we define two sets of binary decision variables as flexibility states at each discrete time step within our prediction horizon:

- s_k for each $k = 0, 1 \ldots, N-1$
- z_k for each $k = 0, 1 \ldots, N-1$

where N represents the length of the prediction horizon for assessing the system's energy flexibility.

The operational logic for the flexibility state is defined as follows:

- $s_k = 1$ & $z_k = 0$: This implies that time instant k is within the flexibility period.
- $s_k = 0$ & $z_k = 1$: This denotes that time instant k is after the end of the flexibility period.
- $s_k = 0$ & $z_k = 0$: This indicates that time instant k is before the start of the flexibility period.

Accompanying these logical conditions are a set of constraints designed to exploit flexibility:

- $u_k \leq 1 - s_k$: This ensures that the control input is set to 0 when $s_k = 1$.
- $s_{k+1} \geq s_k - z_{k+1} \cdot M$: Here, M is a large constant, ensuring that once the system enters the flexibility period, it remains off for consecutive steps.
- $s_k + z_k \leq 1$: This ensures that s_k and z_k are not both 1 at the same time.
- $z_{k+1} \geq z_k$: This ensures the sequence of the flexibility period, indicating that once the period ends, it does not restart.

Figure 4-2 illustrates the operational logic behind the flexibility assessment using binary decision variables. The x-axis represents discrete time steps within the prediction horizon, while the y-axis indicates the binary states (0 or 1) of the decision variables and control signals. The first subplot demonstrates the s_k signal, where a value of '1' signifies a time step within the designated flexibility period, characterized by the HVAC system being off or having the capability to be off. The second subplot shows the z_k signal, where a '1' indicates a time step after the end of the flexibility period. This signal transitions from '0' to '1' at the conclusion of the flexibility period, indicating the system must return to normal operation. The third subplot displays the u_k control signal for the HVAC system. The color-coding in this plot clearly shows the different phases in relation to the flexibility period: the time steps before the flexibility period (marked in coral), the flexibility period itself (highlighted in green), and the time steps following the flexibility period (colored in red).

Mathematical Formulation of Flexibility Assessment

In the framework of flexibility assessment, the primary objective is to determine the maximum period during which the HVAC system with on/off control authority can remain inactive. This goal is achieved by defining the following objective term:

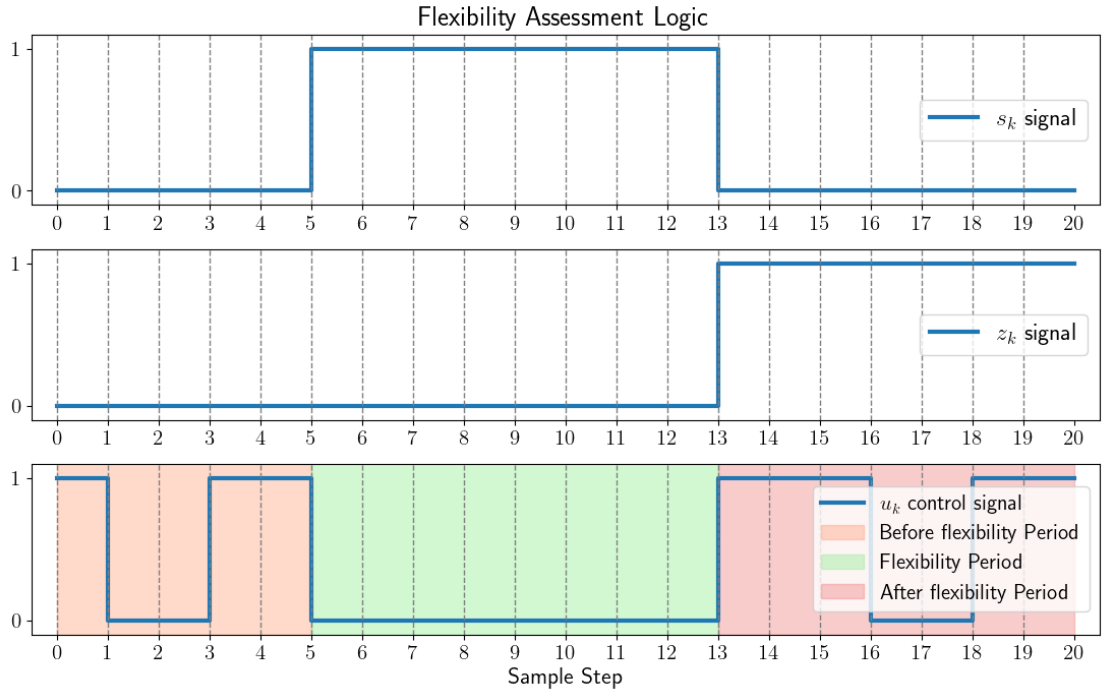

Figure 4-2: Flexibility assessment logic

$$J_{\text{flexi}} = \sum_{k=0}^{N-1} s_k \tag{4-1}$$

Here, J_{flexi} sums the binary variables s_k across the prediction horizon N, quantifying the flexibility period. The assessment problem is formulated as shown in the provided equation.

$$\min_{U_N, S_N, Z_N} \quad J_{\text{flexi}} \tag{4-2}$$

$$\text{s.t.} \quad x_{k+1} = f(x_k, u_k, d_k), \forall k = 0, 1, \ldots, N-1 \tag{4-3}$$

$$u_k \leq 1 - s_k, \forall k = 0, 1, \ldots, N-1 \tag{4-4}$$

$$s_{k+1} \geq s_k - z_{k+1} \cdot M, \forall k = 0, 1, \ldots, N-2 \tag{4-5}$$

$$s_k + z_k \leq 1, \forall k = 0, 1, \ldots, N-1 \tag{4-6}$$

$$z_{k+1} \geq z_k, \forall k = 0, 1, \ldots, N-1 \tag{4-7}$$

$$u_k \in \{0, 1\}, \forall k = 0, 1, \ldots, N-1 \tag{4-8}$$

$$s_k \in \{0, 1\}, \forall k = 0, 1, \ldots, N-1 \tag{4-9}$$

$$z_k \in \{0, 1\}, \forall k = 0, 1, \ldots, N-1 \tag{4-10}$$

$$X_N \in \mathcal{X} \tag{4-11}$$

$$x_0 = x_{initial} \tag{4-12}$$

Where

- The symbols

$$U_N = \begin{bmatrix} u_0 & u_1 & \cdots & u_{N-1} \end{bmatrix}^T$$
$$S_N = \begin{bmatrix} s_0 & s_1 & \cdots & s_{N-1} \end{bmatrix}^T$$
$$Z_N = \begin{bmatrix} z_0 & z_1 & \cdots & z_{N-1} \end{bmatrix}^T$$
$$X_N = \begin{bmatrix} x_0 & x_1 & \cdots & x_{N-1} \end{bmatrix}^T$$

  represent the vectors of decision variables u_k, s_k, z_k and states x_k.

- $u_k \leq 1 - s_k$: This ensures that when $s_k = 1$, the control input should be 0.
- $s_{k+1} \geq s_k - z_{k+1} \cdot M$: M is a constant larger than 1. The constraint ensures that within the flexibility period, control inputs are closed consecutively.
- $s_k + z_k \leq 1$: This ensures that when z_k (time instant k is after the end of the flexibility period), $s_k = 0$.
- $z_{k+1} \geq z_k$: This implies that if k is after the end of the flexibility period, then $k + 1$ is also after the flexibility period.
- $f(x_k, u_k, d_k)$ is the system dynamic as the same as Eq. (3-2). $\mathcal{X}$ is the control physical constraints as the same as Eq. (3-10).

After computing this model, the periods of flexibility can be identified where $s_k = 1$. This symbolizes the moments when the HVAC system can be safely turned off without compromising the system's overall functionality or comfort levels. The underlying optimization problem here focuses on calculating the maximum duration that the device can remain off without impacting the desired environmental conditions.

This MPC-based approach provides a structured and efficient method to evaluate and utilize the flexibility in HVAC operations. One of the key strengths of this framework is its versatility. It is not confined by the specific dynamics of a system, making it applicable to any system with binary input controls. This universality allows the framework to be adapted to various systems, enhancing energy efficiency and operational sustainability across different contexts. The adaptability of this framework to diverse system dynamics emphasizes its potential in a wide range of applications, promoting a more sustainable and efficient approach to energy management in HVAC systems.

4-3-2 Flexibility Exploitation

Upon completing the flexibility assessment in Step 1, grid operators can now act on the results by communicating the determined flexibility period $\mathcal{I}$ back to the Energy Management System (EMS). Then, the EMS recognizes the time stamps ranging from N_{begin} to N_{end} within the prediction horizon of length N as the designated demand response period $\mathcal{I}_{dr}$. This period is visualized as the green area in Figure 4-3, signifying when the HVAC system can afford to be non-operational, allowing for strategic energy conservation during times of surplus generation or low demand.

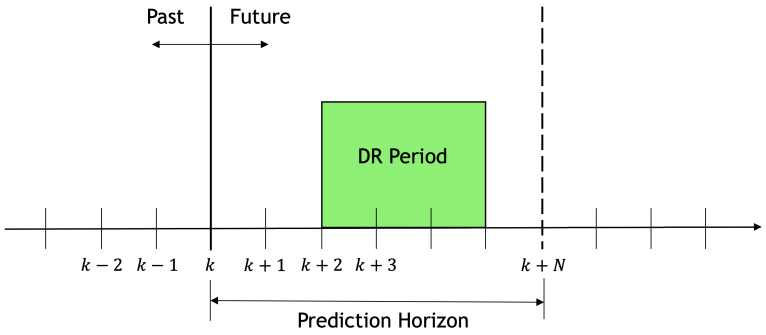

Figure 4-3: Demand Response (DR) Period

During DR period $\mathcal{I}_{dr}$, control inputs are strategically set to zero align with the demand response objectives:

$$u_j = 0 \quad \forall j = N_{begin}, \ldots, N_{end} \tag{4-13}$$

This zero-control-input constraint is incorporated into the set of control constraints within the EMPC framework. It specifically influences the control actions as described in Eq. (3-4). In addition to this specific constraint, all other aspects of the control strategy adhere to the previously developed EMPC framework. This ensures that the overall system maintains its efficiency and effectiveness while dynamically accommodating the specific requirements of demand response events. Furthermore, N_{begin} and N_{end} are treated as dynamic parameters that are updated in real-time to reflect the evolving nature of demand response requests.

The implementation of flexibility exploitation serves not just to adjust energy consumption in reaction to immediate grid needs but also to support the long-term goals of DSM. By effectively utilizing these demand response periods, the system contributes to overall grid stability and efficiency. This dynamic response capability is pivotal in managing the intermittent nature of renewable energy sources, thereby enhancing the resilience and sustainability of the energy grid.

4-4 Simulation Results

To validate the efficacy of our proposed two-step demand-side management strategy, we carried out a series of simulation tests. The data utilized for these simulations corresponds to operational parameters and environmental conditions from March 6, 2023.

In aligning with the first step of our demand-side management strategy, flexibility assessments were conducted at three distinct times during the day, each with a 3-hour prediction horizon. The specific timestamps for these assessments were 7:10, 10:10, and 13:10. Following each flexibility assessment, we immediately proceeded to the second step of the strategy, flexibility exploitation, where the identified flexibility period was designated as the demand response period. It is important to note that after the final assessment period at 13:10, and beyond 16:10, the system reverted to the EMPC strategy that was formulated in Chapter 3.

Figure 4-4 presents the results of our flexibility assessments. The initial phase of the day, especially before 8:00, exhibits limited flexibility due to lower temperatures of tanks. As

the day progresses, the energy flexibility of the system markedly increases at 13:10. During peak water consumption hours, from approximately 13:00 to 15:00, a notable reduction in flexibility is observed.

Figure 4-5 illustrates the simulation test results with the demand response periods marked in green. The results clearly show that the MPC strategy effectively deactivates the heat pump during these periods, thereby fulfilling the demand response request and capitalizing on the system's assessed flexibility.

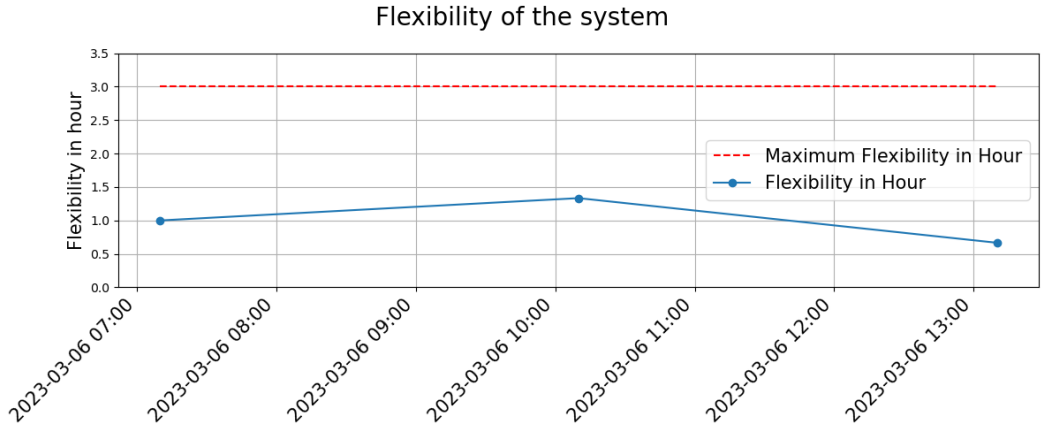

Figure 4-4: Flexibility assessment on March 6, 2023

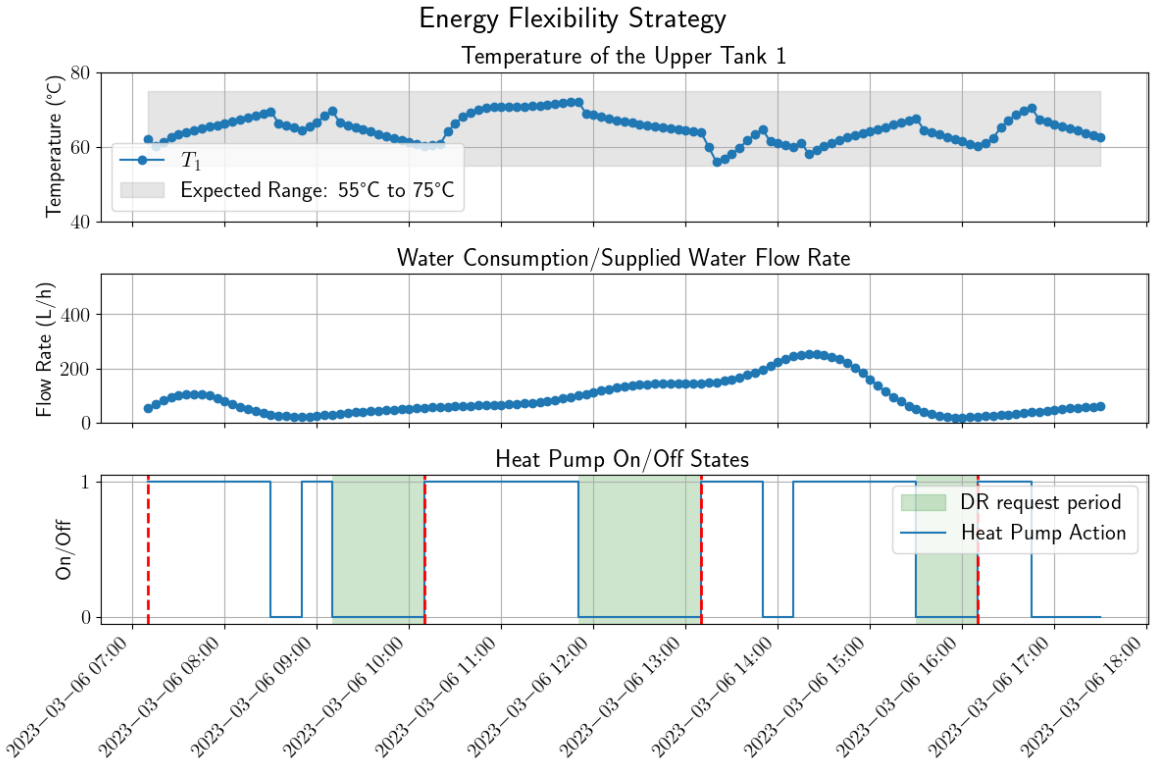

Figure 4-5: Flexibility exploitation on March 6, 2023

4-5 Real Implementation Results

To ascertain the practical viability of our two-step demand-side management strategy, real-time implementation tests were conducted on an operational heat pump system. These tests were instrumental in demonstrating the strategy's performance under actual operational conditions, moving beyond theoretical simulations.

On the test day of December 20, 2023, we enacted a series of DR scenarios in line with our strategic approach. The results depicted in Figure 4-6 confirmed the strategy's effectiveness. The flexibility assessment component of our strategy was set to perform every three hours with a 3-hour prediction horizon, at times precisely 07:23, 10:23, and 13:23. During these assessments, the system successfully identified optimal periods for DR requests, which occurred at 9:43-10:23, 12:43-13:23, and 16:03-16:23.

Our control strategy adhered to these identified periods, fulfilling the DR requests as planned. The exploitation of the flexibility was executed by setting the control inputs to zero during these periods, as shown in the bottom plot of the figure, which represents the heat pump on/off states. The highlighted sections indicate when the DR requests were in effect and the corresponding actions of the heat pump.

Furthermore, during the implementation, the upper temperature of Tank 1 T_1 was closely monitored and successfully maintained within the desired range of $55°C$ to $75°C$ for the majority of the test period. This is evident in the top plot, which shows the temperature of Tank 1. However, during the third DR period, there is a noticeable dip in the temperature of Tank 1 below $55°C$, despite the heat pump being active. This deviation is attributed to two factors: a discrepancy between the predicted and actual water consumption rates and an unusually high demand for hot water on that day, as confirmed by historical data trends. Such deviations, while noted, are within acceptable limits and highlight the importance of accounting for prediction uncertainties and real-time demand fluctuations in DSM strategies.

As shown in Table 4-1, a comparison between the Original Strategy (October 4, 2023) and the DSM Strategy (December 20, 2023) reveals that the DSM Strategy entails a modest increase in energy consumption, from 70 kWh to 73.33 kWh, and in energy cost, from 9.63 to 9.79 Euros. These incremental rises are strategic, allowing us to assess the system's capacity for reduced operation during peak times. Although there is also a slight uptick in the number of temperature violations and in average and maximum temperature deviations, these are within controlled parameters. By permitting these temperature fluctuations, the DSM Strategy effectively reduces peak demand pressures on the energy grid. This not only contributes to a more balanced and efficient system but also showcases the potential for significant improvements in energy sustainability and grid reliability.

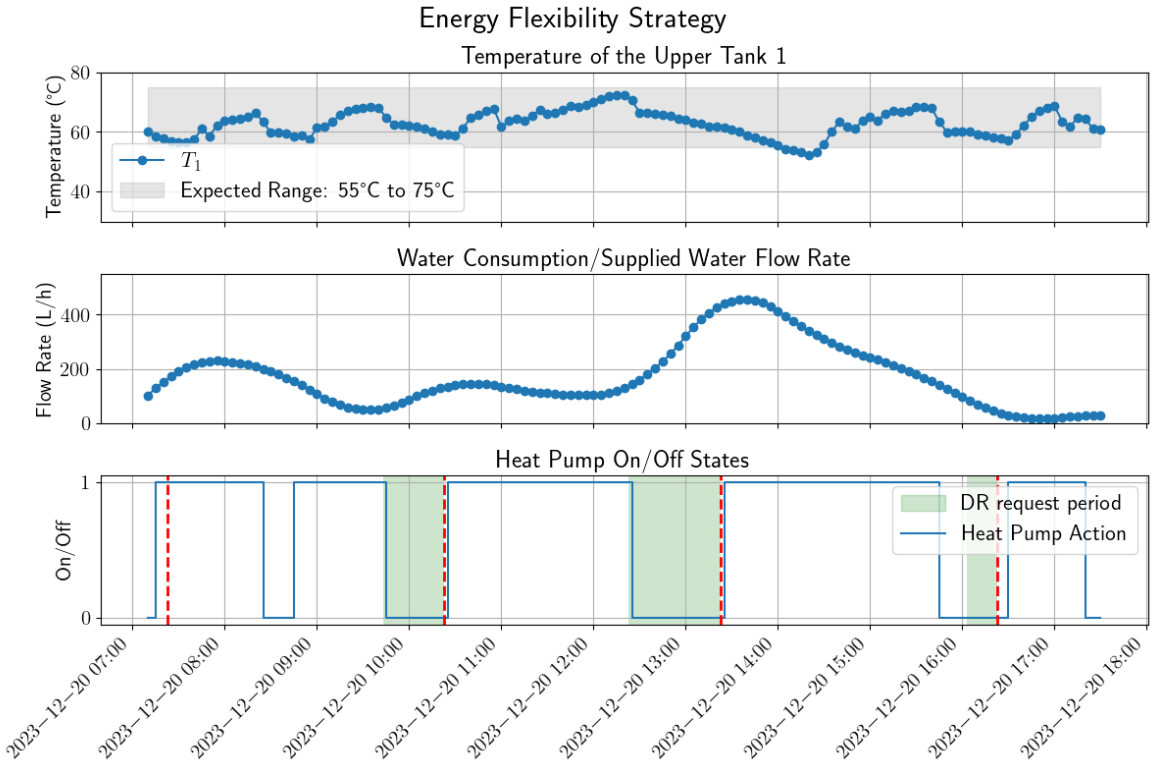

Figure 4-6: Result of the implementation for demand-side management on Dec 20, 2023

	Original Strategy (Oct 4, 2023)	DSM Strategy (Dec 20, 2023)
Energy consumption (kWh)	70	73.33
Energy cost (Euro)	9.63	9.79
The number of violation steps below 60°C (5-min sample time)	23	34
Average violation temperature difference below 60°C (°C)	0.58	0.69
Maximum violation temperature (°C)	7.16	7.74

Table 4-1: Performance of the original strategy on Oct 4, 2023 and the proposed DSM strategy on Dec 20, 2023

Chapter 5

Conclusions

5-1 Summary

The thesis delves into the intricacies of a heat pump system with thermal storage tanks, anchored by a control-oriented model inspired by a real-world system. At its core, the system features a heat pump, modeled using the Coefficient of Performance (COP) to seamlessly link electrical and thermal energies. This is complemented by thermal storage tanks, designed using a stratified tank model that expertly balances efficiency and simplicity. Experimental data guides the optimal configuration of these tanks, suggesting a two-layer design for Tank 1 and a four-layer design for Tank 2, culminating in the formation of the entire system. Refinement of the model includes key adjustments, notably accounting for temperature drops during heat pump deactivation, a crucial factor for system integrity. In a move towards simplification, the model integrates the heat pump and heat exchanger into a single entity. Alongside, the Seasonal Autoregressive Integrated Moving Average (SARIMA) model is introduced for predicting water consumption, adding a layer of predictive capability to the system.

The exploration of economical operation through Model Predictive Control (MPC) is a significant chapter of the research. It goes beyond theoretical frameworks, incorporating practical enhancements like adding slack factors and using a move blocking strategy. This innovative MPC demonstrates its superiority over traditional rule-based control strategies in economic efficiency, as evidenced by both simulations and real-world implementations.

Demand-Side Management (DSM) is another focal point, critical for enhancing energy flexibility. The approach is a two-step demand-side management strategy: first, assessing the system's energy flexibility by quantifying the maximum inactive duration of devices without impacting desired conditions, and second, exploiting this flexibility through Demand Response (DR) requests. The effectiveness of this strategy is validated through rigorous simulations and real implementations.

In conclusion, the research presents a blend of innovative modeling, strategic control, and management techniques, significantly enhancing the performance and flexibility of energy systems. This work not only contributes to academic knowledge but also lays the groundwork for more efficient and sustainable energy management practices in practical scenarios.

5-2 Future Work

The progression of MPC for heat pump systems with thermal storage tanks has highlighted several limitations in the current research, which pave the way for future research and development. These areas aim not only to refine the existing models but also to enhance the practical application and efficiency of the system. Key areas identified for future work, which directly address these limitations, include model validation, demand prediction, and implementation.

- **Enhancing Model Accuracy Through Sensor Optimization:**

  A limitation of the current study is the reliance on limited or less precise data for system modeling, the precision of which greatly influences the accuracy and reliability of MPC. To address this, future initiatives should therefore focus on optimizing sensor placement within the system to capture detailed operational data. The addition of advanced sensors in strategic locations will provide comprehensive insights into system performance. This targeted approach to data collection requires careful consideration of sensor types, their capabilities, and integration within the existing setup. The objective is to create a densely informed model that captures the nuances of the system's operations, thereby enhancing the accuracy and reliability of MPC.

- **Advancing the Demand Prediction Model:**

  The current model for demand prediction is limited by the scope and depth of available data. To address this, future work should concentrate on acquiring more varied and relevant datasets, with a special focus on enhancing water consumption data. This could involve using advanced data analytics to interpret patterns from diverse sources like building occupancy rates and seasonal variations. The implementation of sophisticated machine learning techniques, such as neural networks or ensemble learning methods, should be considered to process this data. These techniques can uncover complex patterns in extensive and varied datasets, greatly improving prediction accuracy. The model should also be designed to incorporate ongoing updates from new data, ensuring its relevance and accuracy over time. This approach to model training and validation requires a robust framework for continuous data analysis and model refinement.

- **Further Implementation:**

  The implementation phase of this research has been limited to local computers, which constrains real-time application and broader scalability. Future work should explore deploying the algorithm on company servers for automated control and real-time adjustments, thereby overcoming these limitations. This involves addressing hardware requirements, cybersecurity, and compatibility with existing IT infrastructure. Additionally, developing a user-friendly interface or dashboard will make the system more accessible and versatile, addressing the current limitation of the system's usability for non-technical staff.

Appendix A

Supplementary Materials

A-1 Additional Experimental Results

This appendix section is devoted to presenting additional experimental results that supplement the findings discussed in the main chapters. These results provide additional insights into the performance and robustness of the proposed control strategies under a variety of operational conditions.

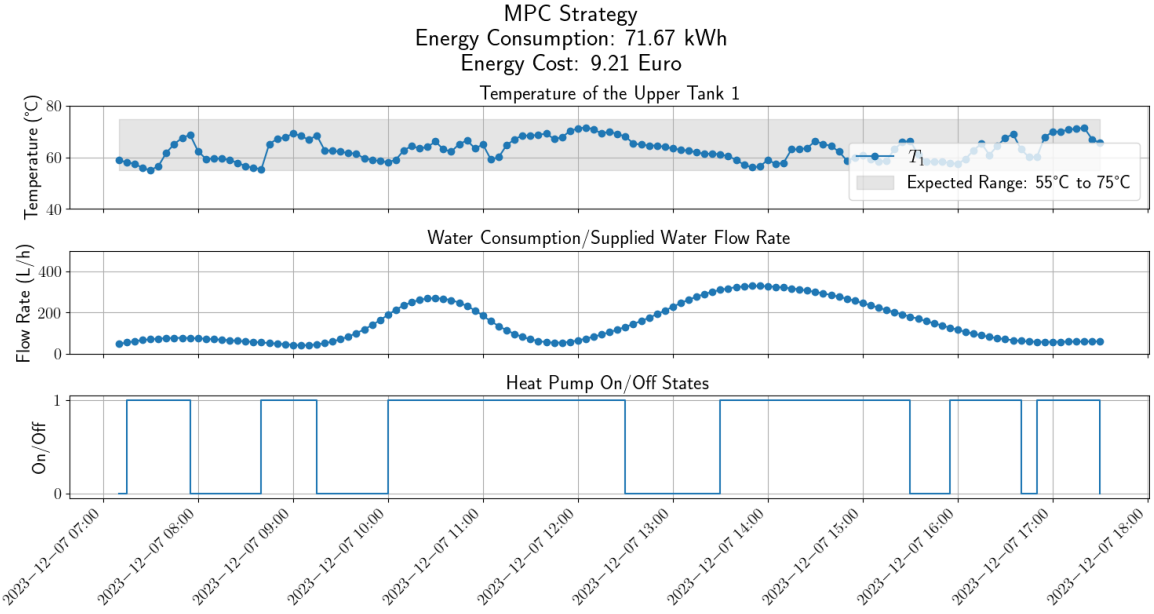

Figure A-1: Result of the implementation for economical operation on Dec 7, 2023

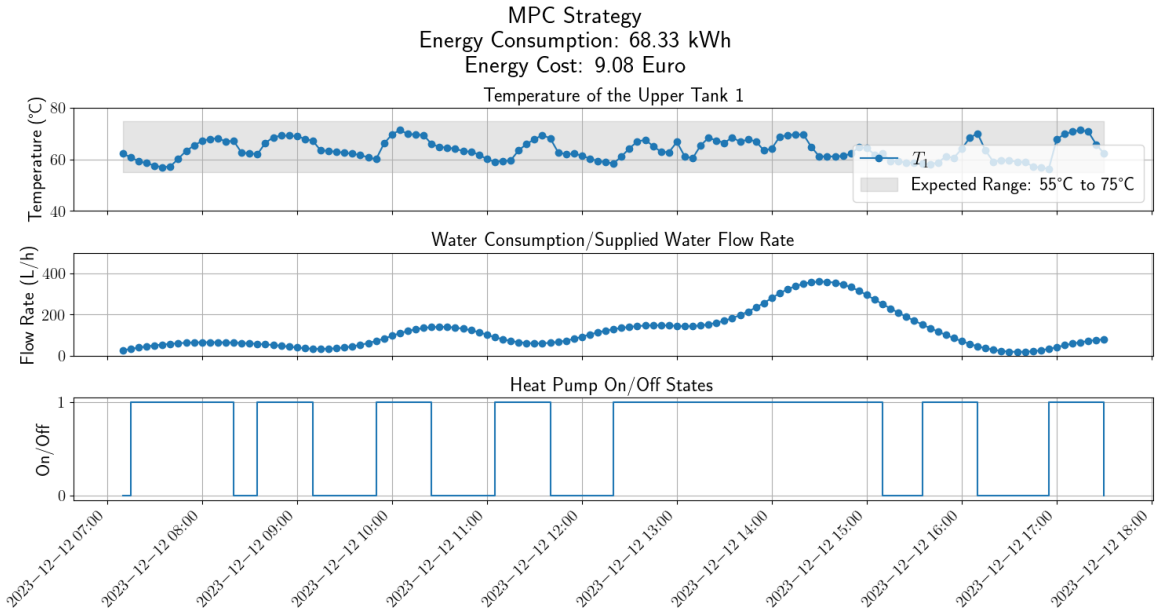

Figure A-2: Result of the implementation for economical operation on Dec 12, 2023

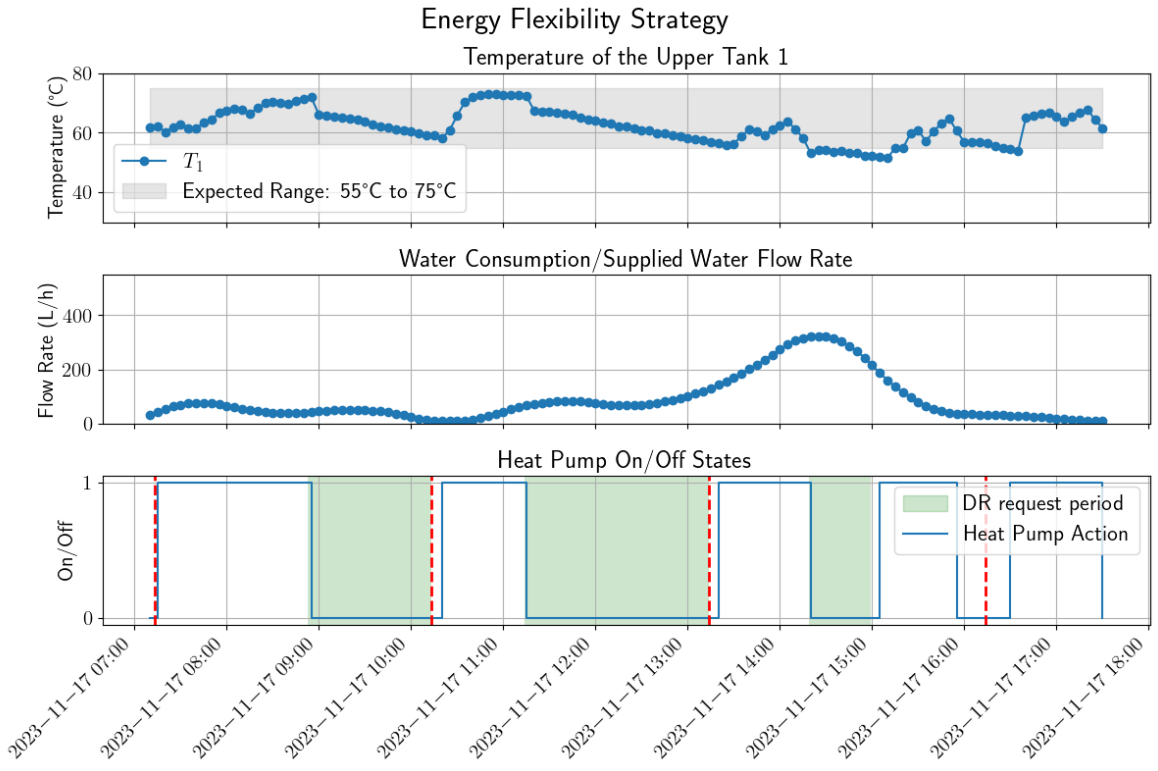

Figure A-3: Result of the implementation for demand-side management on Nov 17, 2023 (DR periods: 8:53-10:13, 11:14-13:14, 14:19-14:59)

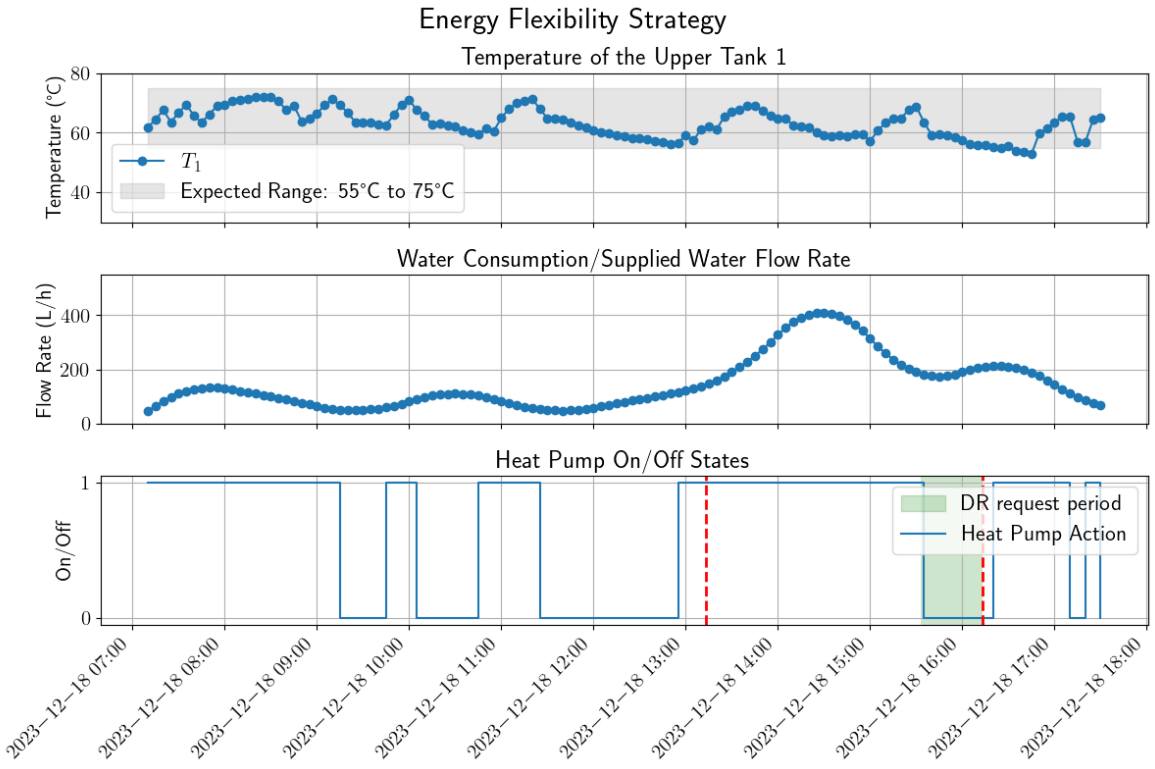

Figure A-4: Result of the implementation for demand-side management on Dec 18, 2023 (DR period: 15:33-16:13)

A-2 Control-Oriented Model Details

A-2-1 Description and identification result of symbols

Table A-1 and Table A-2 respectively summarize the descriptions and identified values of the relevant symbols in **Model 1** and **Model 2**.

Term	Description	Value	Units
Thermal coefficients			
c_p	Specific heat capacity of water	4186	$J/kg \cdot K$
R_{pipes}	Thermal resistance between pipes of the heat pump.	1.46	W/K
R_{pipe1}	Thermal resistance for outlet pipes of the heat pump.	0	W/K
R_{pipe2}	Thermal resistance for inlet pipes of the heat pump.	0.47	W/K
R_{pipe3}	Thermal resistance for outlet pipes of the heat exchanger.	0	W/K
$R_{\text{pipe,upper}}$	Thermal resistance between outlet pipes of the heat exchanger and the upper layer of Tank 1	1.99	W/K
$R_{\text{pipe,bottom}}$	Thermal resistance between outlet pipes of the heat exchanger and the bottom layer of Tank 2	0.65	W/K
R_{12}	Thermal resistance between the 1st and 2nd layers of the water tanks	0.24	W/K
R_{23}	Thermal resistance between the 2nd and 3rd layers of the water tanks	0.001	W/K
R_{34}	Thermal resistance between the 3rd and 4th layers of the water tanks	0.49	W/K
R_{45}	Thermal resistance between the 4th and 5th layers of the water tanks	0.54	W/K
R_{56}	Thermal resistance between the 5th and 6th layers of the water tanks	0.53	W/K
Masses			
m_{pipe1}	Mass of the outlet pipe of the heat pump	0.37	kg
m_{pipe2}	Mass of the inlet pipe of the heat pump	0.17	kg
m_{pipe3}	Mass of the outlet pipe of the heat exchanger	0.37	kg
m_1	Mass of the 1st layers of the water tanks	250	kg
m_2	Mass of the 2nd layers of the water tanks	250	kg
m_3	Mass of the 3rd layers of the water tanks	172.17	kg
m_4	Mass of the 4th layers of the water tanks	95.43	kg
m_5	Mass of the 5th layers of the water tanks	133.52	kg
m_6	Mass of the 6th layers of the water tanks	98.87	kg
Temperatures			
ΔT_{he}	Temperature difference of the heat exchanger	0	°C
ΔT_c	Temperature difference in the demand pipe	2.04	°C
T_s	Temperature of the water in supply pipe	13	°C
Flow rates			
$\dot{m}_s$	Flow rate in the supplement pipe	-	kg/h
$\dot{m}_c$	Flow rate in the demand circulation pipe	957.40	kg/h
$\dot{m}_p$	Flow rate in the main circulation pipe	880	kg/h

Table A-1: Description and identification result of symbols in Model 1

Term	Description	Value	Units
Thermal coefficients			
c_p	Specific heat capacity of water	4186	$J/kg \cdot K$
R_{pipe3}	Thermal resistance for outlet pipes of the heat exchanger.	0.30	W/K
$R_{\text{pipe,upper}}$	Thermal resistance between outlet pipes of the heat exchanger and the upper layer of Tank 1	0	W/K
$R_{\text{pipe,bottom}}$	Thermal resistance between outlet pipes of the heat exchanger and the bottom layer of Tank 2	2	W/K
R_{12}	Thermal resistance between outlet pipes of the 1st and 2nd layers of the water tanks	0.24	W/K
R_{23}	Thermal resistance between the 2nd and 3rd layers of the water tanks	0.24	W/K
R_{34}	Thermal resistance between the 3rd and 4th layers of the water tanks	0.49	W/K
R_{45}	Thermal resistance between the 4th and 5th layers of the water tanks	0.54	W/K
R_{56}	Thermal resistance between the 5th and 6th layers of the water tanks	0.53	W/K
Masses			
m_{pipe3}	Mass of the outlet pipe of the heat exchanger	3.27	kg
m_1	Mass of the 1st layers of the water tanks	250	kg
m_2	Mass of the 2nd layers of the water tanks	250	kg
m_3	Mass of the 3rd layers of the water tanks	169.66	kg
m_4	Mass of the 4th layers of the water tanks	95.38	kg
m_5	Mass of the 5th layers of the water tanks	136.67	kg
m_6	Mass of the 6th layers of the water tanks	98.29	kg
Temperatures			
ΔT_{he}	Temperature difference of the heat exchanger	2.84	°C
ΔT_c	Temperature difference in the demand pipe	1.76	°C
T_s	Temperature of the water in supply pipe	13	°C
ΔT_{off}	Temperature drop of the heat pump's deactivation	2.5	°C
Flow rates			
$\dot{m}_s$	Flow rate in the supplement pipe	-	kg/h
$\dot{m}_c$	Flow rate in the demand circulation pipe	1100	kg/h
$\dot{m}_p$	Flow rate in the main circulation pipe	880	kg/h

Table A-2: Description and identification result of symbols in Model 2

A-2-2 Details of Model 2

For the **Model 2**, we have the following equations:

$$x_{k+1}^3 = \left(x_{k+1}^4 + \frac{Q_{hp}}{m_{\dot{p}} c_p}\right) u_k + \left(x_k^3 - \frac{\left(R_{\text{pipe3}}(x_k^3 - T_k^{\text{amb}})\right) \cdot dk}{m_{\text{pipe3}} c_p}\right)(1-u_k) - \left(\frac{(R_{\text{pipe,upper}}(x_k^3 - x_k^5) + R_{\text{pipe,bottom}}(x_k^3 - x_k^{10})) \cdot dk}{m_{\text{pipe3}} c_p}\right)(1-u_k) \tag{A-1a}$$

$$x_{k+1}^4 = T_{\text{s}} \frac{\dot{m}_s}{\dot{m}_p} + x_k^{10}\left(1 - \frac{\dot{m}_s}{\dot{m}_p}\right) \tag{A-1b}$$

$$x_{k+1}^5 = x_k^5 + \frac{\dot{m}_p c_p \left(x_k^3 - x_k^5\right) u_k - (\dot{m}_c - \dot{m}_s) c_p \triangle T_c - R_{12}(x_k^5 - x_k^6) + \dot{m}_s c_p (x_k^6 - x_k^5)(1-u_k)}{m_1 c_p} dk + \Delta T_{off} \cdot (u_k - u_{k-1}) \cdot u_{k-1} \tag{A-1c}$$

$$x_{k+1}^6 = x_k^6 + \frac{(\dot{m}_p - \dot{m}_s) c_p \left(x_k^5 - x_k^6\right) u_k + R_{12}(x_k^5 - x_k^6) - R_{23}(x_k^6 - x_k^7) + \dot{m}_s c_p (x_k^7 - x_k^6)(1-u_k)}{m_2 c_p} dk \tag{A-1d}$$

$$x_{k+1}^7 = x_k^7 + \frac{(\dot{m}_p - \dot{m}_s) c_p \left(x_k^6 - x_k^7\right) u_k + R_{23}(x_k^6 - x_k^7) - R_{34}(x_k^7 - x_k^8) + \dot{m}_s c_p (x_k^8 - x_k^7)(1-u_k)}{m_3 c_p} dk \tag{A-1e}$$

$$x_{k+1}^8 = x_k^8 + \frac{(\dot{m}_p - \dot{m}_s) c_p \left(x_k^7 - x_k^8\right) u_k + R_{34}(x_k^7 - x_k^8) - R_{45}(x_k^8 - x_k^9) + \dot{m}_s c_p (x_k^9 - x_k^8)(1-u_k)}{m_4 c_p} dk \tag{A-1f}$$

$$x_{k+1}^9 = x_k^9 + \frac{(\dot{m}_p - \dot{m}_s) c_p \left(x_k^8 - x_k^9\right) u_k + R_{45}(x_k^8 - x_k^9) - R_{56}(x_k^9 - x_k^{10}) + \dot{m}_s c_p (x_k^{10} - x_k^9)(1-u_k)}{m_5 c_p} dk \tag{A-1g}$$

$$x_{k+1}^{10} = x_k^{10} + \frac{(\dot{m}_p - \dot{m}_s) c_p \left(x_k^9 - x_k^{10}\right) u_k + R_{56}(x_k^9 - x_k^{10}) + \dot{m}_s c_p (T_s - x_k^{10})(1-u_k)}{m_6 c_p} dk \tag{A-1h}$$

Bibliography

[1] Abdul Afram and Farrokh Janabi-Sharifi. Theory and applications of hvac control systems–a review of model predictive control (mpc). *Building and Environment*, 72:343–355, 2014.

[2] Marcel Ulrich Ahrens, Sverre Stefanussen Foslie, Ole Marius Moen, Michael Bantle, and Trygve Magne Eikevik. Integrated high temperature heat pumps and thermal storage tanks for combined heating and cooling in the industry. *Applied Thermal Engineering*, 189:116731, 2021.

[3] Alessia Arteconi, Neil J Hewitt, and Fabio Polonara. Domestic demand-side management (dsm): Role of heat pumps and thermal energy storage (tes) systems. *Applied Thermal Engineering*, 51(1-2):155–165, 2013.

[4] Brecht Baeten, Frederik Rogiers, Dieter Patteeuw, and Lieve Helsen. Comparison of optimal control formulations for stratified sensible thermal energy storage in space heating applications. In *The 13th International Conference on Energy Storage.*, 2015.

[5] Gianni Bianchini, Marco Casini, Antonio Vicino, and Donato Zarrilli. Demand-response in building heating systems: A model predictive control approach. *Applied Energy*, 168:159–170, 2016.

[6] Felix Bünning, Joseph Warrington, Philipp Heer, Roy S. Smith, and John Lygeros. Robust mpc with data-driven demand forecasting for frequency regulation with heat pumps. *Control Engineering Practice*, 122:105101, 2022.

[7] Duncan S. Callaway and Ian A. Hiskens. Achieving controllability of electric loads. *Proceedings of the IEEE*, 99(1):184–199, 2011.

[8] Luca Cecchinato, Marco Corradi, Ezio Fornasieri, and Lorenzo Zamboni. Carbon dioxide as refrigerant for tap water heat pumps: A comparison with the traditional solution. *International Journal of Refrigeration*, 28(8):1250–1258, 2005.

[9] Alysha M De Livera, Rob J Hyndman, and Ralph D Snyder. Forecasting time series with complex seasonal patterns using exponential smoothing. *Journal of the American Statistical Association*, 106(496):1513–1527, 2011.

[10] Arnaud De Myttenaere, Boris Golden, Bénédicte Le Grand, and Fabrice Rossi. Mean absolute percentage error for regression models. *Neurocomputing*, 192:38–48, 2016.

[11] Francesco D'Ettorre, Mattia De Rosa, Paolo Conti, Daniele Testi, and Donal Finn. Mapping the energy flexibility potential of single buildings equipped with optimally-controlled heat pump, gas boilers and thermal storage. *Sustainable Cities and Society*, 50:101689, 2019.

[12] European Heat Pump Association EHPA. Heat pump record: 3 million units sold in 2022, contributing to repowereu targets, 2022.

[13] Conrado Ermel, Marcus VA Bianchi, Ana Paula Cardoso, and Paulo S Schneider. Thermal storage integrated into air-source heat pumps to leverage building electrification: A systematic literature review. *Applied Thermal Engineering*, page 118975, 2022.

[14] European Network of Transmission System Operators for Electricity. Day ahead prices. https://transparency.entsoe.eu/transmission-domain/r2/dayAheadPrices/show, 2023.

[15] Björn Felten and Christoph Weber. The value (s) of flexible heat pumps–assessment of technical and economic conditions. *Applied Energy*, 228:1292–1319, 2018.

[16] David Fischer and Hatef Madani. On heat pumps in smart grids: A review. *Renewable and Sustainable Energy Reviews*, 70:342–357, 2017.

[17] David Fischer, Tobias Wolf, Jeannette Wapler, Raphael Hollinger, and Hatef Madani. Model-based flexibility assessment of a residential heat pump pool. *Energy*, 118:853–864, 2017.

[18] Lilli Frison, Martin Kleinstück, and Peter Engelmann. Model-predictive control for testing energy flexible heat pump operation within a hardware-in-the-loop setting. In *Journal of Physics: Conference Series*, volume 1343, page 012068. IOP Publishing, 2019.

[19] Linas Gelazanskas and Kelum AA Gamage. Demand side management in smart grid: A review and proposals for future direction. *Sustainable Cities and Society*, 11:22–30, 2014.

[20] C.W. Gellings. The concept of demand-side management for electric utilities. *Proceedings of the IEEE*, 73(10):1468–1470, 1985.

[21] Hessam Golmohamadi, Kim Guldstrand Larsen, Peter Gjøl Jensen, and Imran Riaz Hasrat. Optimization of power-to-heat flexibility for residential buildings in response to day-ahead electricity price. *Energy and Buildings*, 232:110665, 2021.

[22] Hessam Golmohamadi, Kim Guldstrand Larsen, Peter Gjøl Jensen, and Imran Riaz Hasrat. Integration of flexibility potentials of district heating systems into electricity markets: A review. *Renewable and Sustainable Energy Reviews*, 159:112200, 2022.

[23] Dutch Government. Klimaatnota 2022. Technical report, Dutch Government, 2022.

[24] Rasmus Halvgaard, Niels Kjølstad Poulsen, Henrik Madsen, and John Bagterp Jørgensen. Economic model predictive control for building climate control in a smart grid. In *2012 IEEE PES Innovative Smart Grid Technologies (ISGT)*, pages 1–6, 2012.

[25] Dulakshi Santhusitha Kumari Karunasingha. Root mean square error or mean absolute error? use their ratio as well. *Information Sciences*, 585:609–629, 2022.

[26] Zachary Lee, Kartikay Gupta, Kevin J Kircher, and K Max Zhang. Mixed-integer model predictive control of variable-speed heat pumps. *Energy and Buildings*, 198:75–83, 2019.

[27] Yun Li, Neil Yorke-Smith, and Tamas Keviczky. Unlocking energy flexibility from thermal inertia of buildings: A robust optimization approach. *arXiv preprint arXiv:2312.05108*, 2023.

[28] Henrik Lund, Bernd Möller, Brian Vad Mathiesen, and A Dyrelund. The role of district heating in future renewable energy systems. *Energy*, 35(3):1381–1390, 2010.

[29] Frauke Oldewurtel, Alessandra Parisio, Colin N. Jones, Manfred Morari, Dimitrios Gyalistras, Markus Gwerder, Vanessa Stauch, Beat Lehmann, and Katharina Wirth. Energy efficient building climate control using stochastic model predictive control and weather predictions. In *Proceedings of the 2010 American Control Conference*, pages 5100–5105, 2010.

[30] Frauke Oldewurtel, David Sturzenegger, Göran Andersson, Manfred Morari, and Roy S Smith. Towards a standardized building assessment for demand response. In *52nd IEEE Conference on Decision and Control*, pages 7083–7088. IEEE, 2013.

[31] Georgios Papaefthymiou, Bernhard Hasche, and Christian Nabe. Potential of heat pumps for demand side management and wind power integration in the german electricity market. *IEEE Transactions on Sustainable Energy*, 3(4):636–642, 2012.

[32] European Parliament and Council of the European Union. Directive 2009/28/ec of the european parliament and of the council of 23 april 2009 on the promotion of the use of energy from renewable sources and amending and subsequently repealing directives 2001/77/ec and 2003/30/ec, 2009.

[33] Soroush Rastegarpour, Sebastien Gros, and Luca Ferrarini. Mpc approaches for modulating air-to-water heat pumps in radiant-floor buildings. *Control Engineering Practice*, 95:104209, 2020.

[34] Renaldi Renaldi, Arisitides Kiprakis, and Daniel Friedrich. An optimisation framework for thermal energy storage integration in a residential heat pump heating system. *Applied Energy*, 186:520–529, 2017.

[35] Tim Schwickart, Holger Voos, Mohamed Darouach, and Souad Bezzaoucha. A flexible move blocking strategy to speed up model-predictive control while retaining a high tracking performance. In *2016 European Control Conference (ECC)*, pages 764–769. IEEE, 2016.

[36] W. Tang. Model predictive control for heat pump with thermal energy storage. Literature review, September 2023.

[37] Mark van de Ruit, Winfred Mugge, Gaia Cavallo, John Lataire, Daniel Ludvig, and Alfred C Schouten. Quantitative comparison of time-varying system identification methods to describe human joint impedance. *Annual Reviews in Control*, 52:91–107, 2021.

[38] Wenyi Wang, Bin Hu, RZ Wang, Mingwen Luo, Guangpeng Zhang, and Bo Xiang. Model predictive control for the performance improvement of air source heat pump heating system via variable water temperature difference. *International Journal of Refrigeration*, 138:169–179, 2022.

[39] YT Wang, DR Wilson, and DF Neale. Heat-pump control. In *IEE Proceedings D (Control Theory and Applications)*, volume 130, pages 328–332. IET, 1983.

[40] Roger Wimmer, ESFANDIAR Shafai, and HANS P Geering. Model predictive control for heat pump heating systems. In *Proceedings of the IASTED International Conference on Control Applications. Banff, Alberta, Canada*, 2001.

[41] Lei Yuan, Haiyan Zhao, Hong Chen, and Bingtao Ren. Nonlinear mpc-based slip control for electric vehicles with vehicle safety constraints. *Mechatronics*, 38:1–15, 2016.

Glossary

List of Acronyms

AR	Autoregressive
ARIMA	Autoregressive Integrated Moving Average
CO2	Carbon Dioxide
COP	Coefficient of Performance
DR	Demand Response
DSM	Demand-Side Management
EMPC	Economic Model Predictive Control
EMS	Energy Management System
HVAC	Heating, Ventilating and Air-Conditioning
MA	Moving Average
MAPE	Mean Absolute Percentage Error
MI-MPC	Mixed-Integer Model Predictive Control
MPC	Model Predictive Control
RES	Renewable Energy Sources
RMSE	Root Mean Square Error
SARIMA	Seasonal Autoregressive Integrated Moving Average
TES	Thermal Energy Storage
VAF	Variance Accounted For